

# *Detecting and quantifying palaeoseasonality in stalagmites using geochemical and modelling approaches*

Article

Accepted Version

Creative Commons: Attribution-Noncommercial-No Derivative Works 4.0

Baldini, J. U.L., Lechleitner, F. A., Breitenbach, S. F.M., van Hunen, J., Baldini, L. M., Wynn, P. M., Jamieson, R. A., Ridley, H. E., Baker, A. H. ORCID: <https://orcid.org/0000-0003-2697-1350>, Walczak, I. W. and Fohlmeister, J. (2021) Detecting and quantifying palaeoseasonality in stalagmites using geochemical and modelling approaches. *Quaternary Science Reviews*, 254. 106784. ISSN 0277-3791 doi: <https://doi.org/10.1016/j.quascirev.2020.106784> Available at <https://centaur.reading.ac.uk/97596/>

It is advisable to refer to the publisher's version if you intend to cite from the work. See [Guidance on citing](#).

Published version at: <https://www.sciencedirect.com/science/article/pii/S0277379120307460>

To link to this article DOI: <http://dx.doi.org/10.1016/j.quascirev.2020.106784>

Publisher: Elsevier

All outputs in CentAUR are protected by Intellectual Property Rights law, including copyright law. Copyright and IPR is retained by the creators or other copyright holders. Terms and conditions for use of this material are defined in the [End User Agreement](#).

[www.reading.ac.uk/centaur](http://www.reading.ac.uk/centaur)

**CentAUR**

Central Archive at the University of Reading

Reading's research outputs online

1 Detecting and quantifying palaeoseasonality in stalagmites using geochemical  
2 and modelling approaches

3 James U.L. Baldini<sup>1</sup>, Franziska A. Lechleitner<sup>2, 3, 4</sup>, Sebastian F.M. Breitenbach<sup>4</sup>,  
4 Jeroen van Hunen<sup>1</sup>, Lisa M. Baldini<sup>5</sup>, Peter M. Wynn<sup>6</sup>, Robert A. Jamieson<sup>7</sup>, Harriet E. Ridley<sup>1</sup>,  
5 Alexander J. Baker<sup>8</sup>, Izabela W. Walczak<sup>9</sup>, and Jens Fohlmeister<sup>10, 11</sup>

6 <sup>1</sup>Department of Earth Sciences, Durham University, DH1 3LE, United Kingdom.

7 <sup>2</sup>Department of Earth Sciences, University of Oxford, South Parks Road, Oxford OX1 3AN,  
8 United Kingdom.

9 <sup>3</sup> Laboratory for the Analysis of Radiocarbon with AMS (LARA), Department of Chemistry and  
10 Biochemistry, and Oeschger Centre for Climate Change Research, University of Bern,  
11 Freiestrasse 3, 3012 Bern, Switzerland.

12 <sup>4</sup>Department of Geography and Environmental Sciences, Northumbria University,  
13 Newcastle upon Tyne, NE1 8ST, United Kingdom.

14 <sup>5</sup>School of Health & Life Sciences, Teesside University, Middlesbrough, TS1 3BX, United  
15 Kingdom

16 <sup>6</sup>Lancaster Environment Centre, Lancaster University, Lancaster, LA1 4YQ, United Kingdom.

17 <sup>7</sup>School of Earth and Environment, University of Leeds, Leeds, LS2 9JT, United Kingdom

18 <sup>8</sup>National Centre for Atmospheric Science and Department of Meteorology, University of  
19 Reading, RG6 6BB, United Kingdom.

20 <sup>9</sup>Durham Centre for Academic Development, Durham University, Durham, DH1 1TA, United  
21 Kingdom.

22 <sup>10</sup>Potsdam Institute for Climate Impact Research, Telegrafenberg, 14473 Potsdam, Germany.

23 <sup>11</sup>GFZ German Research Centre for Geosciences, Section 'Climate Dynamics and Landscape  
24 Development', Telegrafenberg, 14473 Potsdam, Germany.

25

26

27

28 **Abstract**

29 Stalagmites are an extraordinarily powerful resource for the reconstruction of climatological  
30 palaeoseasonality. Here, we provide a comprehensive review of different types of  
31 seasonality preserved by stalagmites and methods for extracting this information. A new  
32 drip classification scheme is introduced, which facilitates the identification of stalagmites  
33 fed by seasonally responsive drips and which highlights the wide variability in drip types  
34 feeding stalagmites. This hydrological variability, combined with seasonality in Earth  
35 atmospheric processes, meteoric precipitation, biological processes within the soil, and cave  
36 atmosphere composition means that every stalagmite retains a different and distinct (but  
37 correct) record of environmental conditions. Replication of a record is extremely useful but  
38 should not be expected unless comparing stalagmites affected by the same processes in the  
39 same proportion. A short overview of common microanalytical techniques is presented, and  
40 suggested best practice discussed. In addition to geochemical methods, a new modelling  
41 technique for extracting meteoric precipitation and temperature palaeoseasonality from  
42 stalagmite  $\delta^{18}\text{O}$  data is discussed and tested with both synthetic and real-world datasets.  
43 Finally, world maps of temperature, meteoric precipitation amount, and meteoric  
44 precipitation oxygen isotope ratio seasonality are presented and discussed, with an aim of  
45 helping to identify regions most sensitive to shifts in seasonality.

46

47 **1. Introduction**

48 Over the past few decades stalagmites have become one of the most important terrestrial  
49 archives of climate and environmental change. Their widespread distribution, amenability to

50 radiometric dating, and capacity for retaining seasonal to decadal-scale environmental  
51 information have made them indispensable archives for a wide variety of climate information,  
52 most commonly rainfall or temperature variability. The field has developed rapidly, and it is  
53 now clear that stalagmites generally do not record a single climate parameter (e.g., cave  
54 temperature, rainfall amount) exclusively, but instead record a combination of processes. It  
55 is increasingly acknowledged that every stalagmite contains a robust history of some aspect  
56 of environmental change. The issue is one of complexity; generally speaking, the stalagmite  
57 with the least complex signal is considered the ideal. Records generated from stalagmites  
58 with more complex stratigraphies, whose drip flow route changes through time, or that are  
59 influenced by numerous environmental processes, often prove more difficult to interpret.  
60 Some stalagmite records may miss short-lived climate excursions because they are fed by  
61 drips that do not respond to the transient climate forcing in question. Others might lose  
62 sensitivity or respond non-linearly to a climate forcing; for example, a stalagmite might record  
63 droughts faithfully, but miss exceptionally wet intervals when the epikarst (the highly  
64 fractured transition zone between soil and bedrock) is saturated with water. To exacerbate  
65 the issue further, most stalagmite records lack the requisite resolution to detect  
66 palaeoseasonality, an aspect of the climate signal that is increasingly recognised as critical to  
67 the interpretation of geochemical records from stalagmites (Baldini et al., 2019; Morellón et  
68 al., 2009; Moreno et al., 2017). In other words, the desired climate signal is often  
69 compromised by: i) inherent complexities associated with the hydrological transfer of the  
70 climate signal to the stalagmite, ii) overprinting of the desired climate-driven signal by other  
71 environmental variables, and iii) bias introduced via the necessarily selective sampling of the  
72 stalagmite for analysis. The challenge for palaeoclimatologists is to extract and correctly  
73 interpret the desired climate signal from a stalagmite, bearing these complexities in mind.

74 The detection of a seasonality signal within a stalagmite can greatly help interpret all datasets  
75 from a stalagmite sample, of any temporal resolution. For example, the detection of a  
76 seasonal geochemical cycle can contribute to chronological models (Baldini et al., 2002;  
77 Carlson et al., 2018; Ridley et al., 2015b), in some cases permitting the development of high-  
78 precision chronologies over extended time intervals (Ban et al., 2018; Carlson et al., 2018;  
79 Duan et al., 2015; Nagra et al., 2017; Ridley et al., 2015b; Smith et al., 2009). Unlike most  
80 other laminated records (e.g., tree rings, ice cores), high-precision radiometric dates can  
81 anchor stalagmite layer count chronologies, reducing accumulated counting errors. Proxy  
82 information from laminated stalagmites can be linked to environmental variability at seasonal  
83 resolution (Mattey et al., 2010; Orland et al., 2019; Ridley et al., 2015b), allowing much  
84 needed insights into past climatic dynamics that are difficult to obtain otherwise.

85 The fact that stalagmites can reveal palaeoseasonality, a notoriously difficult climate  
86 parameter to reconstruct, is critical for identifying wholesale shifts in climate belts. For  
87 example, monthly-scale geochemical data from a stalagmite has detected variability in the  
88 Intertropical Convergence Zone influence on rainfall seasonality in Central America over the  
89 last two millennia (Asmerom et al., 2020) and the shift from a maritime to a more continental  
90 climate in western Ireland in the early Holocene (Baldini et al., 2002), transitions which must  
91 otherwise be inferred using annual- to centennial-resolution data (e.g., Breitenbach et al.,  
92 2019). High spatial resolution approaches yielding palaeoseasonality can distinguish rainfall  
93 occurring at different times of the year, for example, monsoonal rainfall versus dry season  
94 rainfall (Ban et al., 2018; Ronay et al., 2019), providing a wealth of information not attainable  
95 by other means.

96 Seasonality is one of climate's most important aspects, and this is reflected in the basic  
97 subdivisions of the Köppen system, the most commonly used climate classification scheme  
98 (Köppen, 1918; Peel et al., 2007). Reconstructing past seasonality is not only relevant for pure  
99 palaeoclimatological studies, but also for palaeobotany and archaeology, and for establishing  
100 a benchmark by which to compare recent changes in seasonality during the Anthropocene;  
101 recent research suggests seasonality in rainfall (e.g., Feng et al., 2013) and temperature (e.g.,  
102 Santer et al., 2018) are shifting under modern climate change. This is particularly concerning  
103 because changing seasonality has had broad ecological and social implications in the past. For  
104 example, human dispersal through Asia was limited more by water availability rather than  
105 temperature, and likely followed habitable corridors with favourable rainfall seasonality (Li et  
106 al., 2019; Parton et al., 2015; Taylor et al., 2018). Also, the domestication and dispersal of  
107 crops are linked to rainfall seasonality, because optimal growth conditions depend on  
108 hydrological conditions. In the Fertile Crescent, barley and wheat were sown in autumn,  
109 because in this semi-arid region the winter rains are the limiting factor for their prosperity  
110 (Spengler, 2019). Similarly, abundant evidence now exists that variability in seasonal rainfall  
111 has played a key role in the waxing and waning of major civilisations (Hsiang et al., 2013;  
112 Kennett et al., 2012).

113 Despite the clear importance of reconstructing palaeoseasonality, it is rarely directly  
114 observable in climate proxy records. The obfuscation of seasonality by undersampling or  
115 aliasing is often a consequence of logical and pragmatic choices designed to maximise returns  
116 from available resources. Ideally, analyses would resolve nearly the full climate signal residing  
117 within every stalagmite, but this is neither logistically (given the time and funding required)  
118 nor realistically (given that the karst system transmutes the signal) possible.

119 Here we review both the advantages of obtaining palaeoseasonality information and methods  
120 for its reconstruction using stalagmite geochemistry and modelling, as well as common issues  
121 in extracting this information. A short review of the history of speleothem science and  
122 techniques frames the discussion and highlights how speleothems have become the premier  
123 archives for annual- to sub-annual scale terrestrial climate reconstructions, particularly during  
124 the Quaternary. We also suggest a methodology to maximise the likelihood of successfully  
125 extracting palaeoseasonality information from a stalagmite, including evaluating the  
126 hydrological characteristics of the drip feeding a stalagmite sample prior to collection,  
127 modelling palaeoseasonality from lower resolution data, and determining the seasonality of  
128 the climate at (and in regions near) the site.

129

## 130 **2. Background and technique development**

131 Very early studies demonstrated the potential of stalagmites to record climate information  
132 (Allison, 1923, 1926; Broecker, 1960; Orr, 1952). However, the real growth in the application  
133 of stalagmites as climate archives occurred after the convergence of Thermal Ionisation Mass  
134 Spectrometry (TIMS) uranium-thorium dating of stalagmites in the 1990s (e.g., Edwards et al.,  
135 1987; Edwards and Gallup, 1993) (which allowed accurate dating) and high resolution  
136 sampling techniques in the 2000s (permitting the reconstruction of climate on sub-decadal  
137 timescales). The subsequent development and proliferation of multi-collector inductively  
138 coupled plasma mass spectrometry (MC-ICP-MS) permitted extraordinarily robust (precise  
139 and accurate) chronological control (e.g., Cheng et al., 2013; Hellstrom, 2003; Hoffmann et  
140 al., 2007), while the development of a variety of microanalytical techniques provided climate  
141 proxy information of an unparalleled temporal resolution. The realisation in the late 1990s



142 (Roberts et al., 1998) and early 2000s that stalagmite carbonate trace element compositions  
143 and isotope ratios often vary seasonally (Baldini et al., 2002; Fairchild et al., 2000; McMillan  
144 et al., 2005; Treble et al., 2003; Treble et al., 2005b) opened the door to the investigation of  
145 palaeoseasonality on an unprecedented level.

146

## 147 **2.1. Increasing resolution of analysis**

148 Immense technical progress has facilitated the transition from the first speleothem studies,  
149 which broadly placed periods of speleothem growth into the global climatic context (Harmon,  
150 1979; Hendy and Wilson, 1968; Thompson et al., 1975), to increasingly detailed sub-annual  
151 resolution hydroclimate reconstructions (Fairchild et al., 2001; Johnson et al., 2006; Liu et al.,  
152 2013; Matthey et al., 2008; Maupin et al., 2014; Myers et al., 2015; Ridley et al., 2015b; Ronay  
153 et al., 2019; Treble et al., 2005a). Methodological developments, particularly after the mid-  
154 2000s and particularly with respect to trace element analysis, greatly reduced the required  
155 sample size and increased measurement precision. This included the widespread adoption of  
156 micromilling techniques (Spötl and Matthey, 2006), laser ablation (Müller et al., 2009; Treble  
157 et al., 2003), secondary ionisation mass spectrometry (Baldini et al., 2002; Fairchild et al.,  
158 2001; Finch et al., 2001; Orland et al., 2008, 2009), and the development of protocols for  
159 stable carbon and oxygen isotope measurements with reduced sample sizes (Breitenbach and  
160 Bernasconi, 2011).

161 Here, we apply the recently compiled Speleothem Isotope Synthesis and Analysis (SISAL)  
162 database v1b (Atsawawaranunt et al., 2018; Comas-Bru et al., 2019) to document the  
163 evolution of speleothem stable isotope record resolution. SISAL was created with the primary

164 objective of providing access to a comprehensive repository of published stalagmite  $\delta^{18}\text{O}$   
165 records to the palaeoclimate community and for climate model evaluation (Comas-Bru and  
166 Harrison, 2019; Comas-Bru et al., 2019). SISALv1b contains 455 speleothem records (i.e., SISAL  
167 ‘entities’) from 211 globally distributed caves published since 1992 (Comas-Bru et al., 2019).  
168 More than half the records (264) included in the database cover at least portions of the last  
169 10,000 years.

170 To investigate how stable isotope record resolution has evolved over the last three decades,  
171 we extracted all records from the database and calculated their temporal resolution as the  
172 absolute difference between two consecutive samples. Hiatuses and gaps in the individual  
173 records were excluded from the analysis, as these would have erroneously suggested much  
174 lower resolution than that actually present. In a second step, we performed the same  
175 calculation, considering only Holocene records.

176 The analysis reveals how the number of speleothem stable isotope records steadily increased  
177 with publication year (Figure 1), highlighting the increased popularity of speleothem science  
178 over the past three decades. A trend of increasing temporal resolution with time becomes  
179 apparent after binning all records published in the same year and calculating their mean  
180 resolution (Figure 1). This trend becomes even clearer when only Holocene records are  
181 considered, with a particularly striking increase in resolution over recent years (post-2010)  
182 (records pre-2010: mean resolution = 50.1 years, STDEV = 38.9 years; records between 2010  
183 and 2018: mean resolution = 16.5 years, STDEV = 7.4 years), and is likely related to the  
184 widespread adoption of microanalytical advances. Additionally, a record’s resolution will  
185 typically depend on the time period covered by the record; in general, resolution is higher in  
186 Holocene records compared to the full dataset, which includes older records as well. This

187 partly arises because of greater availability of independent data and information on climate  
188 conditions during more recent time intervals, thus requiring higher resolution records to  
189 tackle relevant research questions. It may also be partially due to typically lower growth rates  
190 during the last glaciation compared to the Holocene. However, overall only nine of the records  
191 in SISALv1b have resolution  $<0.5$  years, allowing for investigations of paleoseasonality. This  
192 highlights the difficulties often encountered with conventional sampling techniques, as this  
193 compilation only includes stable isotope records, and does not consider other methods (e.g.,  
194 laser ablation trace element analysis), which can generate higher resolution time-series. The  
195 increasing resolution possible via technological developments has largely involved the  
196 analysis of trace elements, whereas stable isotope analysis still predominantly relies on  
197 micromilling or drilling techniques.

198

## 199 **2.2. Transition from temperature to rainfall amount to seasonality**

200 Early speleothem palaeoclimate studies focused on using  $\delta^{18}\text{O}$  to generate quantitative cave  
201 temperature records (Gascoyne et al., 1980; Hendy and Wilson, 1968; Lauritzen, 1995;  
202 Lauritzen and Lundberg, 1999), based on the insight that oxygen isotope fractionation during  
203 carbonate deposition is temperature dependent (Epstein et al., 1951; O'Neil et al., 1969), and  
204 building on similar work on marine carbonates (Emiliani, 1955). It was quickly recognised  
205 however that speleothem  $\delta^{18}\text{O}$  is a complex mixed signal reflecting variations in cave  
206 temperature, changes in dripwater isotope composition, and various kinetic effects, which  
207 severely hamper the use of this proxy for quantitative temperature reconstructions  
208 (McDermott, 2004). The subsequent shift in how speleothem  $\delta^{18}\text{O}$  is interpreted led to its  
209 establishment as a proxy for past hydroclimate changes, including atmospheric circulation,

210 regional temperature, moisture source dynamics, and amount of precipitation (Lachniet,  
211 2009).

212 At the same time, the toolkit of geochemical proxies available to speleothem researchers  
213 continued to expand. In particular, trace element concentrations in speleothem carbonate  
214 emerged as tracers for numerous processes, from surface productivity to karst hydrology and  
215 transport (Borsato et al., 2007; Fairchild et al., 2001; Huang and Fairchild, 2001; Treble et al.,  
216 2005a). The combination of multiple proxies measured on the same speleothem provided a  
217 means to disentangle complexities regarding mixed signals in individual proxies and allowed  
218 a progressively deeper understanding of the archive and the associated processes in soil,  
219 karst, atmosphere, and cave. In tandem with these developments regarding the climate proxy  
220 development, monitoring of cave and local atmospheric conditions became increasingly  
221 important, as it was recognised that understanding sometimes highly localised controls on  
222 geochemical signatures is crucial for their interpretation (Genty, 2008; Matthey et al., 2008;  
223 Matthey et al., 2010; Spötl et al., 2005; Verheyden et al., 2008).

224 The presence of annual petrographic cyclicity within stalagmites was recognised very early on  
225 (Allison, 1926). The later identification of visible and luminescent annual banding (Baker et  
226 al., 1993; Broecker, 1960; Shopov et al., 1994) underscored that the deposition, mineralogy,  
227 and chemical composition of speleothems varied seasonally. However, the concept of  
228 seasonal shifts in climate variables (e.g., temperature, precipitation) as contributing to the  
229 net multi-annual climate signal did not gain traction until the early to mid-2000s (Wang et al.,  
230 2001). Cave monitoring revealed drip rate seasonality in Pere Noel Cave, Belgium (Genty and  
231 Deflandre, 1998), Crag Cave, Ireland (Baldini et al., 2006), and in Soreq Cave, Israel (Ayalon et  
232 al., 1998), and seasonality was discussed within the context of a speleothem-based trace

233 element study at Grotta di Ernesto, Italy (Huang et al., 2001). Meteorological data were  
234 compared to seasonal trace element data for an Australian stalagmite (Treble et al., 2003),  
235 and the potential to use seasonal-scale geochemical data to reconstruct the East Asian  
236 Summer Monsoon (EASM) was investigated using a stalagmite from Heshang Cave, China  
237 (Johnson et al., 2006). Studies coupling cave environmental monitoring and ‘farmed’  
238 carbonate precipitates were critical for clarifying the links between hydrological and cave  
239 atmosphere conditions on the chemistry of stalagmites, including at a seasonal scale  
240 (Czuppon et al., 2018; Moerman et al., 2014; Sherwin and Baldini, 2011; Tremaine et al.,  
241 2011). Drip monitoring was also key for establishing how cave hydrology attenuates seasonal  
242 and interannual rainfall variability, and was used to predict ENSO variability preservation  
243 within stalagmites (Chen and Li, 2018; Moerman et al., 2014). These studies all illustrate that  
244 a thorough understanding of annual geochemical cycles requires the development of  
245 extensive cave monitoring records, which highlight the complexities inherent in signal  
246 transfer from surface environment to the stalagmite.

247

### 248 **2.3. Importance of monitoring for understanding the seasonal signal**

249 Monitoring environmental conditions in and above a cave at a high temporal resolution  
250 greatly improves the accuracy of palaeoclimate interpretations derived from stalagmites.  
251 Linking proxy characteristics at a given site with current environmental conditions via  
252 monitoring is relevant for reconstructing past conditions. Although modern conditions may  
253 differ from ancient conditions, monitoring the cave environment elucidates processes  
254 operating at a site, including the timing and extent of ventilation and the general nature of a

255 hydrological signal, acknowledging that some hydrological re-routing may have occurred  
256 through time for certain drip types.

257 Understanding a stalagmite geochemical proxy record is difficult without first understanding  
258 how that signal is transferred and altered from the external environment to the sample.  
259 Environmental changes affecting the seasonal signal fall under four main categories: **i) Earth**  
260 **atmospheric, ii) Meteoric precipitation, iii) biological** (e.g., soil processes), and **iv) cave**  
261 **atmospheric.**

262 **Earth atmospheric** processes affect the seasonality signal retained within stalagmites by  
263 influencing meteoric precipitation isotope ratios at the cave site. Possibly the most common  
264 atmospheric process is the seasonal variation in precipitation  $\delta^{18}\text{O}$  induced by shifts in the  
265 temperature-dependent water vapour-meteoric precipitation fractionation factor. Other  
266 related changes in atmospheric processing include seasonal shifts in moisture source and  
267 pathway of the moisture package to the cave site, as, for example, in monsoonal settings.

268 **Meteoric precipitation:** Meteoric precipitation variability regards the nature of the primary  
269 rainfall amount-derived seasonality signal. Here we include meteoric precipitation amount  
270 and seasonal distribution as separate from 'Earth atmospheric' processes (such as changes in  
271 source moisture source), although clearly the latter affect the former. Meteoric precipitation  
272 is a fundamental control on stalagmite seasonality that is worth considering independently of  
273 other atmospheric processes. Stalagmites deposited in monsoonal climates (e.g., the East  
274 Asian Summer Monsoon, Indian Summer Monsoon, South American Monsoon, and Australian  
275 Summer Monsoon) with distinct wet and dry seasons are excellent examples of samples  
276 whose geochemistry generally (but not always) responds to hydrologic seasonality. In  
277 temperate mid-latitude settings with more evenly distributed rainfall, hydrological shifts

278 might record less seasonal than inter-annual (e.g., ENSO) dynamics or possess a seasonal bias  
279 (see section 3.1) derived from effective infiltration dynamics.

280 **Biological (soil-derived)** seasonality is the least clearly defined control, and predominantly  
281 affects the trace element composition and carbon isotope ratio of cave percolation waters.  
282 However, evidence also exists that increased soil bioproductivity can affect oxygen isotope  
283 ratios by preferential uptake of water during the growing season during intervals with  
284 substantial surface vegetation (Baldini et al., 2005). Trace element transport critically  
285 depends on the biological activity and water supply, both factors that are inherently variable  
286 and not necessarily in-phase. Hydrology can affect biological seasonality, as leaching of  
287 organic matter and trace elements from freshly decomposed litter depends on excess  
288 infiltration. Soils may thus produce a wet season pulse of colloidal material (organics as well  
289 as weathering products) which contributes to an annual peak in trace element concentrations  
290 in some samples; such dynamics are highly site-specific. The evidence for this pulse is derived  
291 both from synchrotron-based stalagmite studies (e.g., Borsato et al., 2007) and daily-scale  
292 automated dripwater collection schemes (Baldini et al., 2012). Treble et al. (2003) suggest  
293 phosphorous enrichment in stalagmite carbonate stemming from seasonal infiltration pulses,  
294 and monitoring at Shihua Cave (China) revealed that organic carbon was transported during  
295 the wet season (Ban et al., 2018; Tan et al., 2006). Whether this pulse is truly independent  
296 from hydrological variability is unclear, but some evidence from dripwater monitoring in  
297 temperate Irish caves suggests that the seasonal trace element pulse is not associated with  
298 increased autumnal water throughput, but rather with seasonal vegetation die-back (Baldini  
299 et al., 2012). In monsoonal north-eastern India biologically-induced litter decomposition  
300 reaches a maximum in early summer (Ramakrishnan and Subhash, 1988), which increases

301 element availability in the soil that can be leached during the entire wet season (Khiewtam  
302 and Ramakrishnan, 1993). The transport of trace elements may also hinge directly on the  
303 presence of natural organic matter in dripwater, which may link the dripwater directly to  
304 surface bioproductivity (Hartland et al., 2012; Hartland et al., 2011). Thus, biological  
305 seasonality is highly site-specific and likely variable through time; this and the complexities  
306 outlined above underscore the importance of dripwater monitoring campaigns.

307 ***Cave atmospheric*** variability can also impart a seasonal signal to a stalagmite geochemical  
308 record. Seasonal changes in cave air mixing with outside air lead to conditions within the cave  
309 that lower cave air carbon dioxide partial pressure ( $p\text{CO}_2$ ) and potentially even contribute to  
310 dripwater evaporation, promoting calcite deposition. Cave atmosphere variability, induced by  
311 ventilation (through thermal gradients or changing wind patterns) therefore affects the  
312 calcite deposition seasonality, as well as kinetic fractionation amount. Excellent examples of  
313 caves whose stalagmites are affected by this variability include New St. Michael's (Gibraltar)  
314 (Mattey et al., 2016; Mattey et al., 2010) and numerous caves in Central Texas (Banner et al.,  
315 2007; Breecker et al., 2012; Cowan et al., 2013; Wong et al., 2011). These effects are discussed  
316 in detail below (Section 3).

### 317 **3. Issues inherent to speleothem-based high-resolution climate reconstructions**

318 Detecting any seasonal component in a stalagmite climate signal includes quantifying growth  
319 rate and input signal seasonality. It is worth noting that the input signal is sometimes  
320 unexpected, and a thorough site monitoring scheme can help identify the main contributing  
321 factors. For example, although many trace elements (and particularly Mg) are affected by  
322 recharge (often via prior carbonate precipitation (PCP) mechanisms (Fairchild and Treble,  
323 2009)), other factors can also influence (seasonal) stalagmite geochemistry. This is the case



324 at ATM Cave, Belize, where various trace elements (including magnesium) increase in  
325 concentration at the beginning of the annual rainy season, and are probably linked to dry  
326 deposition during the preceding dry season followed by transport to the stalagmite with the  
327 onset of the rainy season (Jamieson et al., 2015). In other cases, the advection of atmospheric  
328 aerosols directly into the cave can affect the stalagmite trace element signal (Dredge et al.,  
329 2013). Seasonal non-deposition caused by either drying of the feeder drip or by seasonally  
330 high cave air  $p\text{CO}_2$  can bias any record where every data point integrates more than a few  
331 months of deposition. From this perspective, most stalagmite records integrate  
332 palaeoseasonality information to some extent, but, without appropriate monitoring  
333 strategies in place, deconvolving the extent to which the shifting seasonal signal dominates  
334 the overall record is difficult.

335

### 336 **3.1. Mixing within the aquifer**

337 The degree of recharge mixing within the aquifer and epikarst is a fundamental control on the  
338 preservation of a seasonality signal within stalagmites. A long residence time and/or thorough  
339 mixing within the overlying aquifer can greatly attenuate any hydrological seasonal signal,  
340 and understanding the hydrology feeding a cave drip is therefore critical (Atkinson, 1977;  
341 Ayalon et al., 1998; Baker et al., 1997; Baker and Brunson, 2003; Baker et al., 2019; Kaufman  
342 et al., 2003). For conservation and logistical reasons, monitoring and classification of the drip  
343 should ideally occur prior to sampling a stalagmite.

344 Smart and Friedrich (1987) undertook one of the earliest efforts to comprehensively  
345 categorise cave drips. Their scheme involved measuring drip rates at G.B. Cave, in the Mendip

346 Hills, UK, and parameterising them by plotting maximum drip rate versus the coefficient of  
347 variation (C.V.; the standard deviation divided by the mean multiplied by 100). Baker et al.  
348 (1997) later modified the scheme, dividing drips into six categories (seepage flow, seasonal  
349 drip, percolation stream, shaft flow, vadose flow, subcutaneous flow). Other classification  
350 schemes (e.g., Arbel et al., 2010; Arbel et al., 2008) focussed on analysing drip hydrographs,  
351 and suggested terminology such as 'post-storm', 'seasonal', 'perennial', and 'overflow', which  
352 are broadly consistent with the categories introduced by Smart and Friedrich (1987). The  
353 introduction of automated drip loggers revolutionised the field (Mattey and Collister, 2008),  
354 partly by ensuring that transient hydrological events were not missed. This ensured a  
355 substantially more robust characterisation of drips than that possible via manually measuring  
356 drip rates only during on-site visits.

357 Understanding the hydrology feeding a stalagmite is fundamental for determining if a  
358 stalagmite retains a seasonal signal. Drip rate is controlled by surface processes (e.g.,  
359 meteoric precipitation, evaporation, soil moisture capacity, and susceptibility to runoff) and  
360 aquifer characteristics including reservoir capacity and bedrock permeability (Markowska et  
361 al., 2015; Treble et al., 2013). Bedrock pathways recharging a drip are broadly divisible into  
362 matrix (or 'diffuse') and conduit (or 'fracture') flows (Ayalon et al., 1998; Baker et al., 1997;  
363 Perrin et al., 2003; Smart and Friedrich, 1987), and recent models suggest that many drips are  
364 a combination of the two. Matrix permeability typically refers to either the primary intra-  
365 granular bedrock permeability or to secondary permeability along fine fractures, and is  
366 characterised by a slow response to precipitation events and a large reservoir capacity  
367 (Atkinson, 1977; Smart and Friedrich, 1987). Fracture permeability relates to potentially  
368 solution-enlarged bedding plane partings and joints and is characterised by a rapid to  
369 intermediate response to precipitation events, and a low to moderate storage capacity.

370 Conduit permeability refers to often solutionally-enlarged pipe-like openings >1 cm in  
371 diameter (Atkinson, 1977; Smart and Friedrich, 1987). Such conduit flow is characterised by a  
372 rapid response to storm events followed by a rapid return to baseline flow (Baldini et al.,  
373 2006), and often carries chemically aggressive waters that do not allow secondary carbonate  
374 deposition. Large conduits or bedding planes may intersect a network of more diffuse  
375 hydrological pathways, leading to dual-component flow where the fracture is itself fed by  
376 some diffuse recharge in addition to the fracture flow. The hydrologic permeability of the  
377 fracture flow component compared to the diffuse flow component essentially defines the drip  
378 type; 100% diffuse flow would exhibit no response to storm events, whereas 100% fracture  
379 flow would usually have no drip except for immediately following storm events large enough  
380 to activate the pathway (Figure 2). Most drips would fall along the spectrum between these  
381 two endmembers; a constant base drip (the diffuse flow component) combined with a  
382 variably rapid response to storm events (the fracture flow component).

383 From a seasonality perspective, pure fracture-flow drips vary considerably seasonally but may  
384 experience occasional dripwater undersaturation and/or drying, and consequently the  
385 resultant stalagmite could have abundant microhiatuses (hiatuses in growth too brief to leave  
386 a clear petrographic expression, or appear in chronological models (Baker et al., 2014;  
387 Moseley et al., 2015) also referred to as 'crypto-hiatuses' (Stoll et al., 2015). Drips characterised  
388 by 100% diffuse flow would be stable with little hydrological or biological seasonality. The  
389 likelihood for microhiatuses or drying is low for stalagmites fed by diffuse flow, but the  
390 seasonal signal is probably muted, unless at a site where the seasonal signal is controlled by  
391 a forcing other than hydrological variability (see Section 2.4.). The optimal hydrology for  
392 imparting seasonality onto a stalagmite is a drip fed by moderately diffuse flow that is

393 responsive to monthly-scale shifts in rainfall, but that does not have a substantial fracture  
394 component to transmit event-scale (and possibly undersaturated) water.

395

### 396 **3.2. Non-deposition and seasonal bias in samples**

397 Although growth hiatuses lasting longer than a few years are often (but not always) apparent  
398 within stalagmites as horizons of detrital material followed by competitive growth of  
399 carbonate crystals (Broughton, 1983), brief growth hiatuses occurring seasonally are often  
400 undetectable (though occasionally they have a petrographic manifestation). Thus, the  
401 existence of these microhiatuses is often inferred by applying monitoring data to isolate  
402 intervals through the year where environmental conditions suggest temporary non-  
403 deposition could exist. Because drip rate is one of the fundamental controls on stalagmite  
404 growth (Genty et al., 2001), the use of drip loggers to detect seasonal drying of the stalagmite  
405 feeder drip is important for understanding whether a stalagmite record excludes a certain  
406 season's climate information.

407 Additionally, careful examination of sample petrography can reveal important insights into  
408 the nature of the climate signal retained by a stalagmite. Petrographic microscopy helps in  
409 identifying growth interruptions caused by lack of water, and dissolution features caused by  
410 undersaturated dripwater. An excellent example of this approach exists for Holocene  
411 stalagmites from northern Spain (Railsback et al., 2011; Railsback et al., 2017); the analysis  
412 reveals horizons of dissolution (termed Type 'E' surfaces), interpreted as reflecting occasional  
413 undersaturation of the feeder drip. Other examples of careful petrographic analysis informing  
414 seasonality studies are provided from Drotzky's Cave, Botswana, where the alternating wet

415 and dry seasons are manifested by alternating calcite and aragonite (respectively) couplets  
416 (Railsback et al., 1994) and from Grotta di Carburangeli, Italy, where columnar fabrics were  
417 interpreted as reflected pronounced seasonal variability in drip rates (Frisia, 2015).

418 Cave air carbon dioxide concentrations ( $p\text{CO}_2$ ) have shown to be inversely linked to stalagmite  
419 growth rate (Banner et al., 2007; Sherwin and Baldini, 2011). For example, in a study of three  
420 caves across Texas, it was observed that farmed calcite growth rate was inversely correlated  
421 with cave air  $p\text{CO}_2$  (Banner et al., 2007). Negligible calcite growth and even microhiatuses  
422 occurred during the warmest summer months, when cave air  $p\text{CO}_2$  increased due to low cave  
423 ventilation rates (Banner et al., 2007). Elevated cave air  $p\text{CO}_2$  discourages the dripwater's  
424 thermodynamic tendency to degas  $\text{CO}_2$ , thereby slowing the carbonate precipitation rate. In  
425 most caves where the entrance is located above the rest of the cave, outside air with low  
426  $p\text{CO}_2$  advects into the cave when the outside air density becomes greater than the cave air  
427 density (e.g., Spötl et al., 2005). This is usually driven by temperature gradients; colder, denser  
428 air moves down into a cave during winter, lowering the cave air  $p\text{CO}_2$  and encouraging  
429 stalagmite growth (James et al., 2015). However, cave air  $p\text{CO}_2$  does not act in isolation, but  
430 instead the critical growth determining variable is the differential between cave air  $p\text{CO}_2$  and  
431 dissolved  $\text{CO}_2$  in dripwater (Baldini et al., 2008). Carbonate deposition thus could increase in  
432 the high cave air  $p\text{CO}_2$  season if the dripwater had equilibrated with an atmosphere with even  
433 greater seasonal dissolved  $\text{CO}_2$  increases (e.g., stemming from seasonal soil bioproductivity  
434 increases) which exceed those of the cave atmosphere. These types of drips are generally  
435 quite responsive to rain events, so determining if a seasonal growth bias exists should  
436 incorporate both hydrology and cave atmospheric chemistry. Drips with stable drip rates, that  
437 are not responsive to storm events may have more constant dissolved  $\text{CO}_2$  and therefore

438 seasonal deposition rates that are affected exclusively by cave air  $p\text{CO}_2$  dynamics. However,  
439 several recent publications suggest that dripwater equilibrates not only with soil air, but also  
440 with a reservoir of carbon dioxide within the unsaturated zone of aquifers (termed ‘ground  
441 air’) that may have very high  $p\text{CO}_2$  values (2 to 7%), much higher than typical soils (0.1 to 2%)  
442 (Baldini et al., 2018; Bergel et al., 2017; Markowska et al., 2019; Matthey et al., 2016; Noronha  
443 et al., 2015). Thus, it is possible that drip dissolved  $\text{CO}_2$  is often near-constant, having  
444 equilibrated with a ground air reservoir of near-constant  $p\text{CO}_2$ , and that carbonate  
445 precipitation is anticorrelated with cave air  $p\text{CO}_2$  regardless of drip type, although this  
446 requires further research. The complexities of cave atmospheres are now reasonably well  
447 understood, but more long datasets describing the dissolved  $\text{CO}_2$  of cave drips are essential  
448 for determining the variability of cave percolation waters.

449 Although a temperate-zone (Peel et al., 2007) cave’s tendency to ventilate during the winter  
450 is generally predicable from seasonality in external temperature (James et al., 2015),  
451 occasionally cave geometry provides a more dominant control. In New St. Michael’s Cave in  
452 Gibraltar, ventilation is driven by seasonal changes in wind speed and direction (Matthey et al.,  
453 2016; Matthey et al., 2009). The cave experiences the lowest cave air  $p\text{CO}_2$  values in summer,  
454 and consequently growth (assuming constant drip rate) is biased towards summer (Baker et  
455 al., 2014). The cave’s position high within the Rock of Gibraltar contributes to strong winds  
456 and unusual seasonal ventilation, illustrating how cave position or geometry can dominate  
457 seasonal ventilation patterns. Other examples include Bunker Cave in Germany, where an  
458 essentially horizontal plan with little altitude difference between entrances produces very  
459 little seasonal variability in  $p\text{CO}_2$  (e.g., Riechelmann et al., 2011; Riechelmann et al., 2019),

460 and Císařská Cave (Czech Republic) where a U-shaped cave produces nonlinearities between  
461 air temperature, density, and ventilation (Faimon and Lang, 2013).

462 Because seasonal microhiatuses can lack either a petrological or a geochemical manifestation,  
463 cave monitoring is critical for assessing the likelihood of seasonal non-deposition (Shen et al.,  
464 2013). Stalagmite growth rate modelling, informed by cave monitoring data, can provide  
465 invaluable information regarding how seasonal growth variability affects geochemical climate  
466 proxy records integrating more than one year's worth of growth. For example, seasonal non-  
467 deposition during summer due to either high evapotranspiration-induced drip cessation or  
468 elevated cave air  $p\text{CO}_2$  might bias lower resolution records towards wintertime rainfall values  
469 (generally towards lower  $\delta^{18}\text{O}$  values) (e.g., James et al., 2015) at sites where drip water is not  
470 well mixed. Stoll et al. (2012) used an inverse model to illustrate that rainfall seasonality shifts  
471 relative to the cave air  $p\text{CO}_2$  can greatly affect PCP and consequently stalagmite trace element  
472 concentrations. Baldini et al. (2008) used theoretical stalagmite growth rate equations and  
473 theory developed previously (Buhmann and Dreybrodt, 1985; Dreybrodt, 1980, 1988, 1999),  
474 coupled with monitoring information, to model stalagmite  $\delta^{18}\text{O}$  for various drips within Crag  
475 Cave, Ireland. The results suggest that the amount of time integrated by the analyses, the  
476 nature of the drip, and the ventilation dynamics of the cave, all strongly modulate carbonate  
477  $\delta^{18}\text{O}$  signals.

478 These studies all highlight how characterising the surface and depositional environment is  
479 critical for interpreting the climate signal. Either seasonal microhiatuses or reduced growth  
480 may bias annual- (or coarser-) scale geochemical records towards particular seasons.  
481 Additionally, it is also important to consider how regional climate shifts may have affected a  
482 sample in the past, because modern processes may not have applied throughout the record.

483 Understanding climate signal emplacement processes within stalagmite carbonate is  
484 therefore fundamental for building robust climate records.

485

### 486 **3.3. A drip classification scheme to quantify seasonal responsiveness**

487 Existing drip classification schemes are not designed to characterise the likelihood that a  
488 sampled stalagmite retains a hydrologically induced seasonal signal. However, such  
489 knowledge is crucial if research goals include a component of seasonal climate reconstruction.  
490 Here, we introduce a new drip categorisation scheme that not only permits the identification  
491 of stalagmites most likely to retain a hydrology-modulated seasonal climate signal, but that  
492 also helps predict the general nature of the climate signal within any sample. This is important  
493 for both the accurate interpretation of stalagmite palaeoclimate records, but also for cave  
494 conservation (i.e., to maximise the usefulness of collected samples for the purpose of the  
495 research goals) and for the appropriate usage of research-related resources. A seasonal-  
496 resolution stable isotope record of any length requires considerable resources, and we hope  
497 that this new drip classification scheme will help direct these resources to appropriate  
498 stalagmite samples.

499 The scheme's essence is the collection of (ideally) at least one year of hourly drip rate data  
500 for a drip feeding a stalagmite of interest. For every month, the minimum and maximum  
501 hourly drip rate values are extracted. When plotted, these data reveal the extent to which  
502 the drip is affected by seasonal activation of fracture permeability, and what proportion of  
503 the drip consists of diffuse 'baseflow' (and whether this varies through the year). Drip  
504 categorisation then involves evaluating the distribution of the datapoints, and is described  
505 with terminology broadly consistent with the Smart and Friedrich (1987) scheme. Because the



506 classification scheme uses multiple data points per site, a very large number of possible  
507 combinations of descriptors are possible. For example, some drip sites (e.g., drip site YOK-LD  
508 within Yok Balum Cave, Belize; (Ridley et al., 2015a) are fed by a slow diffuse flow most of the  
509 year, where the minimum and maximum monthly drip rates are almost identical (Figure 3).  
510 However, during wetter months an overflow route is activated, and the maximum drip rate  
511 increases substantially, whereas the minimum remains the same; this would be characterised  
512 as a diffuse drip with a seasonally active overflow component. If this overflow component is  
513 saturated with respect to calcite or aragonite, some seasonal signal may be preserved, but if  
514 the overflow water is undersaturated a stalagmite fed by this drip type has less potential for  
515 seasonal climate reconstructions. Similarly, drip YOK-SK is characterised by almost entirely  
516 invariant diffuse recharge and would not record seasonal changes in recharge (Figure 3). At  
517 another cave site (Leamington Cave, Bermuda, (Walczak, 2016), drip BER-drip #5 is fed by  
518 diffuse recharge during drier intervals of the year, but during wetter months more water is  
519 routed to the diffuse flow, increasing the base flow. Consequently, the drip does experience  
520 some seasonality without risk of undersaturation, and thus a stalagmite fed by it should retain  
521 hydrology-induced seasonality.

522 In this new drip classification plot, the drips that are expected to produce stalagmites that  
523 retain the clearest seasonal signal are those that plot with a slope approaching unity. In other  
524 words, those that are not fed by either an extremely diffuse drip or an extremely flashy drip,  
525 and that consequently respond to seasonal rainfall shifts without transient extreme rapid drip  
526 rate episodes caused by individual storm events (which may lead to dripwater  
527 undersaturation and signal loss). Consequently, the two drip sites plotted in Figure 3 that best  
528 display this type of behaviour (drips YOK-G and BER-drip #5) have both yielded stalagmites  
529 retaining exceptional seasonal signals, stalagmites YOK-G (Ridley et al., 2015b) and BER-SWI-

530 13 (Walczak, 2016). Other drip sites that have a slope approaching unity and have a  
531 pronounced difference between the highest and the lowest set of drip rates (Figure 3B)  
532 should also produce stalagmites with well-developed records of seasonality.

533 Importantly, this drip classification scheme equally helps to identify drips that are unlikely to  
534 produce good seasonality records. For example, stalagmites fed by drips that are invariant  
535 throughout the year would not record hydrologically-induced seasonality (although a  
536 seasonal signal might still be preserved based on non-hydrological factors – see Section 2.4).  
537 Stalagmites fed by drips that have one or more monthly values plotting at the origin (i.e., no  
538 drips for an entire month, Figure 3D) would contain seasonal microhiatuses and would  
539 consequently not record that interval's climate information. Drips where the diffuse flow  
540 component (i.e., the monthly minimum flow) remains constant but the fracture flow  
541 component (i.e., the monthly maximum flow) changes considerably (Figure 3C) may  
542 experience undersaturation and either non-deposition or even corrosion of the stalagmite.

543 This classification scheme comes with some caveats. First, as discussed in Section 2.4., it is  
544 possible that the seasonality signal is imparted onto the stalagmite independent of hydrology.  
545 If seasonal cave ventilation controls the seasonality signal, the application of the scheme  
546 would differ. For example, at a site with strong seasonal ventilation, a stalagmite deposited  
547 by a purely diffuse flow-fed drip would reflect a largely cave atmospheric seasonality signal  
548 (i.e., with no hydrological seasonality). This would reduce the complexity of the geochemical  
549 signal and obviate the need to deconvolve hydrological- and cave atmosphere-induced  
550 seasonality from any geochemical record produced. Second, some drips are so-called  
551 'underflow' drip sites, which respond to recharge linearly up until a maximum drip rate and  
552 then become unresponsive to further drip rate increases. This is often caused by a constriction

553 in the flow pathway leading to the water egress point into the cave. Despite the lack of  
554 variability at high flow, the dripwater is still in dynamic equilibrium with recharge (unlike high  
555 residence time diffuse flow fed sites) and the stalagmite may reflect the dripwater isotopic  
556 variability. Similarly, some drips are affected by piston flow, whereby an increase in hydrologic  
557 head might push through a slug of older water, leading to an instantaneous response to  
558 recharge but of water with a signature more in keeping with 'old' water; careful monitoring  
559 can identify and mitigate these issues (see Section 3.4). Despite these caveats, this drip  
560 evaluation scheme will hopefully provide an efficient means for identifying actively growing  
561 stalagmite samples most likely to record a seasonal climate signal prior to collection of that  
562 sample.

563

#### 564 **3.4. Dripwater oxygen isotope seasonality**

565 The extent that cave dripwater  $\delta^{18}\text{O}$  ( $\delta^{18}\text{O}_{\text{dw}}$ ) values reflect the  $\delta^{18}\text{O}$  of meteoric precipitation  
566 ( $\delta^{18}\text{O}_{\text{p}}$ ) is critical to climate studies and for understanding the palaeoseasonality signal in  
567 particular. Many publications have investigated the relationship between  $\delta^{18}\text{O}_{\text{p}}$  and  $\delta^{18}\text{O}_{\text{dw}}$   
568 (Ayalon et al., 1998; Baker et al., 2019; Baldini et al., 2015; Bar-Matthews et al., 1996; Cruz Jr.  
569 et al., 2005; Duan et al., 2016; Feng et al., 2014; Harmon, 1979; Luo et al., 2014; Markowska  
570 et al., 2016; Mischel et al., 2015; Moquet et al., 2016; Moreno et al., 2014; Oster et al., 2012;  
571 Pu et al., 2016; Riechelmann et al., 2011; Riechelmann et al., 2017; Surić et al., 2017; Tadros  
572 et al., 2016; Tremaine et al., 2011; Verheyden et al., 2008; Wu et al., 2014; Yonge et al., 1985;  
573 Zeng et al., 2015). Depending on the drip site's hydrological characteristics (Arbel et al., 2010;  
574 Baker and Brunsdon, 2003; Smart and Friedrich, 1987),  $\delta^{18}\text{O}_{\text{dw}}$  values may reflect  $\delta^{18}\text{O}_{\text{p}}$  on  
575 timescales ranging from the annual weighted mean (Baker et al., 2019; Cabellero et al., 1996;

576 Chapman et al., 1992; Yonge et al., 1985) to individual (intense) recharge events (Atkinson et  
577 al., 1985; Frappier et al., 2007; Harmon, 1979).

578 Factors such as depth below surface, residence time and mixing of the water within the  
579 unsaturated zone, soil depth and texture, and aquifer hydraulics can vary between drip sites.  
580 Important reservoirs for storage and mixing of effective rainfall are documented as the soil  
581 and epikarst zones (Cabellero et al., 1996; Chapman et al., 1992; Gazis and Feng, 2004; Perrin  
582 et al., 2003; Yonge et al., 1985). Rainwater infiltrating into the soil reservoir is variably lost to  
583 evapotranspiration but in karst regions preferential recharge through dolines and grikes may  
584 occasionally circumvent the soil and related evapotranspiration (e.g., Hess and White, 1989).  
585 Secondary evaporation from infiltrating water can be detected using dripwater  $\delta^{18}\text{O}$  and  $\delta\text{D}$   
586 values plotted relative to the local meteoric water line (Ayalon et al., 1998; Breitenbach et al.,  
587 2015). Bar-Matthews et al. (1996) observed a 1.5 ‰  $\delta^{18}\text{O}_{\text{dw}}$  enrichment relative to rainwater  
588 and attributed this primarily to seasonal evaporation in the soil and epikarst zones above their  
589 Israeli cave site. Evaporative enrichment of infiltrating rainwater is greater in arid and  
590 semiarid regions than in temperate regions where conditions of water excess occur through  
591 much of the year (Markowska et al., 2016; McDermott, 2004). Any excess, non-  
592 evapotranspired water is then transmitted to the epikarst, karst, and finally the cave.  
593 Dripwater residence times in the aquifer or epikarst are highly variable, ranging from minutes  
594 to years, depending on soil thickness, hydraulic properties (Gazis and Feng, 2004), and drip  
595 pathway (e.g., diffuse vs. conduit flow) (Baldini et al., 2006). Mixing of infiltrating rainwater  
596 with existing epikarst water can buffer the climate signal and reduce seasonal  $\delta^{18}\text{O}_{\text{dw}}$   
597 variability from muted to invariant (within analytical error, and assuming no cave  
598 atmosphere-induced seasonality) (Baker et al., 2019; Breitenbach et al., 2019; Onac et al.,

599 2008; Schwarz et al., 2009). At some cave sites,  $\delta^{18}\text{O}_{\text{dw}}$  does not necessarily correlate with  
600  $\delta^{18}\text{O}_{\text{p}}$  shifts, most likely due to mixing within the aquifer (Moquet et al., 2016), underscoring  
601 that different hydrologies produce stalagmites retaining different environmental signals.

602 A recent global compilation of available dripwater monitoring data has further clarified the  
603 relationship between climate (e.g., mean annual temperature and annual precipitation) and  
604  $\delta^{18}\text{O}_{\text{dw}}$  (Baker et al., 2019). In cooler regions where mean annual temperature (MAT) < 10°C,  
605  $\delta^{18}\text{O}_{\text{dw}}$  most closely reflects the amount-weighted  $\delta^{18}\text{O}_{\text{p}}$  (i.e., evaporation from the soil and  
606 epikarst does not exert much influence). In seasonal climates with MAT between 10°C and  
607 16°C,  $\delta^{18}\text{O}_{\text{dw}}$  values generally reflect the recharge-weighted  $\delta^{18}\text{O}_{\text{p}}$  (see Fig. 1 of (Baker et al.,  
608 2019). In regions where MAT > 16°C,  $\delta^{18}\text{O}_{\text{dw}}$  is generally higher relative to amount-weighted  
609 precipitation  $\delta^{18}\text{O}_{\text{p}}$  because fractionation processes related to evaporative effects on stored  
610 karst water are more substantial (Baker et al., 2019). Stalagmite  $\delta^{18}\text{O}$  records from regions  
611 experiencing high temperatures and/or aridity will probably not reflect rainfall  $\delta^{18}\text{O}$  (Baker  
612 et al., 2019).

613

### 614 **3.5. The uniqueness of each stalagmite record**

615 Recent publications have made a case for the importance of replication in stalagmite  
616 geochemical records (Wong and Breecker, 2015; Zeng et al., 2015), which is a worthwhile and  
617 useful goal. Producing the same geochemical record from multiple samples ensures that no  
618 analytical issues exist and can facilitate correlating records whose growth intervals overlap in  
619 regions and for time periods with high signal-to-noise ratios. Particularly in cases where  
620 evidence for a short-lived climate anomaly exists, replication from within the same sample

621 and from other stalagmites is critical. However, stalagmite geochemistry is affected by a  
622 myriad of variables, and the precise combination of factors affecting any one sample are  
623 essentially unique. Thus, every stalagmite retains a different component of the environmental  
624 signal, and a lack of reproducibility does not necessarily indicate that a record is 'incorrect' or  
625 flawed. Even stalagmites that are affected by strong kinetic effects retain accurate  
626 environmental data; it is a matter of recognising this control, and basing any interpretations  
627 accordingly.

628 Unless two stalagmites are fed by a very similar drip type (often two samples growing near  
629 each other whose feeder drips share the same hydrological pathway), stalagmite records  
630 from the same cave may not match. This is a clear consequence of the diversity of possible  
631 drip pathways feeding individual stalagmites. For example, a stalagmite growing underneath  
632 a diffuse drip fed by an extremely low hydrologic permeability pathway that is unresponsive  
633 to large rain events would not contain the same record as a stalagmite growing underneath a  
634 drip with no diffuse component but that is instead fed by fracture flow. The former (diffuse  
635 flow-fed) stalagmite may retain long-term climate information but lack seasonal-scale  
636 information, whereas the latter (fracture flow-fed) stalagmite may retain some seasonal  
637 environmental information, but may also experience occasional undersaturation following  
638 large rain events, leading to microhiatuses and information loss. The fracture flow-fed  
639 stalagmite may have a more rapid overall growth rate, but may experience flow re-routing  
640 and stochastic drip variability due to solutational enlargement of the fracture pathway,  
641 potentially leading to a shorter overall growth interval due to the eventual diversion of water  
642 away from the stalagmite. Once cave- and site-specific ventilation factors are considered as  
643 well, it is apparent that no two stalagmites can yield precisely the same record; rather it is

644 imperative to understand the environmental conditions recorded by each individual sample.  
645 If the goal is to reconstruct seasonality, it is important to understand the nature of the  
646 seasonality signal for each potential sample, e.g., whether the sample is affected by  
647 hydrological seasonality or cave atmospheric seasonality. In the latter case, it is then  
648 favourable to select a stalagmite from a diffuse flow drip in order to simplify the extraction of  
649 the seasonal ventilation signal.

650 The considerable range of stalagmite records possible, even from the same site, is potentially  
651 advantageous. The individuality of stalagmite records may yield a powerful tool for the  
652 quantitative reconstruction of historically elusive environmental variables. For example,  
653 differences in oxygen isotope ratios between two samples from the same site could reflect  
654 in-cave temperature-induced kinetic fractionation effects, and modelling (Deininger and  
655 Scholz, 2019; Deininger et al., 2016; Dreybrodt, 1988; Dreybrodt and Deininger, 2014;  
656 Riechelmann et al., 2013) could theoretically yield the cave temperature, potentially even at  
657 a seasonal resolution. This perspective is consistent with the recent appreciation that  
658 speleothems deposited at isotopic equilibrium are extremely rare (Daëron et al., 2019;  
659 Mickler et al., 2006) and that kinetic effects are an integral part of the environmental signal  
660 retained by stalagmites (Millo et al., 2017; Sade and Halevy, 2017). The concept that kinetic  
661 effects are undesirable is a vestige of early studies attempting to extract absolute  
662 palaeotemperatures from stalagmite oxygen isotope ratios, in which case kinetic effects do  
663 indeed interfere with the extraction of the desired signal. However, because stalagmite  $\delta^{18}\text{O}$   
664 values are no longer considered pure in-cave temperature proxies, kinetic effects no longer  
665 present a serious issue, provided that they are considered within any interpretations. In fact,  
666 because kinetic effects often vary in sync with the primary rainfall signal (e.g., kinetic effects

667 tend to occur during drier periods accentuating the already elevated stalagmite  $\delta^{18}\text{O}$  and  $\delta^{13}\text{C}$   
668 signature) they tend to help the climate signal stand out above background noise.

669 Stalagmite climate reconstructions are usually based around one record or an overlapping  
670 series of records; future research could use the differences between two records (considering  
671 in-cave kinetic effects) to reconstruct aspects of the environmental signal, including seasonal  
672 temperature shifts. Recent research utilising several stalagmites from along the same  
673 moisture trajectory across a wide region to reconstruct oxygen isotope systematics and  
674 temperature represent an exciting development in speleothem climate sciences (Deininger  
675 et al., 2017; Hu et al., 2008; McDermott et al., 2011; Wang et al., 2017), and similar  
676 methodologies could reveal in-cave fractionation processes that are ultimately relatable to  
677 temperature, potentially on a seasonal-scale. For example, changes in outside temperature-  
678 induced ventilation may affect samples fed by different hydrologies differently (promoting  
679 more kinetic fractionation in the slower dripping sample), and comparing the isotope ratio  
680 records may reveal the range of external seasonal temperature variability. We suggest that  
681 the comparison of multiple coeval stalagmite geochemical records from within the same cave  
682 site is a crucial research frontier that is well worth investigating further.

683

#### 684 **4. Analysis techniques**

685 Detection of seasonal variations in stalagmite geochemical parameters requires sampling or  
686 analysis at sufficiently high spatial resolution to mitigate signal averaging (Figure 4). Sampling  
687 frequency should approach monthly resolution to detect a seasonality signal and to avoid  
688 aliasing issues during intervals with slower growth. This necessitates careful consideration



689 prior to analysis to ensure both sufficient resolution to detect seasonal-scale variability, and  
690 sufficient material for the analysis method. In addition to the pre-analysis considerations, we  
691 also recommend publishing complete micro-analytical data tables, in order to increase  
692 transparency. Below we discuss common microanalytical techniques capable of  
693 palaeoseasonality reconstruction and compare advantages and disadvantages of each.

694

#### 695 **4.1. Sampling for palaeoseasonality**

696 Sub-sampling stalagmites for geochemical analysis requires careful planning and execution.  
697 We recommend a thorough reconnaissance of a sample's petrography using microscopy prior  
698 to geochemical analysis. The conversion of a sample into polished thin sections can provide  
699 critical information but is destructive. Reflected light microscopy provides a non-  
700 destructive alternative that can yield crucial information regarding crystal growth habit, the  
701 location of possible hiatuses, inclusions, and porosity.

702 The various methods available for the extraction of proxy data all require different sample  
703 amounts depending on analytical limits of detection and other factors (Fairchild et al., 2006).  
704 Methods are broadly categorizable as destructive and non-destructive, depending on the  
705 amount of material required. The former is further divisible into: i) macro-destructive (e.g.,  
706 cuttings for fluid inclusion studies, low-concentration proxies like biomarkers or DNA) (e.g.,  
707 Blyth et al., 2011; Vonhof et al., 2006; Wang et al., 2019a), ii) meso-destructive (e.g.,  
708 conventional and micro-milling for U-series samples, stable isotopes, ICP-OES,  $^{14}\text{C}$ ) (e.g.,  
709 Lechleitner et al., 2016a; Ridley et al., 2015b; Spötl and Matthey, 2006), and iii) micro-  
710 destructive (e.g., laser ablation or secondary ionization mass spectrometer (SIMS) analyses  
711 for traditional and non-traditional isotope systems, element concentrations or ratios) (Baldini

712 et al., 2002; Luetscher et al., 2015; Treble et al., 2007; Webb et al., 2014; Welte et al., 2016).  
713 Non-destructive methods include (but are not restricted to): i) simple desktop scanning and  
714 photography, ii)  $\mu$ XRF line scanning and mapping (e.g., Breitenbach et al., 2019; Scropton et  
715 al., 2018), iii) synchrotron analyses (e.g., Frisia et al., 2005; Vanghi et al., 2019; Wang et al.,  
716 2019b; Wynn et al., 2014), iv) phosphor mapping via beta-scanning (e.g., Cole et al., 2003), v)  
717 reflected light, and fluorescence, including confocal laser fluorescent microscopy (CLFM) (e.g.,  
718 Orland et al., 2012) and other microscopy techniques (e.g. SEM, EMPA, RAMAN), or vi) X-ray  
719 Computed Tomography (CT) scanning (e.g., Walczak et al., 2015; Wortham et al., 2019). The  
720 choice of technique should consider suitability for answering the targeted research questions,  
721 and logistical considerations such as sample sectioning. Although the list above categorises  
722 techniques based on their destructiveness, it does not account for sample preparation; for  
723 example, SIMS analysis uses only a small amount of sample (i.e., essentially non-destructive),  
724 but requires sectioning of the stalagmite into centimetre-scale cubes, polishing and epoxy-  
725 mounting. Another major consideration is the length of the record required; it is possible  
726 (though labour-intensive) to produce seasonal-scale records extending hundreds or even  
727 thousands of years using micromilling, but this is not practical using SIMS, unless automated  
728 protocols allowing for unattended analysis can be developed (Orland et al., 2019).

729 Although macro-destructive sampling can inform interpretations based on higher resolution  
730 data, it cannot generally reconstruct seasonality on its own. Thus, here we discuss only  
731 selected meso-, micro-, and non-destructive techniques. The focus is first on ‘conventional  
732 drilling’ and ‘micromilling’ of powder samples, which probably are the most widely used  
733 techniques to obtain material for inorganic chemistry, followed by the highly versatile, fast,  
734 and cost-effective laser ablation sampling (LA-ICP-MS). SIMS requires substantial sample  
735 preparation, offers excellent resolution and is a good choice in situations requiring in-depth

736 characterisation of a short interval. Synchrotron- $\mu$ XRF (SR- $\mu$ XRF) has advanced considerably  
737 over the past decade, and it is now possible to obtain high-resolution (0.5-5  $\mu$ m) quantitative  
738 trace element data non-destructively through fast scanning of large samples (Borsato et al.,  
739 2019). Below we describe the relevance and applicability of these techniques towards the  
740 reconstruction of palaeoseasonality.

741

#### 742 **4.1.1. Conventional drilling**

743 Conventional drilling (or 'spot-sampling') (Fairchild et al., 2006) is the drilling of powders from  
744 discrete spots, that are normally separated by unsampled material, and is still amongst the  
745 most widely used methods to obtain carbonate powders from speleothems. This method is  
746 comparably fast and, with a sufficiently small drill bit (typical  $\varnothing$  ca. 0.2-1 mm), can achieve a  
747 spatial resolution of up to 0.3-0.5 mm along the growth axis, although more frequently the  
748 resolution is  $\sim$ 1 mm. Conventional drilling is ideally performed with instruments that allow  
749 computer-aided control of x-y-z dimensions, such as Sherline<sup>®</sup> or Mercantek<sup>®</sup> instruments.

750 With typical stalagmite growth rates of 0.1 to 0.2 mm year<sup>-1</sup>, this technique is usually  
751 inadequate when targeting sub-annual resolution (Figure 5). If used on samples with growth  
752 rates approaching twice the sampling interval, aliasing may occur and unfavourably affect the  
753 recovery of high-frequency variability (Fairchild et al., 2006). Furthermore, this type of spot  
754 sampling usually does not integrate all the carbonate material, i.e. the time slices at the top  
755 and bottom of the hole are under-represented in the average for the drill-hole; this  
756 undersampling could miss short-lived climate excursions. Consequently, we cannot  
757 recommend conventional drilling for recovering a seasonal signal, although the technique is  
758 effective at quickly producing a lower-resolution record and is well suited for longer records

759 of climate (e.g., those covering multiple glacial cycles), and for screening potential target  
760 stalagmites. Additionally, conventional drilling is possible on a large stalagmite slab, obviating  
761 the need for sectioning into multiple smaller slabs. A related technique which is preferred for  
762 sampling at seasonal scale is micromilling, discussed below.

763

#### 764 **4.1.2. Micromilling**

765 Micromilling refers to continuous sample cutting along a trench parallel to a stalagmite's  
766 growth axis (Fairchild et al., 2006; Spötl and Matthey, 2006). Usually performed with computer-  
767 controlled milling devices (such as the ESI/New Wave micromill) this technique can achieve  
768 ~20-micron spatial resolution (e.g., Myers et al., 2015), but is critically dependent on the  
769 textural characteristics of the sample. Dense columnar, fascicular, radiaxial, or radial fibrous  
770 calcites are the most suitable material, but needle-like aragonite can also be sampled,  
771 although gaps between needle-shaped crystals may lead to loss of sample and require  
772 painstaking cleaning procedures. The sample morphology throughout the stalagmite also  
773 warrants consideration. Planar, parallel, and laterally continuous laminae across the sample  
774 are ideal, but often stalagmite laminae appear curved in a slabbed sample. These are normally  
775 convex, but in some cases are concave (particularly in the case of a 'splash' cup), and with  
776 laminae that thin towards the edges. The greater such curvature, the narrower the  
777 micromilling trough required for sub-annual (seasonal-scale) sampling (Figure 5), because a  
778 wider trench would integrate material from other laminae. Similarly, the sample should allow  
779 2-3 mm sampling into the depth of the sample slab, and ideally the growth layers should not  
780 taper out in the third dimension. X-ray and Neutron CT scans can help visualise the 3D internal

781 structure of the sample (Walczak et al., 2015; Wortham et al., 2019), and the appropriate  
782 milling depth.

783 The determination of the x, y, and z dimensions of the sampling increment is the first step of  
784 any sampling strategy (Figure 5). For seasonal resolution, this strategy will ideally permit a  
785 very small y-axis increment (the y-axis is parallel to the stalagmite growth axis). The other  
786 dimensions must then allow the collection of enough carbonate for analysis (typically 50-120  
787  $\mu\text{g}$  for carbon and oxygen stable isotopes). Depending on sample characteristics and desired  
788 resolution, dimensions of  $y = 10\text{-}100 \mu\text{m}$  and  $x = 10\text{-}300 * y \mu\text{m}$  (parallel to visible growth  
789 layers on the slab) are ideal (Figure 5). The sampling depth (z-axis) is best minimised because  
790 lamina behaviour into the sample is often unknown, unless CT scans of the sample exist.  
791 Larger sample masses are occasionally needed for non-traditional proxies.

792 A common issue in the speleothem sciences is the precise correlation between two datasets  
793 obtained via different means, for example a micromilled stable isotope dataset and a LA-  
794 ICPMS derived trace element dataset. Annual- to decadal-scale correlations are usually  
795 possible, but rarely are the records correlative on the seasonal- or even annual-scale.  
796 Comparisons are achievable using very careful measurements from a datum (often the  
797 stalagmite top), with or without the use of banding as 'landmarks' (e.g., (Johnson et al., 2006;  
798 Treble et al., 2005a)). A recent technological advance is the development of software, such  
799 the open-source GIS-based QGIS software (Linzmeier et al., 2018), which integrates micro-  
800 imaging and analysis into a single spatial reference frame. This approach is particularly useful  
801 for organising different analyses derived from differently sectioned portions of samples and  
802 has been successfully applied to stalagmite data (Orland et al., 2019).

803 The problem of correlating different types of data is to some extent avoidable by sampling  
804 sufficient material with the micromill for both stable isotope and trace elemental analysis via  
805 ICP-MS. The sampled powder is divided into two aliquots, one for each analytical technique.  
806 The resultant trace element and stable isotope data permit zero-lag cross-correlations and  
807 highly robust interpretations of different environmental processes (e.g., Jamieson et al.,  
808 2016).

809 For example, if planned multi-proxy analyses require 0.8 mg of carbonate powder (e.g., stable  
810 isotope ratios,  $^{14}\text{C}$ , and trace elements), and a 50  $\mu\text{m}$  spatial resolution is desired using a  
811 milling bit diameter of 0.8 mm, a 0.05 mm x 4.15 mm x 1 mm trench would suffice (assuming  
812 calcite density of 2.7 g/cm<sup>3</sup> and no sample loss via incomplete recovery); sample loss and a  
813 particularly low-density sample would require a larger volume. An often-overlooked  
814 additional consideration involves the corners that are initially unsampled when milling  
815 trenches (red corner areas, Figure 5). Depending on the drill bit diameter and trench  
816 dimensions, the corners at each end of the trench would lead to unwanted integration of  
817 material from several sample increments and thus time slices. Use of a smaller milling bit  
818 diameter minimizes this effect. Additionally, a 50% reduction of this sampling effect is  
819 achieved if a trench is milled along the growth axis prior to the high-resolution milling, or if  
820 the milled trench is adjacent to a longitudinal cut (Figure 5). Material from the first trench can  
821 be used for reconnaissance studies. Another approach yielding similar results involves  
822 collecting the desired powder, and then moving the milling bit along the horizontal sampling  
823 track (i.e., parallel to the growth layer) for a distance corresponding to half the width of the  
824 milling bit. This powder is then discarded (or collected as auxiliary powder), and the milling  
825 bit returns to the original position, ready to produce the next aliquot of powder. Either of  
826 these sampling approaches effectively reduce spatial integration of sample (Kennett et al.,

827 2012; Myers et al., 2015; Ridley et al., 2015b), thereby increasing the likelihood of obtaining  
828 a clear seasonal signal (Figure 6).

829 Other issues include growth layers that slope inward rather than geometrically perfect layers  
830 (where the layering is perpendicular to section) and the use of tapered rather than cylindrical  
831 drill bits, which would fail to sample some carbonate at depth during each run. A study  
832 comparing micromilling/IRMS and SIMS techniques on annually layered otoliths found that  
833 an offset existed between the two techniques (with SIMS yielding values  $\sim 0.5\%$  lower) and  
834 that the amplitude of annual oxygen isotope signal derived via micromilling was  
835 approximately half of the SIMS signal; both of these observations are potentially explained by  
836 deviations from an ideal sample geometry, and consequently greater integration of unwanted  
837 material arising from micromilling (Helser et al., 2018). Despite these differences, both  
838 techniques were able to detect annual isotope ratio cycles (Helser et al., 2018). A thorough  
839 reconnaissance of the sample using CT scanning or other means to characterise its geometry  
840 in advance of slabbing can minimise these issues.

841 Other minor issues include the possible conversion of aragonite to calcite during milling,  
842 which would result in a decrease in  $\delta^{18}\text{O}$  values of  $0.02\%$  for every 1% aragonite converted  
843 to calcite (Waite and Swart, 2015). This effect may have implications for modelling oxygen  
844 isotope variability or calculating deviations from equilibrium deposition. However, using a  
845 slower rotation rate of the milling bit (500-800 rpm) will minimise, or even eliminate, this  
846 effect. A final recommendation is to run micromilled samples through the IRMS non-  
847 sequentially (i.e., out of stratigraphic order). Ideally the laboratory environment is static and  
848 will not affect results, but any unaccounted for diurnal changes (e.g., lab temperature) may  
849 affect the analyses in a cyclical way. Running samples non-sequentially both helps ensures

850 that any cycles detected (e.g., a seasonal cycle) are not analytical artefacts and helps to  
851 identify issues, if they exist (e.g., a persistent cycle when samples are arranged in the order  
852 that they were run).

853

#### 854 **4.1.3. LA-ICPMS**

855 Laser Ablation Inductively Coupled Plasma Mass Spectrometry (LA-ICPMS) is a beam method  
856 sampling technique. A polished speleothem slab is analysed by ablating small portions of  
857 material using a laser within a sample cell. The laser (typically an ArF excimer laser at a 193  
858 nm wavelength) physically ablates the sample, aerosolising the material which is then carried  
859 into the ICP-MS system by a carrier gas (typically helium and/or argon, with helium yielding a  
860 greater signal intensity (Luo et al., 2018)) where trace element concentrations are measured  
861 and quantified against standards of known compositions. The specific mass spectrometer set-  
862 up depends on the research question; for example, by using a quadrupole ICP-MS for  
863 elemental measurements using a reference isotope, or a multi-collector ICP-MS for isotope  
864 ratio analyses. Additional analytical set-ups are compatible with LA-ICPMS, including reaction  
865 cells, triple-quadrupoles, and split-stream analysis using two mass spectrometers in tandem  
866 (Frick et al., 2016; Kylander-Clark et al., 2013; Woodhead et al., 2016).

867 The advantages of LA-ICPMS for speleothem trace element analysis are numerous and include  
868 excellent spatial resolution (down to ~3 microns (Müller and Fietzke, 2016), using a  
869 rectangular aperture with long axis oriented along laminae) whilst preserving low detection  
870 limits (Figure 6). Although historically LA-ICPMS instruments used round 'spots', some laser  
871 ablation instruments are now fitted with rectangular masks (apertures), resulting in  
872 rectangular spots optimised for speleothem analysis, where the ablation spot is oriented



873 perpendicular to speleothem growth axis, along the x-axis (Müller et al., 2009). This permits  
874 the ablation of a surface area equivalent to large circular spot sizes, while retaining high  
875 spatial resolution in the growth direction (similar to the micromill sampling described in  
876 4.1.2). The speed of analysis via this method is also exceptionally high, with typical scan speed  
877 of  $10 \mu\text{m s}^{-1}$  (e.g., (Jamieson et al., 2015)). Two-volume laser cells are now available,  
878 minimising sample damage incurred via sectioning and ensuring consistent aerosol flow  
879 within the cell. The coupling of a laser ablation system with a large-capacity gas exchange  
880 device even allows analysis under atmospheric air (Tabersky et al., 2013) although with  
881 somewhat elevated limits of detection. This technique is particularly suitable for large  
882 stalagmites, or archaeological samples, because it minimises physical sample destruction by  
883 requiring less sectioning.

884 The presence of a localised impurity can produce a trace elemental concentration peak even  
885 in the absence of a laterally contiguous geochemical horizon with that geochemistry. LA-  
886 ICPMS can produce elemental maps that can verify the spatial continuity of geochemical  
887 laminae of interest, particularly when combined with a square aperture (Evans and Müller,  
888 2013; Rittner and Müller, 2012; Treble et al., 2005b; Woodhead et al., 2007). This permits the  
889 resolution of spatial relationships with greater confidence, and can corroborate  
890 interpretations based on stacked and parallel line scans, thereby avoiding issues related to  
891 the overinterpretation of a small number of points. Other microanalytical techniques (e.g.,  
892 SIMS, synchrotron,  $\mu\text{XRF}$ , etc.) can also produce elemental maps, but LA-ICPMS techniques  
893 can provide greater spatial coverage more rapidly.

894 The most significant disadvantage to LA-ICPMS is related to difficulties with standardisation.  
895 The use of matrix matched standards (i.e., made of the same material as the sample) during

896 laser ablation analysis is ideal, but the limited availability, variable degrees of standard  
897 homogeneity, and accurate standardisation of carbonate materials are ongoing challenges.  
898 Orland et al. (2014) and later Müller et al. (2015) provide promising tests for a carbonate  
899 standard, albeit for a limited range of elements. Many analyses are standardised with  
900 somewhat greater uncertainty than is ideal using glasses such as NIST 620 or 622. These  
901 analyses are often regarded as semi-quantitative, with high levels of confidence regarding  
902 variability and data trends but uncertainty regarding absolute values. Another minor  
903 disadvantage is lack of precise knowledge regarding the position of individual analytical spots.  
904 The sheer number of analyses possible via this technique (often >10,000) and indistinct,  
905 continuous track means that the exact position of any one individual spot is often difficult to  
906 determine precisely, complicating the correlation with other climate proxies. This  
907 disadvantage is mitigatable by precise notetaking, syn-analytical microscopy recording,  
908 careful reflected light imaging, cross-correlation, application of QGIS or similar software, and  
909 judicious 'wobble-matching' with other proxy records, as well as creating marker laser lines at  
910 certain intervals to further help to constrain spatial uncertainties.

911

#### 912 **4.1.4. Secondary ionisation mass spectrometry**

913 Secondary ionisation mass spectrometry (SIMS) uses a primary beam of positive (often  
914 caesium) or negative (often oxygen) ions to impact a sample surface under a vacuum,  
915 'sputtering' secondary ions into a mass spectrometer (Wiedenbeck et al., 2012). A positively  
916 charged primary beam (commonly Cs<sup>+</sup>) ionises negative secondary ions (e.g. C<sup>-</sup>, O<sup>-</sup>), and a  
917 negatively charged primary beam (commonly O<sup>-</sup>) ionises positive secondary ions (e.g., Mg<sup>2+</sup>,  
918 Sr<sup>2+</sup>). The sputtered secondary ions are then accelerated into a double-focusing mass

919 spectrometer, and counted by ion detectors (electron multiplier or Faraday cup). This  
920 analytical technique can yield both trace element analysis and stable isotope ratio data in  
921 speleothem carbonate at the micron scale, with very little damage to the sample, and with  
922 very high sensitivity (Figure 6).

923 The spatial resolution typically ranges between 1 to 10  $\mu\text{m}$  spot size and 1-2  $\mu\text{m}$  spot depth  
924 for trace elements, with stable isotope analyses historically restricted to 20–30  $\mu\text{m}$  resolution  
925 (Fairchild and Baker, 2012) but now capable of achieving 10  $\mu\text{m}$  resolution (Orland et al.,  
926 2019). This represents a very high-resolution method for stable isotope analysis within  
927 speleothem carbonate, and is therefore ideal for detecting palaeoseasonality (Fairchild et al.,  
928 2006). The analysis resolution for trace elements is second only to using synchrotron  
929 radiation, but with the added advantage of full quantification of concentration data and the  
930 ability to cover much greater areas of sample. Matrix matched materials, typically calcium  
931 carbonate, are used for standardisation to ensure consistent ionisation of chemical species  
932 and ablation rates (Fairchild and Treble, 2009).

933 Early studies of SIMS-derived trace element trends in speleothems helped to demonstrate  
934 that many stalagmites retained a seasonal signal (Baldini et al., 2002; Finch et al., 2001;  
935 Roberts et al., 1998), representing a considerable shift in resolving power compared to the  
936 former decadal- to centennial-scale of analysis previously possible. The presence of annual  
937 trace element cycles was quickly established as the norm rather than the exception for  
938 shallow cave sites, even in the absence of visible speleothem laminations (Fairchild et al.,  
939 2001). Divalent alkaline earth metals such as magnesium and barium were suggested as  
940 palaeohydrological proxies, phosphorus as indicative of bioproductivity, and strontium as  
941 reflecting calcite growth rate and/or PCP (Fairchild et al., 2001; Fairchild et al., 2000; Treble

942 et al., 2003). However, need for better empirical transfer functions between speleothems and  
943 external climatic processes, and partitioning between drip waters and speleothem calcite,  
944 complicated interpretations (Fairchild et al., 2001). Subsequent process-based studies have  
945 revealed the complexity involved in interpreting trace elements at seasonal scales,  
946 highlighting the role they play in complexation with organic matter as colloids (Borsato et al.,  
947 2007), in speleothem diagenesis (Martin-Garcia et al., 2014), and the complex controls on  
948 transfer through vegetation/soil/epikarst (Hartland et al., 2009; Hartland et al., 2012), as well  
949 as controls on partitioning via internal cave microclimate and crystallographic structures  
950 (Fairchild and Treble, 2009). The use of trace element cycles obtained via SIMS as  
951 chronological markers is exemplified through the work of Smith et al. (2009), where the ability  
952 of trace element cycles to provide relative age constraints at a finer spatial resolution than  
953 traditional U-series age models is unambiguously demonstrated.

954 A frontier for SIMS trace element measurements lies in the potential of combining these trace  
955 element records with stable isotope measurements undertaken at sub-annual scale. Prior to  
956 the advent of SIMS techniques for stable isotope analysis, there were very few combined  
957 trace element – stable isotope studies due to the incompatibility of analytical resolution  
958 between the two parameters (Orland et al., 2014). However, the analysis of stable isotopes  
959 by SIMS now achieves a spatial resolution capable of allowing direct comparability between  
960 both isotopic and trace element indicators of seasonality (Orland et al., 2014).

961 SIMS stable isotope studies have investigated the  $\delta^{18}\text{O}$ ,  $\delta^{13}\text{C}$  and  $\delta^{34}\text{S-SO}_4$  dynamics in  
962 stalagmite records (typical uncertainties ( $2\sigma$ ):  $\delta^{18}\text{O} = 0.2\text{‰}$  (Orland et al., 2019);  $\delta^{13}\text{C} = 0.6\text{-}$   
963  $0.7\text{‰}$  (Oerter et al., 2016; Sliwinski et al., 2015);  $\delta^{34}\text{S} = 1.6\text{‰}$  ( $1\sigma$ ) at 70 ppm S concentrations  
964 (Wynn et al., 2010)). Whereas each of these isotope ratios reflects changing surface

965 environmental conditions over inter-annual timescales, only the  $\delta^{18}\text{O}$  measurements by SIMS  
966 can produce records of intra-annual seasonality. Analysis of  $\delta^{13}\text{C}$  in speleothem carbonate  
967 cannot be undertaken simultaneously with  $\delta^{18}\text{O}$ , and any available records in the literature  
968 (e.g., (Pacton et al., 2013)) are not undertaken at seasonal resolution. The apparent lack of  
969 seasonal change in cave dripwater  $\delta^{34}\text{S-SO}_4$  (Borsato et al., 2015) has also so far prevented  
970 SIMS speleothem sulphur isotope measurements at the seasonal scale (Wynn et al., 2010).  
971 Treble et al. (2005a) produced the first  $\delta^{18}\text{O}$  record unambiguously linking seasonal cycles in  
972 speleothem oxygen isotopes to rainfall dynamics, and corroborated these interpretations  
973 with trace element cycles and contemporary rainfall monitoring. Subsequent work at Soreq  
974 Cave, Israel, further developed the technique to detect seasonality and links with rainfall  
975 dynamics across a range of time periods (Orland et al., 2012; Orland et al., 2009; Orland et al.,  
976 2014). Coupled annual variability in fluorescence and  $\delta^{18}\text{O}$  provided a seasonal marker of  
977 annual variability in rainfall from before the climate instrumental record (Orland et al., 2012;  
978 Orland et al., 2009). Careful correlation between fluorescent banding,  $\delta^{18}\text{O}$  and trace element  
979 measurements, and surface environmental conditions demonstrated that the fluorescent  
980 banding represented seasonal organic colloid flux variability into the cave.

981 Despite the clear advantages of utilising SIMS stable isotope analyses of speleothem  
982 carbonate to reveal seasonal patterns of rainfall delivery and drivers of climatic change, the  
983 technique also comes with its analytical challenges, including the considerable impact of  
984 geometric imperfections (e.g., sample topography, porosity, inclusions, cracks, etc) (Kita et  
985 al., 2011; Pacton et al., 2013; Treble et al., 2005a). In most instances, the ability to control the  
986 precise location of SIMS analyses enable geometric imperfections to be avoided, provided  
987 good surface mapping can be used to identify optimal locations for analysis and post

988 processing can be used to see any geometric imperfections in each analysis pit (Orland et al.,  
989 2009). This is in contrast to micromilling, where large swathes of sample are often bulked  
990 together regardless of sample porosity or imperfections. The need to use matrix matched  
991 standard materials presents similar problems of availability and homogeneity for the accuracy  
992 of data analysis as encountered with LA-ICPMS. However, recent improvements in this area,  
993 alongside improvements in sample preparation techniques have been substantial enough to  
994 enable accurate correction for instrumental drift (Valley and Kita, 2009). The impact of trace  
995 element content on carbonate  $\delta^{18}\text{O}$  and  $\delta^{13}\text{C}$  analyses also requires careful consideration  
996 (Sliwinski et al., 2017), but can be corrected following careful standardisation and is generally  
997 not a problem encountered through speleothem analysis where the trace element content is  
998 typically less than 1 weight %. An emerging analytical frontier concerns the impact of water  
999 and/or organic content on SIMS carbonate  $\delta^{18}\text{O}$  and  $\delta^{13}\text{C}$ , requiring careful pre-screening of  
1000 sample material and simultaneous analysis of OH- and CH- respectively (Orland et al., 2012;  
1001 Orland et al., 2015; Orland et al., 2019; Wycech et al., 2018).

1002 Despite these issues, SIMS remains an appealing choice for palaeoseasonality reconstruction  
1003 using stalagmites due to its sensitivity and resolution. SIMS has produced some of the highest  
1004 resolution records of palaeoseasonality available and will continue to play an important role  
1005 in linking stalagmite records to seasonal changes in environmental conditions, particularly  
1006 across discrete, short-lived events. Although the technique is not suitable for building long  
1007 records, the comparison of discrete timeslices permits seasonality to be contrasted for key  
1008 intervals (Orland et al., 2012; Orland et al., 2015; Orland et al., 2019).

1009

#### 1010 **4.1.5. Synchrotron**

1011 The application of Synchrotron Radiation micro X-Ray Fluorescence (SR- $\mu$ XRF) to the study of  
1012 speleothem carbonate opened up new possibilities in terms of greater resolving power for  
1013 geochemical analysis (Kuczumow et al., 2003; Kuczumow et al., 2001). Based on the emission  
1014 of electromagnetic radiation from charged electrons accelerated in an orbit, synchrotron  
1015 radiation generates secondary radiation from speleothem carbonate based on the  
1016 characteristic fluorescent properties of chemical elements. The excellent spatial resolution of  
1017 analysis (0.5–5 microns), low detection limits, low background, and the ability to  
1018 quantitatively map trace element variability across a given area has enabled the study of  
1019 speleothem geochemical structures at the sub-annual timescale and in two dimensions  
1020 (Figure 6). The use of XANES (X-Ray Absorption Near Edge structure) can define the oxidation  
1021 state of the element under consideration, thereby adding further resolving power to  
1022 determine environmental processes.

1023 Applications range from using SR- $\mu$ XRF to determine long-term (100 year) secular changes in  
1024 elemental signals (Frisia et al., 2005), high resolution event imaging across sub-annual to  
1025 multi-annual timescales (Badertscher et al., 2014; Frisia et al., 2008; Vanghi et al., 2019; Wang  
1026 et al., 2019b), and for investigating petrological controls on geochemical composition (Frisia  
1027 et al., 2018; Ortega et al., 2005; Vanghi et al., 2019). However, it is at the seasonal scale of  
1028 analysis where the resolving power of synchrotron radiation has really pushed the boundaries  
1029 of speleothem science.

1030 No conventional dating technique provides an absolute timeframe at the sub-annual scale of  
1031 speleothem carbonate deposition. However, linking the seasonality of external  
1032 environmental processes to speleothem petrology and geochemical characteristics can yield  
1033 a monthly scale resolution of trace element content. SR- $\mu$ XRF was used to determine the

1034 coincidence of trace element distributions and physical calcite characteristics within annual  
1035 stalagmite laminations (Borsato et al., 2007). Based on the annually laminated stalagmite  
1036 ER78 from Ernesto Cave, Italy, a suite of trace elements (P, Cu, Zn, Br, Y, and Pb) were found  
1037 to form an annual peak, coincident with a characteristic thin (0.5-4  $\mu\text{m}$ ) brown UV-fluorescent  
1038 layer in each annual couplet. The brown colouration of each UV-fluorescent layer is probably  
1039 due to organic acids derived from high rates of water infiltration during each autumn (Frisia  
1040 et al., 2000; Huang et al., 2001; Orland et al., 2014). The transport of trace elements is  
1041 associated with colloidal organic molecules (Hartland et al., 2010; Hartland et al., 2012), and  
1042 leads to the incorporation of this distinctive elemental suite on a seasonal basis associated  
1043 with the autumnal rains (the 'autumnal pulse' as described in Section 2.4). SR- $\mu\text{XRF}$  permits  
1044 the detection of variability inherent to each individual year, which then can be contrasted  
1045 against the symmetrical mean annual profile. Any differences (e.g., double peaks or shoulder  
1046 peaks) provide an indication that the rainfall distribution throughout that year deviated from  
1047 the mean annual profile. Strontium was observed to vary inversely to colloiddally transported  
1048 elements (Borsato et al., 2007), possibly due to competition for binding to defect sites, thus  
1049 limiting incorporation into the calcite lattice. SR- $\mu\text{XRF}$  revealed seasonal patterns of zinc, lead,  
1050 phosphorus, and strontium within speleothem Obi84 from Obir Cave, Austria, whose  
1051 concentration peaks also coincided with the dark coloured visible laminae. These were  
1052 similarly interpreted as hydrological event markers associated with autumnal infiltration, but  
1053 could also result from dry deposition of aerosols (Dredge et al., 2013).

1054 SR- $\mu\text{XRF}$  2D mapping within speleothem Obi84 over three annual cycles demonstrated the  
1055 effects of several infiltration events each year, present as short-lived peaks in Zn  
1056 concentration and which build in magnitude towards the main autumnal flush (Wynn et al.,  
1057 2014) (Figure 6). Using these event peaks as markers of autumnal flushing permitted



1058 attribution of annual sulphate cycles to summer high and winter low concentrations. At the  
1059 Obir Cave site, these seasonal shifts in speleothem sulphate content were attributed to  
1060 temperature-driven cave ventilation and associated cave air  $p\text{CO}_2$  variability which controlled  
1061 the dripwater pH and the sulphate:carbonate ratio. Wynn et al. (2018) later verified this  
1062 proposed seasonal mechanism using controlled laboratory experiments, thereby permitting  
1063 the extraction of seasonal temperature information based on the annual sulphate cycle's  
1064 topology. SR- $\mu\text{XRF}$  can thus extract geochemical expressions of seasonality, and the technique  
1065 is well-suited to investigating changing rainfall and temperature seasonality dynamics back  
1066 through time.

1067

#### 1068 **4.1.6. Data analysis**

1069 Following the geochemical analyses and data processing, the information must be  
1070 interpreted. For techniques producing tens to hundreds of data points, this is not particularly  
1071 challenging. On the other hand, techniques such as LA-ICPMS can produce tens of thousands  
1072 of data points for multiple elements, and can greatly increase the processing time on common  
1073 spreadsheet programmes. To circumvent these issues, it is possible to simplify the data using  
1074 a Principal Component Analysis (PCA), a multivariate statistical analysis technique which  
1075 extracts modes of variation from large multivariate timeseries datasets that best describe  
1076 overall variability of those datasets. The technique is ideal for large multivariate stalagmite-  
1077 derived LA-ICPMS datasets (Borsato et al., 2007; Jamieson et al., 2015; Orland et al., 2014).  
1078 PCA has also been used to extract a seasonal signal from trace elemental concentrations even  
1079 in the absence of visible laminae and applied towards the development of a chronology (Ban  
1080 et al., 2018).

1081 Comparing the intra-annual amplitude of a geochemical signal (Orland et al., 2012; Orland  
1082 et al., 2009; Orland et al., 2014; Orland et al., 2019) from monthly-resolved datasets is ideal  
1083 for extracting seasonal information from an otherwise difficult to interpret dataset. For  
1084 example, Ridley et al. (2015b) used the well-developed annual carbon isotope cycles with  
1085 their Belizean stalagmite to extract seasonal amplitudes, which were then interpreted in  
1086 terms of the strength of the seasonal ITCZ incursion into southern Belize. Orland et al.  
1087 (2015) used the topology of oxygen isotope variability within individual growth bands in a  
1088 Chinese stalagmite to clarify the origin the oxygen isotope variability. Spectral analysis of  
1089 well-dated samples can also reduce data complexity (Myers et al., 2015). For example,  
1090 Asmerom et al. (2020) used a wavelet analysis to reconstruct the strength of the wet season  
1091 in Central America over the last two millennia, and to show that modern seasonality in  
1092 rainfall was only emplaced in the 15<sup>th</sup> Century. Extracting a meaningful metric from  
1093 numerous more complex data using statistical techniques is one way of simplifying a  
1094 complex geochemical dataset.

1095

## 1096 **5. Modelling techniques**

1097 Many efforts at modelling both the hydrology feeding a stalagmite and the climate signal  
1098 within exist. Proxy system models (PSMs) describe how geological or chemical archives are  
1099 imprinted with climate signal (Evans et al., 2013). In terms of stalagmite-specific models,  
1100 several exciting geochemical models now exist which can explore the emplacement of a  
1101 geochemical signal in a stalagmite (Wong and Breecker, 2015), often based on established  
1102 processes which govern stalagmite precipitation (e.g., (Buhmann and Dreybrodt, 1985)). Two  
1103 recent examples (specifically of disequilibrium isotope fractionation processes proxy system

1104 models) are the IsoCave model, which can examine disequilibrium isotope effects in  
1105 speleothems and related implications for speleothem isotope thermometry (Guo and Zhou,  
1106 2019), and the ISOLUTION model which similarly helps to better understand the effect of  
1107 these disequilibrium isotope fractionation processes on stalagmite proxy records (Deininger  
1108 and Scholz, 2019). The I-STAL model allows the simulation of PCP and how this affects  
1109 dripwater Mg, Sr, and Ba (Stoll et al., 2012). A number of models looking specifically at drip  
1110 hydrology now exist (e.g., KarstHydroModel (Baker and Bradley, 2010; Treble et al., 2003)),  
1111 and these are extremely useful for understanding how the rainfall input signal is transformed  
1112 before reaching the stalagmite. Rather than using hydrological or geochemical modelling, a  
1113 recent publication introduced a Monte Carlo approach to model rainfall and temperature  
1114 seasonality in a stalagmite from La Garma Cave, northern Spain, over the Holocene (Baldini  
1115 et al., 2019). Here, we build on this work and compare both synthetic and real-world input  
1116 data to the results of the second-generation model.

1117 The model requires some widely available types of input data, including: i) a stalagmite-based  
1118  $\delta^{18}\text{O}$  record, ii) a record of regional mean annual temperature (MAT) of any resolution (e.g.,  
1119 borehole, marine sediments, stalagmite fluid inclusions) over the interval of interest, iii)  
1120 monthly-scale modern instrumental records of rainfall and temperature above the site (or as  
1121 close as possible to the site), and iv) cave air temperature and its relationship with above  
1122 ground temperature. The relationship between meteoric precipitation  $\delta^{18}\text{O}$  and temperature  
1123 at the site is useful but not required information because regional or global meteoric  
1124 precipitation  $\delta^{18}\text{O}$  and temperature equations can provide a suitable alternative.

1125 Essentially, the model assumes that the MAT of the cave site is similar to the MAT of the  
1126 regional temperature input record (ii above), and produces a sine function around this value

1127 of an amplitude reflecting modern temperature seasonality, but with random variability  
1128 added to the absolute minimum and maximum temperatures (the amount of randomness is  
1129 user-defined). A second sine function reflects the rainfall seasonality, and whereas the  
1130 temperature wave's polarity is fixed (i.e., summers are always warmer than winters), the  
1131 rainfall seasonality sine wave's polarity is allowed to flip randomly. The seasonal extreme  
1132 values associated with either sine function are fixed to the same calendar months, linked to  
1133 the timing of the modern minima and maxima.

1134 These two sine waves produce synthetic monthly temperature and rainfall values, which are  
1135 then converted to  $\delta^{18}\text{O}_p$  based ideally on local temperature-rainfall  $\delta^{18}\text{O}$  relationships, or in  
1136 cases where this relationship is not known, to more global equations (e.g., (Schubert and  
1137 Jahren, 2015)). It is assumed that the  $\delta^{18}\text{O}_p$  is conveyed to the dripwater (see discussion  
1138 regarding evapotranspiration, Section 4.3) and that this is converted to carbonate  $\delta^{18}\text{O}$  using  
1139 the Tremaine equation (Tremaine et al., 2011) at ambient cave air temperature adjusted  
1140 according to observed relationships between outside and inside air. This equation was chosen  
1141 as most appropriate because its empirical nature accounts for in-cave disequilibrium  
1142 fractionation processes more completely than other equations. The model therefore  
1143 considers seasonal changes in rainfall but is independent of total annual rainfall. The annual  
1144 amount-weighted mean modelled carbonate  $\delta^{18}\text{O}$  value is then compared with the actual  
1145 measured carbonate  $\delta^{18}\text{O}$  value, and if it is within a certain user-defined value, it is logged as  
1146 a successful simulation. If the difference between the modelled and actual carbonate  $\delta^{18}\text{O}$  is  
1147 greater than this value (generally  $\sim 0.1$  per mil), the simulation is logged as unsuccessful. 1,000  
1148 of these coupled temperature and rainfall simulations are conducted per time slice, all the

1149 successful and unsuccessful simulations are logged, and the mean monthly modelled rainfall  
1150 and temperature values calculated from the successful simulations.

1151

### 1152 **5.1 Test Runs: Gradual shifts in rainfall polarity**

1153 The model reproduces shifts in rainfall polarity in synthetic datasets well (Figure 7). In one  
1154 experiment, the input  $\delta^{18}\text{O}$  dataset was created by using i) a temperature sine function that  
1155 was set as invariant (i.e., it maintained its polarity and amplitude throughout the run), and ii)  
1156 a rainfall sine function that shifted in polarity completely over 14 model years. The wettest  
1157 month in the input rainfall record was April in Year 1, gradually changing polarity to November  
1158 by Year 14. As such, model Year 7 was characterised by no seasonality (Figure 7). The model  
1159 was run without *a priori* knowledge of these shifts other than the mean annually-resolved  
1160 synthetic  $\delta^{18}\text{O}$  record, MAT, 'modern' seasonality range, and cave temperature (i.e., the  
1161 simulations were run 'modeller blind'), but the output reproduced the shifting rainfall pattern  
1162 very well. The gradual shift in rainfall polarity is detected, and the lack of seasonality in the  
1163 input rainfall signal during Year 7 is reproduced. The input temperature data had a 15 °C  
1164 annual temperature range, and two model simulations were conducted: one derived using an  
1165 annual seasonal temperature range of  $10 \pm 6$  °C, and a second using an annual seasonal  
1166 temperature range of  $15 \pm 6$  °C. In the case of the lower annual temperature range, the model  
1167 overestimates rainfall seasonality in order to compensate for the inappropriate annual  
1168 temperature range, but still detects shifts in rainfall polarity (Figure 7). When the more  
1169 appropriate temperature range is used, the simulation captures both the amplitude and  
1170 polarity of the shifting rainfall input signal. However, this experiment highlights a limitation

1171 of this modelling approach;  $\delta^{18}\text{O}$  data is explicable both in terms of rainfall and temperature  
1172 seasonality shifts, and an unknown annual temperature range introduces uncertainties.

1173 A second experiment involved synthetic temperature and rainfall input records with both  
1174 considerable inter-annual variability and noise introduced (Figure 8). Notably, one model year  
1175 (Year 4) had the polarity of the rainfall signal completely reversed. Again, the model was able  
1176 to extract the salient features of the input data very well. Reproduced were inter-annual  
1177 variations in rainfall and temperature, and, importantly, the model detected the reversed  
1178 seasonality of the rainfall signal in Year 4 (Figure 8).

1179

## 1180 **5.2 Application to a stalagmite $\delta^{18}\text{O}$ dataset from a seasonally arid continental region**

1181 The first version of the model was run successfully across the Holocene using a  $\delta^{18}\text{O}$  dataset  
1182 derived from the maritime climate of northern Spain (Baldini et al., 2019). Here, we apply the  
1183 model to a dataset from Bir-Uja Cave in the Keklik-Too mountain ridge, Kyrgyzstan, a location  
1184 characterised by extremely strong seasonal fluctuations in both temperature and rainfall. The  
1185 cave ( $40^{\circ}29'\text{N}$ ,  $72^{\circ}35'\text{E}$ ) is  $\sim 60$  m long and is developed at an altitude of  $\sim 1,325$  m above sea  
1186 level (Fohlmeister et al., 2017). The input data consisted of the  $\delta^{18}\text{O}$  dataset from stalagmite  
1187 Keklik1 reported on in Fohlmeister et al. (2017), a 500-year long, centennial-resolution  
1188 borehole temperature record from the Tian Shan mountains ( $\sim 461$  km to the north of the  
1189 cave site) (Huang et al., 2000), instrumental precipitation and temperature records since 1880  
1190 C.E. from Tashkent, Uzbekistan ( $\sim 300$  km to the east) (Menne et al., 2012), and cave  
1191 temperature (Fohlmeister et al., 2017). The  $\delta^{18}\text{O}$  input data were decadal-resolved, and the  
1192 stalagmite was dated using a recently developed radiocarbon technique (Fohlmeister and

1193 Lechleitner, 2019; Fohlmeister et al., 2017; Lechleitner et al., 2016b). The Keklik1 record  
1194 extends from 2011 C.E. back to 1150 C.E., but the borehole record only extends back to 1500  
1195 C.E., so the interval modelled only extends to 1500 C.E. On average, the site receives ~450  
1196 mm of precipitation per year (based on Global Network of Isotopes in Precipitation data from  
1197 Tashkent), with ~80% falling from November to April. Summers are very dry, with August (the  
1198 driest month) receiving ~5 mm of rainfall. Monthly temperatures range from -1.4 °C in January  
1199 to 25.0 °C in July, with a MAT of 12.1 °C. Stalagmite Keklik1 was located ~40 meters from the  
1200 cave entrance and was collected in October 2011. Cave temperature varies seasonally, from  
1201 12 °C from the end of November until April, to a maximum of 16.5 °C in May. The site is  
1202 characterised by near 100% relative humidity in the cold season which drops considerably to  
1203 ~60% during the warmer months (Fohlmeister et al., 2017).

1204 Unlike the Spanish GAR-01 record which extended back to ~13,500 years BP and was  
1205 modelled using 100-year timeslices (Baldini et al., 2019), the Keklik1  $\delta^{18}\text{O}$  record was  
1206 modelled using annual timeslices. The timings of the minimum and maximum values of the  
1207 modelled temperature sine function were fixed at January and July, respectively. These  
1208 months were also designated as the minimum/maximum of the modelled rainfall sine wave,  
1209 which fits present day observations, but the sine function's polarity was not prescribed in  
1210 advance.

1211 Baldini et al. (2019) noted that the modelled temperature curve for northern Iberia closely  
1212 resembled a previously published temperature reconstruction for the region (Martin-Chivelet  
1213 et al., 2011) with a temporal resolution that exceeded the information provided by the low-  
1214 resolution input dataset. Although no annual-scale MAT record exists in the Kyrgyzstan region  
1215 for the last 500 years, summer temperatures are well constrained by tree ring records. A

1216 comparison of the modelled July temperature derived from the Keklik1  $\delta^{18}\text{O}$  record reveals a  
1217 very good match with the NTREND AG2 temperature anomalies (~300 km to the north of the  
1218 cave site) (Anchukaitis et al., 2017; Cook et al., 2013) (Figure 9). The model's ability to  
1219 reconstruct palaeotemperature may reflect the fact that the probability of a successful model  
1220 run is maximised when modelled temperature approximates the actual temperature shift.  
1221 Successful model runs with a different (and incorrect) temperature pattern are possible with  
1222 certain modelled rainfall simulations, but the mean monthly temperature values (reflecting  
1223 the mean of all successful runs) will be biased towards model simulations with the correct  
1224 temperature shift. The apparently robust reconstruction of warm-season palaeotemperature  
1225 is an unexpected and exciting model outcome, but one that requires further evaluation.

1226 The rainfall reconstruction reproduces many of the same features highlighted by Fohlmeister  
1227 et al. (2017). In particular, decreases in the winter rainfall contributions in the late 1500s, the  
1228 mid-1700s, and the early 1800s are apparent in both records. Although to a certain extent  
1229 this is expected because the  $\delta^{18}\text{O}$  record is integral to both reconstructions, it is interesting  
1230 that the two reconstructions use two fundamentally different techniques (numerical versus  
1231 geochemical modelling) to estimate the importance of winter rainfall to the overall annual  
1232 water budget at the site, and arrive at broadly similar results. For example, a winter rainfall  
1233 peak occurs in 1797 CE in both records and transitions to drier winters by 1815 CE, with ~22%  
1234 and ~50% reductions in winter rainfall implied by the model and  $\delta^{18}\text{O}$  data, respectively. The  
1235 model underestimating the reduction in rainfall probably arises because of the model's  
1236 utilisation of smooth sine waves rather than more step-like functions; in other words,  
1237 although it is possible for one month per year to have zero rainfall in the model, the adjacent  
1238 two months must necessarily have some rainfall, whereas in reality, several dry months per



1239 summer could occur. The use of step functions would permit the incorporation of several dry  
1240 months annually and would amplify apparent shifts in seasonal rainfall amounts. Modelled  
1241 DJFM rainfall compares reasonably well with GHCN rainfall from Tashkent (Figure 9),  
1242 particularly considering that the Tashkent meteorological station is ~300 km away from and  
1243 ~1,000 m lower in altitude than the cave site.

1244

### 1245 **5.3 Limitations to the modelling technique and future work**

1246 Several limitations to the presented modelling technique exist. First, the timing of the rainfall  
1247 minima and maxima versus temperature signal could affect the model's efficacy; for example,  
1248 if the rainiest month occurs three months after (or before) the warmest month, the use of  
1249 the sine function means that all outcomes are possible. This is because the maxima/minima  
1250 in one parameter's sine function occur at the nodes of the other sine wave, effectively making  
1251 both sine waves independent of each other. At many sites, temperature and rainfall are  
1252 intrinsically linked and their seasonal cycle broadly synchronous, but the above may be an  
1253 issue at some locations. Additionally, the model would require a differently shaped rainfall-  
1254 function to model rainfall at locations with two distinct rainy intervals every year, such as low  
1255 latitude sites affected by the ITCZ twice each year.

1256 The current version of the model does not incorporate evapotranspiration, and this is an  
1257 obvious oversimplification. This may have repercussions for sites like Kyrgyzstan that  
1258 experience a pronounced hot and dry season with negative effective infiltration. Similarly,  
1259 variable kinetic fractionation almost certainly occurred within the cave (Fohlmeister et al.,  
1260 2017) but is not considered within the model. Future versions of the model will incorporate

1261 both evapotranspiration and kinetic effects, but the model currently likely overcomes this  
1262 limitation simply by reducing rainfall amount for months with high evapotranspiration rates.  
1263 Potentially, coupling the new model discussed here with a dripwater isotope evolution model  
1264 (e.g., ISOLUTION (Deininger and Scholz, 2019)) could produce very robust results. The model  
1265 also cannot identify intervals characterized by changes in moisture pathway or fractionation  
1266 amount; rather, it highlights intervals that are not explicable in terms of changes in  
1267 temperature or rainfall amount seasonality (intervals where the model cannot converge on  
1268 any solutions), and thus points to the involvement of other processes.

1269 The model is allowed to randomly vary MAT above or below the low-resolution temperature  
1270 input record, but only within user-defined bounds. Too great a range of permissible MAT  
1271 values would allow essentially any outcome. For example, if there were no limits to minimum  
1272 winter temperature, a low  $\delta^{18}\text{O}$  value could be modelled as either a very cold winter with a  
1273 subdued rainfall seasonality or as a mild winter but with substantial winter rain. Limiting the  
1274 temperature seasonality to reasonable bounds (for example, based modern interannual MAT  
1275 variability) permits assessing whether any given month is warmer or colder than the low-  
1276 resolution temperature input, but may underestimate the total amount of cooling and  
1277 warming. In extreme cases, this may manifest itself as a failure to converge upon any  
1278 successful model, thus highlighting timeslices that require closer inspection and potentially  
1279 an alternative explanation.

1280 As discussed in Section 5.2, the utilisation of step functions to describe rainfall seasonality  
1281 may facilitate the modelling of climate for sites where several months receive similar amounts  
1282 of rainfall. Future studies should investigate the ramifications of function choice on output.  
1283 Additionally, theoretically arriving at a mathematical solution utilising the relevant equations

1284 and input data is possible, obviating the need for MC simulations, and future research will  
1285 investigate this possibility. Finally, future models could incorporate options for geochemical  
1286 modelling of drip and carbonate chemistry.

1287

## 1288 **6. Regional seasonality**

1289 In this section we analyse global meteoric precipitation and temperature data to highlight  
1290 regions experiencing pronounced seasonal variability in temperature, precipitation amount,  
1291 and precipitation  $\delta^{18}\text{O}$  (Figures 10 and 11), helping to facilitate the identification of cave sites  
1292 sensitive to seasonality. This also highlights locations that are at the margins of such regions,  
1293 where seasonality may have affected the record in the past, despite the lack of a modern  
1294 influence.

1295

### 1296 **6.1. Identification of seasonally sensitive regions**

1297 WorldClim Version 2 data were obtained at a 2.5 minute ( $\sim 4.5$  km at the equator) spatial  
1298 resolution (Fick and Hijmans, 2017). Inland continental regions within the mid- to high-  
1299 latitudes of the Northern Hemisphere (e.g., central and northern Canada, eastern Russia,  
1300 northeast China, and Mongolia) are characterised by the greatest mean annual temperature  
1301 range (Figure 10a). A greater annual temperature range is characteristic of continental  
1302 climates due to the reduced oceanic influence, with ocean water's high heat capacity and  
1303 moderating influence on air temperature. The lowest mean annual temperature ranges occur  
1304 in the low latitudes (where insolation remains high year-round) and maritime regions of the

1305 world (where oceans moderate temperature variability) (Figure 10a). The pattern of global  
1306 temperature seasonality (herein calculated as the maximum temperature of the warmest  
1307 month minus the minimum temperature of the coldest month averaged over the period 1970  
1308 – 2000 based on WorldClim Version 2 data) is consistent with the geographic pattern of cave  
1309 air ventilation reported in (James et al., 2015), a study concerning the role of outside  
1310 temperature seasonality in the seasonal ventilation of caves.

1311 Seasonality in precipitation amount (Figure 10b) is greatest in the low latitudes due to the  
1312 annual migration of the Intertropical Convergence Zone (ITCZ) and monsoonal systems that  
1313 cause distinct wet and dry seasons, along the western coast of North America, southern South  
1314 America, and Europe where seasonal westerlies preferentially bring enhanced winter  
1315 precipitation, and bordering the Mediterranean where a ‘Mediterranean climate’  
1316 characterised by wet-winters and dry-summer dominates (Figure 10b). The lowest  
1317 precipitation amount seasonality occurs in arid and semi-arid regions of the world and the  
1318 non-coastal mid- to high-latitudes of the northern and southern hemispheres.

1319 Global seasonality in amount-weighted  $\delta^{18}\text{O}_p$  (Figure 11) approximates the pattern of  
1320 temperature seasonality (Figure 10a), with the greatest annual range in  $\delta^{18}\text{O}_p$  observed at  
1321 Northern Hemisphere continental interior and high latitude sites (e.g., northeast Asia, central  
1322 Canada, northern Greenland). In addition, high altitude sites (e.g., the Andes in western South  
1323 America, the Caucasus Mountains at the intersection of Europe and Asia) also exhibit higher  
1324 annual WM  $\delta^{18}\text{O}_p$  ranges due to the altitude effect. The lowest  $\delta^{18}\text{O}_p$  seasonality occurs within  
1325 maritime (e.g., NW Europe, SW and SE Australia) and arid/semi-arid regions (e.g., East Africa,  
1326 eastern Brazil, South Africa). Many stalagmite records are from temperate regions where  
1327 modern MAT ranges from 10 to 16 °C (Baldini et al., 2019; Baldini et al., 2015; Ban et al., 2018;

1328 Huang et al., 2001; Johnson et al., 2006; Orland et al., 2014). Global cave dripwater  $\delta^{18}\text{O}$  data  
1329 reveal that caves from regions with this MAT range have dripwater chemistry that reflects  
1330 recharge-weighted  $\delta^{18}\text{O}_p$  (Baker et al., 2019). The seasonal distribution of  $\delta^{18}\text{O}_p$  is therefore a  
1331 critical control in the case of many different stalagmite samples.

1332 In other cases, very pronounced seasonality inherent in stalagmite geochemical records are  
1333 not due to seasonality in  $\delta^{18}\text{O}_p$ , but instead to seasonality in rainfall amount (Ridley et al.,  
1334 2015b) and associated shifts in bioproductivity (Baldini et al., 2005) or PCP (Fairchild and  
1335 Hartland, 2010; Fairchild et al., 2006). Seasonality in temperature can also induce cave  
1336 ventilation in temperate zone caves during the winter (providing the cave geometry is  
1337 appropriate), promoting carbonate deposition within the cave and biasing annual- to decadal-  
1338 scale records towards the winter season rainfall (James et al., 2015). The maps provided  
1339 herein can help identify regions containing speleothems retaining the desired seasonal signal,  
1340 and determine what the most likely control is on any seasonal signal found within a  
1341 stalagmite. Furthermore, the maps help highlight cave sites that are located on the  
1342 peripheries of climatologically seasonal zones at present, where past seasonality shifts could  
1343 have influenced a record. Examples include the Sahel and southern Belize (Figure 12), both  
1344 currently at the very northern extent of the ITCZ, where a small ITCZ shift to the south would  
1345 produce both severe drying and a substantial decrease in rainfall seasonality. This perspective  
1346 was underscored by recent results from Central America that used monthly-scale rainfall  
1347 proxy data over the last two millennia to suggest that the region has only been affected by  
1348 the ITCZ since ~1400 C.E., and that the ITCZ influence may wane in the near future (Asmerom  
1349 et al., 2020) (Figure 12).

1350

## 1351 **6.2. Complexities despite strong seasonality: northeast India as an example**

1352 The seasonality maps presented here highlight regions most likely to contain stalagmites  
1353 which retain seasonal signals in temperature, rainfall amount, or  $\delta^{18}\text{O}_p$ . However, they also  
1354 illustrate that not all seasonal variations in  $\delta^{18}\text{O}_p$  are explicable in regional temperature or  
1355 rainfall amount terms. In many cases, complex moisture source variability overprints  
1356 temperature-induced seasonality, hampering the use of models such as the one presented in  
1357 Section 5. Here, we discuss the Indian Summer Monsoon (ISM) as an example of such a  
1358 situation, and focus specifically on Mawmluh Cave in Meghalaya, northeast India, one of the  
1359 most seasonal locations on Earth in terms of rainfall amount (Fig. 10). In Meghalaya,  
1360 hydroclimate is characterised by extreme seasonality, as the plateau constitutes the first  
1361 topographic barrier for moisture-laden air masses travelling inland from the Bay of Bengal  
1362 (Murata et al., 2007; Prokop and Walanus, 2003). At present, the ISM brings ~80% of the  
1363 annual rainfall to the cave site, inducing extreme amounts of rainfall (up to 12 meters per  
1364 year (Breitenbach et al., 2015). The seasonal precipitation cycle is reflected in rainfall  $\delta^{18}\text{O}$   
1365 composition (Berkelhammer et al., 2012; Breitenbach et al., 2010). Rainfall  $\delta^{18}\text{O}$  becomes  
1366 progressively lighter during the ISM, but this effect is only partially driven by increasing  
1367 precipitation intensity and the amount effect because the period of maximum precipitation  
1368 (June-August) precedes maximum  $^{18}\text{O}$  depletion (August-October) (Breitenbach et al., 2010)).  
1369 Instead, the  $^{18}\text{O}$ -depletion results predominantly from the moisture source shifting from a  
1370 proximal location (the Bay of Bengal) in the early and late ISM to a more distal location (the  
1371 open Indian Ocean) during the peak ISM (longer transport times resulting in more Rayleigh  
1372 distillation). Rainfall and dripwater  $\delta^{18}\text{O}$  at Mawmluh Cave are thus highly seasonal, but the  
1373 relationship between temperature, rainfall amount, and rainfall  $\delta^{18}\text{O}$  is not straightforward

1374 (Breitenbach et al., 2010; Breitenbach et al., 2015). Additional complexity arises from the  
1375 filtering and buffering capacity of the karst aquifer through which rainwater percolates *en*  
1376 *route* to a stalagmite. Although a clear seasonal dripwater  $\delta^{18}\text{O}$  cycle exists, with its lowest  
1377 value approximating ISM rainfall  $\delta^{18}\text{O}$ , its annual amplitude is compressed, reflecting buffering  
1378 in the karst (Breitenbach et al., 2015). This further complicates the interpretation of  $\delta^{18}\text{O}$   
1379 records from these stalagmites, and information from independent proxies that are sensitive  
1380 to processes dominating during the winter season is required to disentangle such processes.  
1381 Combining summer-sensitive  $\delta^{18}\text{O}$  with winter-sensitive Mg/Ca (reflecting PCP) permitted  
1382 disentangling ISM strength and the degree of dry season dryness in a stalagmite from  
1383 Mawmluh Cave (Myers et al., 2015; Ronay et al., 2019). Such a multi-proxy approach,  
1384 supported by local monitoring and karst process modelling, allows robust interpretations of  
1385 seasonal-scale climate from stalagmites, even when the proxy seasonality is driven by more  
1386 complex processes than temperature or rainfall amount alone.

1387

## 1388 **8. Future directions and recommendations**

1389 In this review, we introduce and discuss several concepts that we hope will facilitate the  
1390 development and interpretation of robust seasonal-resolution climate records  
1391 from stalagmites, will improve the extraction and interpretation of seasonal information from  
1392 stalagmites, and promote future discussion, including: **A)** that replication of records should  
1393 not always be an expectation without *a priori* knowledge that the drip type and  
1394 environmental conditions responsible for the deposition of the stalagmites are comparable  
1395 (e.g., some stalagmites retain seasonal information, whereas others do not), **B)** that every  
1396 stalagmite-based geochemical record is different and records a unique component of the

1397 environmental signal of varying complexity (i.e., each stalagmite retains an accurate history  
1398 of its environment; the question is whether or not this history can be deconvolved), and **(C)**  
1399 that the application of at least one year's worth of hourly-resolved drip rate monitoring  
1400 combined with a new drip classification scheme presented here may help identify stalagmites  
1401 retaining a seasonal signal. Furthermore, we have **(D)** developed global seasonality maps of  
1402 temperature (as was done previously by (James et al., 2015)), meteoric precipitation amount,  
1403 and meteoric precipitation  $\delta^{18}\text{O}$  ratios which allow the identification of regions sensitive to  
1404 different types of seasonality recordable by stalagmites. The maps facilitate predicting what  
1405 type of seasonality potentially affects modern stalagmite samples from that region. They also  
1406 assist in palaeoclimate interpretations by identifying locations proximal to regions with  
1407 pronounced seasonality, where past migration of key atmospheric circulation systems could  
1408 have altered the geochemical record retained by a stalagmite. On a similar note, we **(E)**  
1409 present a model that interprets annual- to centennial-scale stalagmite  $\delta^{18}\text{O}$  records in terms  
1410 of seasonal temperature and meteoric precipitation seasonality shifts. Although we stress  
1411 that this model only highlights one possible interpretation (that the data were modulated  
1412 primarily by regional long-term mean annual temperature variability combined with  
1413 seasonality shifts in rainfall and temperature), often this interpretation is the most  
1414 parsimonious. The modelling technique also helps identify time intervals when altered  
1415 seasonality cannot account for the observed isotope shifts, suggesting that another variable  
1416 needs consideration. We **(F)** discuss four major controls on the seasonality signal within  
1417 stalagmites: i) Earth atmospheric, ii) Meteoric precipitation, iii) biological (e.g., soil processes),  
1418 and iv) cave atmospheric, and **(G)** discuss a case study from India that serves as an example  
1419 of a stalagmite whose seasonal signal is not derived from rainfall amount or regional



1420 temperature, but instead results from seasonal shifts in air mass trajectories (i.e., affected by  
1421 seasonal shifts in Earth atmospheric processes).

1422 Stalagmites are remarkable archives of information regarding climate (on both seasonal and  
1423 longer timescales), surface and cave environmental conditions, dry deposition, moisture  
1424 source pathway, marine aerosols contributions, and hydrological routing. Replication of proxy  
1425 records present strong support for palaeoclimatic interpretations, and should remain a goal  
1426 of any stalagmite science research programme, but unless the climate signal-to-noise ratio of  
1427 a region is unusually high, replication is only possible when comparing stalagmites deposited  
1428 under similar conditions. A thorough understanding of the environmental processes affecting  
1429 both entire caves (e.g., ventilation) as well as individual stalagmites (e.g., drip rate) facilitates  
1430 replication efforts. The geochemical record from even adjacent stalagmites will reflect  
1431 numerous processes, some of which are common to the two samples but many which are  
1432 not, and only through a thorough understanding of the processes affecting each sample are  
1433 robust (and replicable) climate interpretations achievable. However, unless analytical issues  
1434 exist, non-replication does not imply that one record is incorrect; rather it generally implies  
1435 that the two records simply record different environmental parameters.

1436 Cave monitoring prior to the collection of a stalagmite will increase the likelihood of obtaining  
1437 a record of the desired sensitivity to seasonal climate shifts, or other desired forcing. We  
1438 recommend monitoring the drip feeding the stalagmite for at least one year using an  
1439 automated drip logger and plotting the results in a diagram similar to Figure 3 to evaluate a  
1440 stalagmite's likelihood of retaining hydrological seasonality. We recommend monitoring  
1441 multiple sites within the cave and selecting the most appropriate stalagmite for collection  
1442 based on the monitoring results. It is worth bearing in mind that unless the seasonality signal

1443 in a stalagmite is conveyed via seasonal cave ventilation, stalagmites fed by diffuse flow drips  
1444 with long residence times may not retain seasonal information. Other drips that are  
1445 seasonally either dry or undersaturated with respect to carbonate will lead to the formation  
1446 of microhiatuses in the stalagmites and signal loss for that particular season. Monitoring a  
1447 stalagmite's drip rate and drip chemistry for as long as possible represents one of the simplest  
1448 but most effective means of understanding the potential climate signal contained within a  
1449 sample prior to collection. This also has implications for cave conservation and protection  
1450 efforts, because clearly formulated research goals and drip monitoring prior to stalagmite  
1451 sample collection can greatly reduce the number of samples removed from a cave for  
1452 research purposes.

1453 If sample growth rate permits, we suggest that the extraction of the palaeoseasonality signal  
1454 over long timescales is best achieved via micromilling, leaving no gap between adjacent  
1455 samples, or LA-ICPMS. The major disadvantages of micromilling is that it is resource intensive,  
1456 and that many samples may not have growth rates high enough to permit the required  
1457 resolution; the major disadvantage of LA-ICPMS is that the trace element signature of a  
1458 stalagmite is often dominated by site-specific factors such as temperature, sea spray, volcanic  
1459 aerosols, fire, variable throughput of colloidal material, or rainfall, and consequently aligning  
1460 the data with other records is sometimes complex. Micromilled carbonate powders that are  
1461 divided into two or more aliquots that are subsequently analysed for stable isotope ratios,  
1462 trace elements, and other geochemical proxies can provide very robust interpretations (e.g.,  
1463 Jamieson et al., 2016). This eliminates issues of cross-correlation and enables a powerful  
1464 multiproxy approach, where each stable isotope ratio value is linked directly and  
1465 unambiguously to numerous elemental concentration values. The technique can yield

1466 important information regarding palaeoseasonality but is considerably more resource  
1467 intensive than running multiple LA-ICPMS tracks parallel to each other and the micromilled  
1468 stable isotope track. An alternative is to produce a long decadal-scale isotope ratio traverse  
1469 complemented by higher resolution transects or maps across key intervals of interest using  
1470 LA-ICPMS, SIMS, synchrotron, or  $\mu$ XRF to corroborate interpretations based on the longer  
1471 transects. In the future, proxy mapping at micron-scale resolution using these techniques will  
1472 help reduce uncertainties related to geometric ambiguities such as those associated with  
1473 crystal boundaries and improve the robustness of interpretations.

1474

## 1475 **9. Conclusions**

1476 The reconstruction of palaeoseasonality using stalagmites is an exciting research direction  
1477 that has yet to mature into its full potential. Numerous records of palaeoseasonality exist, but  
1478 few direct reconstructions extend before the last two millennia. Ideally, future studies  
1479 concluding that a decadal- to annual-scale isotope ratio record is affected by seasonality  
1480 changes should support this by either using short windows of sub-annual data or by  
1481 modelling.

1482 Any climate proxy record is affected by inherent complexities in climate signal transfer to the  
1483 stalagmite and by selective sampling of the stalagmite for analysis. A high-resolution (sub-  
1484 annual to annual-scale) sampling strategy coupled with appropriate site monitoring  
1485 maximises the likelihood of extracting a signal approximating the climate input signal. For long  
1486 records annual- to decadal-scale resolution is ideal, and shorter records could benefit from  
1487 an even higher resolution if resources permit. Large shifts in isotope ratios could reflect

1488 changes in seasonality, potentially associated with the migration of key atmospheric  
1489 circulation systems over the cave site. New models incorporating seasonality can provide  
1490 information regarding whether observed geochemical shifts are interpretable in terms of  
1491 altered seasonality, and these represent an exciting and inexpensive new research tool. A  
1492 seasonal-scale sampling strategy over short intervals of interest can verify these model  
1493 interpretations, and LA-ICPMS or line-scan  $\mu$ XRF represent potentially the most efficient  
1494 methods to achieve this; other alternatives include monthly-scale micromilling, synchrotron  
1495 analysis (SR- $\mu$ XRF), and SIMS.

1496 The robust interpretation of stalagmite geochemical records in terms of seasonality  
1497 represents a key challenge for the next decade. Achieving this is complicated by multiple in-  
1498 cave and exogenic environmental forcings with dynamic seasonality, including: rainfall,  
1499 temperature, humidity, bioproductivity, cave air  $p\text{CO}_2$ , drip rate, source moisture region and  
1500  $\delta^{18}\text{O}$ , and moisture mass trajectory from the source region. Even apparently straightforward  
1501  $\delta^{18}\text{O}$  records from regions with high signal-to-noise ratios typically interpretable as either  
1502 varying total annual rainfall or summer rainfall may instead reflect another parameter instead  
1503 (e.g., a change in moisture source or rainfall seasonality), as is the case with the Indian  
1504 Summer Monsoon. Most records would benefit from a rigorous multi-proxy approach utilising  
1505 not only multiple geochemical proxy datasets, but also site monitoring and new modelling  
1506 approaches. Similarly, focussing research efforts at the same well-understood cave sites both  
1507 maximises the quality of interpretations and contributes to the conservation of caves and  
1508 stalagmite samples. The application of multiple stalagmites from the same site but with  
1509 different drip rates and affected by different amounts of disequilibrium fractionation may  
1510 provide the key to reconstructing formerly elusive climate variables, such as temperature.

1511 Instead of representing an irresolvable issue, we suggest that disequilibrium fractionation  
1512 may present opportunities to quantify temperature, potentially even at seasonal resolutions.  
1513 Similarly, multi-proxy data could yield seasonal information even in the absence of seasonal  
1514 sampling resolution; if two or more independent proxies reflect different seasonal data,  
1515 combining the proxies could yield palaeoseasonality.

1516 Over the past few decades stalagmites have provided some of the most iconic records in  
1517 palaeoclimatology. In the future, stalagmites will continue to not only provide long records of  
1518 exceptional quality, but they will also provide rare glimpses into palaeoseasonality at  
1519 unprecedented temporal resolution. Recent microanalytical advances have facilitated the  
1520 construction of exquisitely resolved stalagmite-based climate records; we are now at a stage  
1521 where the interpretation of these records is catching up with their remarkable technical  
1522 aspects. Extracting quantitative and accurate seasonal climate information from these  
1523 geochemical records is a key challenge over the next decade, and, if this is achieved,  
1524 stalagmites will truly be considered in a class of their own as climate archives.

1525

## 1526 **Acknowledgements**

1527 We thank SISAL and PAGES for access to the SISAL database v1b. Portions of this research  
1528 were funded by European Research Council Grant #240167. Tim Horscroft is thanked for his  
1529 support in facilitating the preparation of the manuscript. Ian Orland and an anonymous  
1530 reviewer are thanked for detailed constructive reviews that greatly improved the manuscript.  
1531 Alex Iveson is thanked for useful comments regarding LA-ICPMS.

1532

1533 **References:**

- 1534 Allison, V.C., 1923. The growth of stalagmites and stalactites. *Journal of Geology* 31, 106-125.
- 1535 Allison, V.C., 1926. The antiquity of the deposit in Jacob's cavern. *American Museum of Natural*  
1536 *History, Anthropological Papers* 19, 204-225.
- 1537 Anchukaitis, K.J., Wilson, R., Briffa, K.R., Buntgen, U., Cook, E.R., D'Arrigo, R., Davi, N., Esper, J.,  
1538 Frank, D., Gunnarson, B.E., Hegerl, G., Helama, S., Klesse, S., Krusic, P.J., Linderholm, H.W., Myglan,  
1539 V., Osborn, T.J., Zhang, P., Rydval, M., Schneider, L., Schurer, A., Wiles, G., Zorita, E., 2017. Last  
1540 millennium Northern Hemisphere summer temperatures from tree rings: Part II, spatially resolved  
1541 reconstructions. *Quaternary Sci. Rev.* 163, 1-22.
- 1542 Arbel, Y., Greenbaum, N., Lange, J., Inbar, M., 2010. Infiltration processes and flow rates in  
1543 developed karst vadose zone using tracers in cave drips. *Earth Surface Processes and Landforms* 35,  
1544 1682-1693.
- 1545 Arbel, Y., Greenbaum, N., Lange, J., Shtober-Zisu, N., Grodek, T., Wittenberg, L., Inbar, M., 2008.  
1546 Hydrologic classification of cave drips in a Mediterranean climate, based on hydrograph separation  
1547 and flow mechanisms. *Israel Journal of Earth Sciences* 57, 291-310.
- 1548 Asmerom, Y., Baldini, J.U.L., Pruffer, K.M., Polyak, V.J., Ridley, H.E., Aquino, V.V., Baldini, L.M.,  
1549 Breitenbach, S.F.M., Macpherson, C.G., Kennett, D.J., 2020. Intertropical convergence zone  
1550 variability in the Neotropics during the Common Era. *Science Advances* 6, eaax3644.
- 1551 Atkinson, T.C., 1977. Diffuse flow and conduit flow in limestone terrain in the Mendip Hills, Somerset  
1552 (Great Britain). *Journal of Hydrology* 35, 93-110.
- 1553 Atkinson, T.C., Hess, J.W., Harmon, R.S., 1985. Stable isotope variations in recharge to a karstic  
1554 aquifer, Yorkshire dales, England. *Annales de la Société Géologique de Belgique* 108, 225.

1555 Atsawawaranunt, K., Comas-Bru, L., Mozhdehi, S.A., Deininger, M., Harrison, S.P., Baker, A., Boyd,  
1556 M., Kaushal, N., Ahmad, S.M., Brahim, Y.A., Arienzo, M., Bajo, P., Braun, K., Burstyn, Y., Chawchai, S.,  
1557 Duan, W.H., Hatvani, I.G., Hu, J., Kern, Z., Labuhn, I., Lachniet, M., Lechleitner, F.A., Lorrey, A., Perez-  
1558 Mejias, C., Pickering, R., Scropton, N., Members, S.W.G., 2018. The SISAL database: a global resource  
1559 to document oxygen and carbon isotope records from speleothems. *Earth System Science Data* 10,  
1560 1687-1713.

1561 Ayalon, A., Bar-Matthews, M., Sass, E., 1998. Rainfall-recharge relationships within a karstic terrain  
1562 in the Eastern Mediterranean semi-arid region, Israel:  $\delta^{18}\text{O}$  and  $\delta\text{D}$  characteristics *Journal of*  
1563 *Hydrology* 207, 18-31.

1564 Badertscher, S., Borsato, A., Frisia, S., Cheng, H., Edwards, R.L., Tuysuz, O., Fleitmann, D., 2014.  
1565 Speleothems as sensitive recorders of volcanic eruptions - the Bronze Age Minoan eruption recorded  
1566 in a stalagmite from Turkey. *Earth Planet. Sci. Lett.* 392, 58-66.

1567 Baker, A., Barnes, W.L., Smart, P.L., 1997. Variations in the discharge and organic matter content of  
1568 stalagmite drip waters in Lower Cave, Bristol. *Hydrol Process* 11, 1541-1555.

1569 Baker, A., Bradley, C., 2010. Modern stalagmite  $\delta^{18}\text{O}$ : Instrumental calibration and forward  
1570 modelling. *Global and Planetary Change* 71, 201-206.

1571 Baker, A., Brunsdon, C., 2003. Non-linearities in drip water hydrology: an example from Stump Cross  
1572 Caverns, Yorkshire. *J Hydrol* 277, 151-163.

1573 Baker, A., Hartmann, A., Duan, W., Hankin, S., Comas-Bru, L., Cuthbert, M.O., Treble, P.C., Banner, J.,  
1574 Genty, D., Baldini, L.M., Bartolomé, M., Moreno, A., Pérez-Mejías, C., Werner, M., 2019. Global  
1575 analysis reveals climatic controls on the oxygen isotope composition of cave drip water. *Nature*  
1576 *Communications* 10, 2984.

1577 Baker, A., Smart, P.L., Edwards, R.L., Richards, D.A., 1993. Annual growth banding in a cave  
1578 stalagmite. *Nature* 364, 518-520.

1579 Baker, A.J., Matthey, D.P., Baldini, J.U.L., 2014. Reconstructing modern stalagmite growth from cave  
1580 monitoring, local meteorology, and experimental measurements of dripwater films. *Earth and*  
1581 *Planetary Science Letters* 392, 239-249.

1582 Baldini, J.U.L., Bertram, R.A., Ridley, H.E., 2018. Ground air: A first approximation of the Earth's  
1583 second largest reservoir of carbon dioxide gas. *Sci. Total Environ.* 616-617, 1007-1013.

1584 Baldini, J.U.L., McDermott, F., Baker, A., Baldini, L.M., Matthey, D.P., Railsback, L.B., 2005. Biomass  
1585 effects on stalagmite growth and isotope ratios: A 20th century analogue from Wiltshire, England.  
1586 *Earth Planet. Sci. Lett.* 240, 486-494.

1587 Baldini, J.U.L., McDermott, F., Baldini, L.M., Ottley, C.J., Linge, K.L., Clipson, N., Jarvis, K.E., 2012.  
1588 Identifying short-term and seasonal trends in cave drip water trace element concentrations based on  
1589 a daily-scale automatically collected drip water dataset. *Chem. Geol.* 330, 1-16.

1590 Baldini, J.U.L., McDermott, F., Fairchild, I.J., 2002. Structure of the 8200-year cold event revealed by  
1591 a speleothem trace element record. *Science* 296, 2203-2206.

1592 Baldini, J.U.L., McDermott, F., Fairchild, I.J., 2006. Spatial variability in cave drip water  
1593 hydrochemistry: Implications for stalagmite paleoclimate records. *Chem. Geol.* 235, 390-404.

1594 Baldini, J.U.L., McDermott, F., Hoffmann, D.L., Richards, D.A., Clipson, N., 2008. Very high-frequency  
1595 and seasonal cave atmosphere  $P_{CO_2}$  variability: Implications for stalagmite growth and oxygen  
1596 isotope-based paleoclimate records. *Earth Planet. Sci. Lett.* 272, 118-129.

1597 Baldini, L.M., Baldini, J.U.L., McDermott, F., Arias, P., Cueto, M., Fairchild, I.J., Hoffmann, D.L.,  
1598 Matthey, D.P., Müller, W., Nita, D.C., Ontañón, R., Garcá-Moncó, C., Richards, D.A., 2019. North



1599 Iberian temperature and rainfall seasonality over the Younger Dryas and Holocene. *Quaternary*  
1600 *Science Reviews* 226, 105998.

1601 Baldini, L.M., McDermott, F., Baldini, J.U.L., Arias, P., Cueto, M., Fairchild, I.J., Hoffmann, D.L.,  
1602 Matthey, D.P., Müller, W., Nita, D.C., Ontañón, R., Garcá-Moncó, C., Richards, D.A., 2015. Regional  
1603 temperature, atmospheric circulation, and sea-ice variability within the Younger Dryas Event  
1604 constrained using a speleothem from northern Iberia. *Earth Planet. Sci. Lett.* 419, 101-110.

1605 Ban, F.M., Baker, A., Marjo, C.E., Duan, W.H., Li, X.L., Han, J.X., Coleborn, K., Akter, R., Tan, M.,  
1606 Nagra, G., 2018. An optimized chronology for a stalagmite using seasonal trace element cycles from  
1607 Shihua Cave, Beijing, North China. *Scientific Reports* 8, 4551.

1608 Banner, J.L., Guilfoyle, A., James, E.W., Stern, L.A., Musgrove, M., 2007. Seasonal variations in  
1609 modern speleothem calcite growth in Central Texas, USA. *J Sediment Res* 77, 615-622.

1610 Bar-Matthews, M., Ayalon, A., Matthews, A., Sass, E., Halicz, L., 1996. Carbon and oxygen isotope  
1611 study of the active water-carbonate system in a karstic Mediterranean cave: Implications for  
1612 paleoclimate research in semiarid regions. *Geochim. Cosmochim. Acta* 60, 337-347.

1613 Bergel, S.J., Carlson, P.E., Larson, T.E., Wood, C.T., Johnson, K.R., Banner, J., Breecker, D.O., 2017.  
1614 Constraining the subsoil carbon source to cave-air CO<sub>2</sub> and speleothem calcite in central Texas. 217,  
1615 112-127.

1616 Berkelhammer, M., Sinha, A., Stott, L., Cheng, H., Pausata, F.S.R., Yoshimura, K., 2012. An abrupt  
1617 shift in the Indian Monsoon 4000 years ago. *Geophysical Monograph Series* 198, 75-87.

1618 Blyth, A.J., Baker, A., Thomas, L.E., Van Calsteren, P., 2011. A 2000-year lipid biomarker record  
1619 preserved in a stalagmite from north-west Scotland. *J. of Quaternary Sci.* 26, 326-334.

1620 Borsato, A., Frisia, S., Fairchild, I.J., Somogyi, A., Susini, J., 2007. Trace element distribution in annual  
1621 stalagmite laminae mapped by micrometer-resolution X-ray fluorescence: implications for  
1622 incorporation of environmentally significant species. *Geochim. Cosmochim. Acta* 71, 1494-1512.

1623 Borsato, A., Frisia, S., Hellstrom, J., Treble, P., Johnson, K., Howard, D., Greig, A., 2019. Fast high-  
1624 resolution synchrotron micro-XRF mapping of annually laminated stalagmites, European Geoscience  
1625 Union General Assembly. EGU, Vienna.

1626 Borsato, A., Frisia, S., Wynn, P.M., Fairchild, I.J., Miorandi, R., 2015. Sulphate concentration in cave  
1627 dripwater and speleothems: long-term trends and overview of its significance as proxy for  
1628 environmental processes and climate changes. *Quaternary Sci. Rev.* 127, 48-60.

1629 Breecker, D.O., Payne, A.E., Quade, J., Banner, J.L., Ball, C.E., Meyer, K.W., Cowan, B.D., 2012. The  
1630 sources and sinks of CO<sub>2</sub> in caves under mixed woodland and grassland vegetation. *Geochim.  
1631 Cosmochim. Acta* 96, 230-246.

1632 Breitenbach, S.F.M., Adkins, J.F., Meyer, H., Marwan, N., Kumar, K.K., Haug, G.H., 2010. Strong  
1633 influence of water vapor source dynamics on stable isotopes in precipitation observed in Southern  
1634 Meghalaya, NE India. *Earth and Planetary Science Letters* 292, 212-220.

1635 Breitenbach, S.F.M., Bernasconi, S.M., 2011. Carbon and oxygen isotope analysis of small carbonate  
1636 samples (20 to 100  $\mu$ g) with a GasBench II preparation device. *Rapid Commun. Mass Spectrom.*  
1637 25, 1910-1914.

1638 Breitenbach, S.F.M., Lechleitner, F.A., Meyer, H., Diengdoh, G., Matthey, D., Marwan, N., 2015. Cave  
1639 ventilation and rainfall signals in dripwater in a monsoonal setting – a monitoring study from NE  
1640 India. *Chemical Geology* 402, 111-124.

1641 Breitenbach, S.F.M., Plessen, B., Waltgenbach, S., Tjallingii, R., Leonhardt, J., Jochum, K.P., Meyer, H.,  
1642 Goswami, B., Marwan, N., Scholz, D., 2019. Holocene interaction of maritime and continental climate

1643 in Central Europe: New speleothem evidence from Central Germany. *Global and Planet. Change* 176,  
1644 144-161.

1645 Broecker, W.S., 1960. Radiocarbon measurements and annual rings in cave formations. *Nature* 185,  
1646 93-94.

1647 Broughton, P.L., 1983. Environmental Implications of competitive growth fabrics in stalactitic  
1648 carbonate. *International Journal of Speleology*. 13, 31-41.

1649 Buhmann, D., Dreybrodt, W., 1985. The kinetics of calcite dissolution and precipitation in  
1650 geologically relevant situations of karst areas. 2. closed system. *Chemical Geology* 53, 109-124.

1651 Cabellero, E., Jimenez de Cisneros, C., Reyes, E., 1996. A stable isotope study of cave seepage waters.  
1652 *Applied Geochemistry* 11, 583-587.

1653 Carlson, P.E., Miller, N.R., Banner, J.L., Breecker, D.O., Casteel, R.C., 2018. The potential of near-  
1654 entrance stalagmites as high-resolution terrestrial paleoclimate proxies: Application of isotope and  
1655 trace-element geochemistry to seasonally-resolved chronology. *Geochimica et Cosmochimica Acta*  
1656 235, 55-75.

1657 Chapman, J.B., Ingraham, N.L., Hess, J.W., 1992. Isotopic investigation of infiltration and unsaturated  
1658 zone flow processes at Carlsbad Caverns. *Journal of Hydrology* 133, 343-363.

1659 Chen, C.-J., Li, T.-Y., 2018. Geochemical characteristics of cave drip water respond to ENSO based on  
1660 a 6-year monitoring work in Yangkou Cave, Southwest China. *Journal of Hydrology* 561, 896-907.

1661 Cheng, H., Lawrence Edwards, R., Shen, C.-C., Polyak, V.J., Asmerom, Y., Woodhead, J., Hellstrom, J.,  
1662 Wang, Y., Kong, X., Spötl, C., Wang, X., Calvin Alexander, E., 2013. Improvements in  $^{230}\text{Th}$  dating,  
1663  $^{230}\text{Th}$  and  $^{234}\text{U}$  half-life values, and U–Th isotopic measurements by multi-collector inductively  
1664 coupled plasma mass spectrometry. *Earth and Planetary Science Letters* 371-372, 82-91.

1665 Cole, J.M., Nienstedt, J., Spataro, G., Rasbury, E.T., Lanzirrotti, A., Celestian, A.J., Nilsson, M., Hanson,  
1666 G.N., 2003. Phosphor imaging as a tool for in situ mapping of ppm levels of uranium and thorium in  
1667 rocks and minerals. *Chem. Geol.* 193, 127-136.

1668 Comas-Bru, L., Harrison, S.P., 2019. SISAL: Bringing Added Value to Speleothem Research.  
1669 *Quaternary* 2, 7.

1670 Comas-Bru, L., Harrison, S.P., Werner, M., Rehfeld, K., Scropton, N., Veiga-Pires, C., Ahmad, S.M.,  
1671 Brahim, Y.A., Mozhdehi, S.A., Arienzo, M., Atsawawaranunt, K., Baker, A., Braun, K., Breitenbach, S.,  
1672 Burstyn, Y., Chawchai, S., Columbu, A., Deininger, M., Demeny, A., Dixon, B., Hatvani, I.G., Hu, J.,  
1673 Kaushal, N., Kern, Z., Labuhn, I., Lachniet, M.S., Lechleitner, F.A., Lorrey, A., Markowska, M., Nehme,  
1674 C., Novello, V.F., Oster, J., Perez-Mejias, C., Pickering, R., Sekhon, N., Wang, X.F., Warken, S.,  
1675 Atkinson, T., Ayalon, A., Baldini, J., Bar-Matthews, M., Bernal, J.P., Boch, R., Borsato, A., Boyd, M.,  
1676 Brierley, C., Cai, Y.J., Carolin, S., Cheng, H., Constantin, S., Couchoud, I., Cruz, F., Denniston, R.,  
1677 Dragusin, V., Duan, W.H., Ersek, V., Finne, M., Fleitmann, D., Fohlmeister, J., Frappier, A., Genty, D.,  
1678 Holzkamper, S., Hopley, P., Johnston, V., Kathayat, G., Keenan-Jones, D., Koltai, G., Li, T.Y., Lone,  
1679 M.A., Luetscher, M., Matthey, D., Moreno, A., Moseley, G., Psomiadis, D., Ruan, J.Y., Scholz, D., Sha,  
1680 L.J., Smith, A.C., Strikis, N., Treble, P., Unal-Imer, E., Vaks, A., Vansteenberge, S., Voarintsoa, N.R.G.,  
1681 Wong, C., Wortham, B., Wurtzel, J., Zhang, H., Grp, S.W., 2019. Evaluating model outputs using  
1682 integrated global speleothem records of climate change since the last glacial. *Clim Past* 15, 1557-  
1683 1579.

1684 Cook, E.R., Krusic, P.J., Anchukaitis, K.J., Buckley, B.M., Nakatsuka, T., Sano, M., Asia2K, P., 2013.  
1685 Tree-ring reconstructed summer temperature anomalies for temperate East Asia since 800 CE. *Clim.*  
1686 *Dynam.* 41, 2957-2972.

1687 Cowan, B.D., Osborne, M.C., Banner, J.L., 2013. Temporal variability of cave air PCO<sub>2</sub> in Central  
1688 Texas. *J Cave Karst Stud* 75, 38-50.

1689 Cruz Jr., F.W., Karmann, I., Vianna, J., O., Burns, S.J., Ferrari, J.A., Vuille, M., Sial, A.N., Moreira, M.Z.,  
1690 2005. Stable isotope study of cave percolation waters in subtropical Brazil: Implications for  
1691 paleoclimate inferences from speleothems. *Chemical Geology* 220, 245-262.

1692 Czuppon, G., Demény, A., Leél-Össy, S., Óvari, M., Stieber, J., Kiss, K., Kármán, K., Surányi, G.,  
1693 Haszpra, L., 2018. Cave monitoring in the Béke and Baradla caves (Northeastern Hungary):  
1694 implications for the conditions for the formation cave carbonates. *International Journal of*  
1695 *Speleology*, 13-28.

1696 Daëron, M., Drysdale, R.N., Peral, M., Huyghe, D., Blamart, D., Coplen, T.B., Lartaud, F., Zanchetta,  
1697 G., 2019. Most Earth-surface calcites precipitate out of isotopic equilibrium. *Nat Commun* 10.

1698 Deininger, M., McDermott, F., Mudelsee, M., Werner, M., Frank, N., Mangini, A., 2017. Coherency of  
1699 late Holocene European speleothem delta O-18 records linked to North Atlantic Ocean circulation.  
1700 *Clim. Dynam.* 49, 595-618.

1701 Deininger, M., Scholz, D., 2019. ISOLUTION 1.0: an ISOTOpe evoLUTION model describing the stable  
1702 oxygen (delta O-18) and carbon (delta C-13) isotope values of speleothems. *International Journal of*  
1703 *Speleology* 48, 21-32.

1704 Deininger, M., Werner, M., McDermott, F., 2016. North Atlantic Oscillation controls on oxygen and  
1705 hydrogen isotope gradients in winter precipitation across Europe; implications for palaeoclimate  
1706 studies. *Clim Past* 12, 2127-2143.

1707 Dredge, J., Fairchild, I.J., Harrison, R.M., Fernandez-Cortes, A., Sanchez-Moral, S., Jurado, V., Gunn, J.,  
1708 Smith, A., Spotl, C., Matthey, D., Wynn, P.M., Grassineau, N., 2013. Cave aerosols: distribution and  
1709 contribution to speleothem geochemistry. *Quaternary Sci. Rev.* 63, 23-41.

1710 Dreybrodt, W., 1980. Deposition of calcite from thin films of natural calcareous solutions and the  
1711 growth of speleothems. *Chem. Geol.* 29, 89-105.

- 1712 Dreybrodt, W., 1988. Processes in karst systems - physics, chemistry and geology. Springer, Berlin,  
1713 New York.
- 1714 Dreybrodt, W., 1999. Chemical kinetics, speleothem growth and climate. *Boreas* 28, 347-356.
- 1715 Dreybrodt, W., Deininger, M., 2014. The impact of evaporation to the isotope composition of DIC in  
1716 calcite precipitating water films in equilibrium and kinetic fractionation models. *Geochim.*  
1717 *Cosmochim. Acta* 125, 433-439.
- 1718 Duan, F.C., Wu, J.Y., Wang, Y.J., Edwards, R.L., Cheng, H., Kong, X.G., Zhang, W.H., 2015. A 3000-yr  
1719 annually laminated stalagmite record of the Last Glacial Maximum from Hulu Cave, China.  
1720 *Quaternary Res.* 83, 360-369.
- 1721 Duan, W., Ruan, J., Luo, W., Li, T., Tian, L., Zeng, G., Zhang, D., Bai, Y., Li, J., Tao, T., Zhang, P., Baker,  
1722 A., Tan, M., 2016. The transfer of seasonal isotopic variability between precipitation and drip water  
1723 at eight caves in the monsoon regions of China. *Geochim. Cosmochim. Acta* 183, 250-266.
- 1724 Edwards, L.R., Chen, J.H., Wasserburg, G.J., 1987.  $^{238}\text{U}$ - $^{234}\text{U}$ - $^{230}\text{Th}$ - $^{232}\text{Th}$  systematics and the  
1725 precise measurement of time over the past 500,000 years. *Earth Planet. Sci. Lett.* 81, 175-192.
- 1726 Edwards, R.L., Gallup, C.D., 1993. Dating of the Devils Hole Calcite Vein. *Science* 259, 1626-1627.
- 1727 Emiliani, C., 1955. Pleistocene temperatures. *Journal of Geology* 63, 538-578.
- 1728 Epstein, S., Buchsbaum, R., Lowenstam, H.A., Urey, H.C., 1951. Carbonate-water isotopic  
1729 temperature scale. *Bulletin of the Geological Society of America* 62, 417-427.
- 1730 Evans, D., Müller, W., 2013. LA-ICPMS elemental imaging of complex discontinuous carbonates: An  
1731 example using large benthic foraminifera. *J. Anal. At. Spectrom.* 28, 1039-1044.
- 1732 Evans, M.N., Tolwinski-Ward, S.E., Thompson, D.M., Achukaitis, K.J., 2013. Applications of proxy  
1733 system modeling in high resolution paleoclimatology. *Quaternary Science Reviews* 76, 16-28.

- 1734 Faimon, J., Lang, M., 2013. Variances in airflows during different ventilation modes in a dynamic U-  
1735 shaped cave. *Int J Speleol* 42, 115-122.
- 1736 Fairchild, I.J., Baker, A., 2012. *Speleothem Science: From Processes to Past Environments*. Wiley-  
1737 Blackwell, Chichester, UK.
- 1738 Fairchild, I.J., Baker, A., Borsato, A., Frisia, S., Hinton, R.W., McDermott, F., Tooth, A.F., 2001. Annual  
1739 to sub-annual resolution of multiple trace-element trends in speleothems. *J. Geol. Soc. London* 158,  
1740 831-841.
- 1741 Fairchild, I.J., Borsato, A., Tooth, A.F., Frisia, S., Hawkesworth, C.J., Huang, Y., McDermott, F., Spiro,  
1742 B., 2000. Controls on trace element (Sr-Mg) compositions of carbonate cave waters: implications for  
1743 speleothem climatic records. *Chem. Geol.* 166, 255-269.
- 1744 Fairchild, I.J., Hartland, A., 2010. Trace element variations in stalagmites: controls by climate and by  
1745 karst system processes. *EMU Notes in Mineralogy* 10, 259-287.
- 1746 Fairchild, I.J., Smith, C.L., Baker, A., Fuller, L., Spotl, C., Matthey, D., McDermott, F., Eimp, 2006.  
1747 Modification and preservation of environmental signals in speleothems. *Earth Sci. Rev.* 75, 105-153.
- 1748 Fairchild, I.J., Treble, P.C., 2009. Trace elements in speleothems as recorders of environmental  
1749 change. *Quaternary Sci. Rev.* 28, 449-468.
- 1750 Feng, W., Casteel, R.C., Banner, J.L., Heinze-Fry, A., 2014. Oxygen isotope variations in rainfall, drip-  
1751 water and speleothem calcite from a well-ventilated cave in Texas, USA: Assessing a new  
1752 speleothem temperature proxy. *Geochim. Cosmochim. Acta* 127, 233-250.
- 1753 Feng, X., Porporato, A., Rodriguez-Iturbe, I., 2013. Changes in rainfall seasonality in the tropics.  
1754 *Nature Climate Change* 3, 811-815.

- 1755 Fick, S.E., Hijmans, R.J., 2017. WorldClim 2: new 1-km spatial resolution climate surfaces for global  
1756 land areas. *Int J Climatol* 37, 4302-4315.
- 1757 Finch, A.A., Shaw, P.A., Weedon, G.P., Holmgren, K., 2001. Trace element variation in speleothem  
1758 aragonite: potential for palaeoenvironmental reconstruction. *Earth and Planetary Science Letters*  
1759 186, 255-267.
- 1760 Fohlmeister, J., Lechleitner, F.A., 2019. STAlagmite dating by radiocarbon (star): A software tool for  
1761 reliable and fast age depth modelling. *Quat Geochronol* 51, 120-129.
- 1762 Fohlmeister, J., Plessen, B., Dudashvili, A.S., Tjallingii, R., Wolff, C., Gafurov, A., Cheng, H., 2017.  
1763 Winter precipitation changes during the Medieval Climate Anomaly and the Little Ice Age in arid  
1764 Central Asia. *Quaternary Sci. Rev.* 178, 24-36.
- 1765 Frappier, A.B., Sahagian, D., Carpenter, S.J., González, L.A., Frappier, B.R., 2007. Stalagmite stable  
1766 isotope record of recent tropical cyclone events. *Geology* 35.
- 1767 Frick, D.A., Schuessler, J.A., von Blanckenburg, F., 2016. Development of routines for simultaneous in  
1768 situ chemical composition and stable Si isotope ratio analysis by femtosecond laser ablation  
1769 inductively coupled plasma mass spectrometry. *Analytica Chimica Acta* 938, 33-43.
- 1770 Frisia, S., 2015. Microstratigraphic logging of calcite fabrics in speleothems as tool for palaeoclimate  
1771 studies. *Int J Speleol* 44, 1-16.
- 1772 Frisia, S., Borsato, A., Fairchild, I.J., McDermott, F., 2000. Calcite fabrics, growth mechanisms, and  
1773 environments of formation in speleothems from the Italian Alps and southwestern Ireland. *J*  
1774 *Sediment Res* 70, 1183-1196.
- 1775 Frisia, S., Borsato, A., Fairchild, I.J., Susini, J., 2005. Variations in atmospheric sulphate recorded in  
1776 stalagmites by synchrotron micro-XU and XANES analyses. *Earth Planet. Sci. Lett.* 235, 729-740.



- 1777 Frisia, S., Borsato, A., Hellstrom, J., 2018. High spatial resolution investigation of nucleation, growth  
1778 and early diagenesis in speleothems as exemplar for sedimentary carbonates. *Earth Sci. Rev.* 178, 68-  
1779 91.
- 1780 Frisia, S., Borsato, A., Susini, J., 2008. Synchrotron radiation applications to past volcanism archived  
1781 in speleothems: An overview. *J. Volcanol. Geotherm. Res.* 177, 96-100.
- 1782 Gascoyne, M., Schwarcz, H.P., Ford, D.C., 1980. A palaeotemperature record for the mid-Wisconsin  
1783 in Vancouver Island. *Nature* 285, 474-476.
- 1784 Gazis, C., Feng, X.H., 2004. A stable isotope study of soil water: evidence for mixing and preferential  
1785 flow paths. *Geoderma* 119, 97-111.
- 1786 Genty, D., 2008. Palaeoclimate research in Villars Cave (Dordogne, SW France). *Int J Speleol* 37, 173-  
1787 191.
- 1788 Genty, D., Baker, A., Vokal, B., 2001. Intra- and inter-annual growth rate of modern stalagmites.  
1789 *Chemical Geology* 176, 191-212.
- 1790 Genty, D., Deflandre, G., 1998. Drip flow variations under a stalactite of the Père Noël cave  
1791 (Belgium). Evidence of seasonal variations and air pressure constraints. *J Hydrol* 211, 208-232.
- 1792 Guo, W., Zhou, C., 2019. Patterns and controls of disequilibrium isotope effects in speleothems:  
1793 Insights from an isotope-enabled diffusion-reaction model and implications for quantitative  
1794 thermometry. *Geochimica et Cosmochimica Acta* 267, 196-226.
- 1795 Harmon, R.S., 1979. An isotopic study of groundwater seepage in the Central Kentucky karst. *Water*  
1796 *Resources Research* 15, 476.

1797 Hartland, A., Fairchild, I.J., Lead, J.R., 2009. Colloids in karstic percolation waters: Implications for the  
1798 interpretation of trace element variations in speleothems. *Geochim. Cosmochim. Acta* 73, A498-  
1799 A498.

1800 Hartland, A., Fairchild, I.J., Lead, J.R., Baker, A., 2010. Fluorescent properties of organic carbon in  
1801 cave dripwaters: Effects of filtration, temperature and pH. *Sci. Total Environ.* 408, 5940-5950.

1802 Hartland, A., Fairchild, I.J., Lead, J.R., Borsato, A., Baker, A., Frisia, S., Baalousha, M., 2012. From soil  
1803 to cave: Transport of trace metals by natural organic matter in karst dripwaters. *Chem. Geol.* 304,  
1804 68-82.

1805 Hartland, A., Fairchild, I.J., Lead, J.R., Zhang, H., Baalousha, M., 2011. Size, speciation and lability of  
1806 NOM-metal complexes in hyperalkaline cave dripwater. *Geochim. Cosmochim. Acta* 75, 7533-7551.

1807 Hellstrom, J., 2003. Rapid and accurate U/Th dating using parallel ion-counting multi-collector ICP-  
1808 MS. *J. Anal. At. Spectrom.* 18, 1346-1351.

1809 Helser, T.E., Kastle, C.R., McKay, J.L., Orland, I.J., Kodzon, R., Valley, J.W., 2018. Evaluation of  
1810 micromilling/conventional isotope ratio mass spectrometry and secondary ion mass spectrometry of  
1811  $\delta^{18}\text{O}$  values in fish otoliths for sclerochronology. *Rapid Commun Mass Spectrom* 32, 1781-1790.

1812 Hendy, C.H., Wilson, A.T., 1968. Paleoclimatic data from speleothems. *Nature* 216, 48-51.

1813 Hess, J.W., White, W.B., 1989. Water Budget and Physical Hydrology, in: B., W.W., White, E.L. (Eds.),  
1814 *Karst Hydrology: Concepts from the Mammoth Cave Area*. Springer-Verlag, Boston, pp. 105-126.

1815 Hoffmann, D.L., Prytulak, J., Richards, D.A., Elliott, T.R., Coath, C.D., Smart, P.L., Scholz, D., 2007.  
1816 Procedures for accurate U and Th isotope measurements by high precision MC-ICPMS. *Int. J. Mass*  
1817 *Spectrom. Ion Processes* 264, 97-109.

- 1818 Hsiang, S.M., Burke, M., Miguel, E., 2013. Quantifying the Influence of Climate on Human Conflict.  
1819 Science 341, 1235367.
- 1820 Hu, C., Henderson, G.M., Huang, J., Xie, S., Sun, Y., Johnson, K.R., 2008. Quantification of Holocene  
1821 Asian monsoon rainfall from spatially separated cave records. Earth Planet. Sci. Lett. 266, 221-232.
- 1822 Huang, S.P., Pollack, H.N., Shen, P.Y., 2000. Temperature trends over the past five centuries  
1823 reconstructed from borehole temperatures. Nature 403, 756-758.
- 1824 Huang, Y., Fairchild, I.J., 2001. Partitioning of Sr<sup>2+</sup> and Mg<sup>2+</sup> into calcite under karst-analogue  
1825 experimental conditions. Geochim. Cosmochim. Acta 65, 47-62.
- 1826 Huang, Y., Fairchild, I.J., Borsato, A., Frisia, S., Cassidy, N.J., McDermott, F., Hawkesworth, C.J., 2001.  
1827 Seasonal variations in Sr, Mg and P in modern speleothems (Grotta di Ernesto, Italy). Chem. Geol.  
1828 175, 429-448.
- 1829 IAEA, 2001. GNIP Maps and Animations. , Vienna.
- 1830 IAEA/WMO, 2001. Global Network of Isotopes in Precipitation. The GNIP Database.
- 1831 James, E., Banner, J., Hardt, B., 2015. A global model for cave ventilation and seasonal bias in  
1832 speleothem paleoclimate records.
- 1833 Jamieson, R.A., Baldini, J.U.L., Brett, M.J., Taylor, J., Ridley, H.E., Ottley, C.J., Prufer, K.M.,  
1834 Wassenburg, J.A., Scholz, D., Breitenbach, S.F.M., 2016. Intra- and inter-annual uranium  
1835 concentration variability in a Belizean stalagmite controlled by prior aragonite precipitation: A new  
1836 tool for reconstructing hydro-climate using aragonitic speleothems. Geochim. Cosmochim. Acta 190,  
1837 332-346.

1838 Jamieson, R.A., Baldini, J.U.L., Frappier, A.B., Müller, W., 2015. Volcanic ash fall events identified  
1839 using principle component analysis of a high-resolution speleothem trace element dataset. *Earth  
1840 and Planetary Science Letters* 426, 36-45.

1841 Johnson, K.R., Hu, C., Belshaw, N.S., Henderson, G.M., 2006. Seasonal trace-element and stable-  
1842 isotope variations in a Chinese speleothem: The potential for high-resolution paleomonsoon  
1843 reconstruction. *Earth and Planetary Science Letters* 244, 394-407.

1844 Kaufman, A., Bar-Matthews, M., Ayalon, A., Carmi, I., 2003. The vadose flow above Soreq Cave,  
1845 Israel: a tritium study of the cave waters. *Journal of Hydrology* 273, 155-163.

1846 Kennett, D.J., Breitenbach, S.F.M., Aquino, V.V., Asmerom, Y., Awe, J., Baldini, J.U.L., Bartlein, P.,  
1847 Culleton, B.J., Ebert, C., Jazwa, C., Macri, M.J., Marwan, N., Polyak, V., Prufer, K.M., Ridley, H.E.,  
1848 Sodemann, H., Winterhalder, B., Haug, G.H., 2012. Development and Disintegration of Maya Political  
1849 Systems in Response to Climate Change. *Science* 338, 788-791.

1850 Khiewtam, R.S., Ramakrishnan, P.S., 1993. Litter and fine root dynamics of a relict sacred grove  
1851 forest at Cherrapunji in north-eastern India. *Forest Ecology and Management* 60, 327-344.

1852 Kita, N.T., Huberty, J.M., Kozdon, R., Beard, B.L., Valley, J.W., 2011. High-precision SIMS oxygen,  
1853 sulfur and iron stable isotope analyses of geological materials: accuracy, surface topography and  
1854 crystal orientation. *Surf. Interface Anal.* 43, 427-431.

1855 Köppen, W., 1918. Classification of climates according to temperature, precipitation and course of  
1856 the year. *Petermanns Mitt* 64, 193-203.

1857 Kuczumow, A., Genty, D., Chevallier, P., Nowak, J., Ro, C.U., 2003. Annual resolution analysis of a  
1858 SW-France stalagmite by X-ray synchrotron microprobe analysis. *Spectrochim Acta B* 58, 851-865.

- 1859 Kuczumow, A., Vekemans, B., Schalm, O., Gysels, K., Ro, C.U., Van Grieken, R., 2001. Analysis of  
1860 speleothems by electron and X-ray microprobes. *J. Anal. At. Spectrom.* 16, 90-95.
- 1861 Kylander-Clark, A.R.C., Hacker, B.R., Cottle, J.M., 2013. Laser-ablation split-stream ICP  
1862 petrochronology. *Chemical Geology* 345, 99-112.
- 1863 Lachniet, M.S., 2009. Climatic and environmental controls on speleothem oxygen-isotope values.  
1864 *Quaternary Science Reviews* 28, 412-432.
- 1865 Lauritzen, S., 1995. High Resolution Paleotemperature Proxy Record for the Last Interglaciation  
1866 Based on Norwegian Speleothems. *Quaternary Res.* 43, 133-146.
- 1867 Lauritzen, S., Lundberg, J., 1999. Calibration of the speleothem delta function: an absolute  
1868 temperature record for the Holocene in northern Norway. *Holocene* 9, 659-669.
- 1869 Lechleitner, F.A., Baldini, J.U.L., Breitenbach, S.F.M., Fohlmeister, J., McIntyre, C., Goswami, B.,  
1870 Jamieson, R.A., van der Voort, T.S., Prufer, K., Marwan, N., Culleton, B.J., Kennett, D.J., Asmerom, Y.,  
1871 Polyak, V., Eglinton, T.I., 2016a. Hydrological and climatological controls on radiocarbon  
1872 concentrations in a tropical stalagmite. *Geochim. Cosmochim. Acta* 194, 233-252.
- 1873 Lechleitner, F.A., Fohlmeister, J., McIntyre, C., Baldini, L.M., Jamieson, R.A., Hercman, H.,  
1874 Gąsiorowski, M., Pawlak, J., Stefaniak, K., Socha, P., Eglinton, T.I., Baldini, J.U.L., 2016b. A novel  
1875 approach for construction of radiocarbon-based chronologies for speleothems. *Quat Geochronol* 35,  
1876 54-66.
- 1877 Li, F., Vanwezer, N., Boivin, N., Gao, X., Ott, F., Petraglia, M., Roberts, P., 2019. Heading north: Late  
1878 Pleistocene environments and human dispersals in central and eastern Asia. *Plos One* 14, e0216433.
- 1879 Linzmeier, B.J., Kitajima, K., Denny, A.C., Cammack, J.N., 2018. Making maps on a micrometer scale.  
1880 *Eos* 99.

1881 Liu, Y.H., Henderson, G.M., Hu, C.Y., Mason, A.J., Charnley, N., Johnson, K.R., Xie, S.C., 2013. Links  
1882 between the East Asian monsoon and North Atlantic climate during the 8,200 year event. *Nat.*  
1883 *Geosci.* 6, 117-120.

1884 Luetscher, M., Boch, R., Sodemann, H., Spotl, C., Cheng, H., Edwards, R.L., Frisia, S., Hof, F., Müller,  
1885 W., 2015. North Atlantic storm track changes during the Last Glacial Maximum recorded by Alpine  
1886 speleothems. *Nat Commun* 6, 6344.

1887 Luo, T., Hu, Z., Zhang, W., Günther, D., Liu, Y., Zong, K., Hu, S., 2018. Reassessment of the influence  
1888 of carrier gases He and Ar on signal intensities in 193 nm excimer LA-ICP-MS analysis. *Journal of*  
1889 *Analytical Atomic Spectrometry* 33, 1655-1663.

1890 Luo, W., Wang, S., Zeng, G., Zhu, X., Liu, W., 2014. Daily response of drip water isotopes to  
1891 precipitation in Liangfeng Cave, Guizhou Province, SW China. *Quaternary International* 349, 153-158.

1892 Markowska, M., Baker, A., Andersen, M.S., Jex, C.N., Cuthbert, M.O., Rau, G.C., Graham, P.W.,  
1893 Rutledge, H., Mariethoz, G., Marjo, C.E., Treble, P.C., Edwards, N., 2016. Semi-arid zone caves:  
1894 Evaporation and hydrological controls on delta O-18 drip water composition and implications for  
1895 speleothem paleoclimate reconstructions. *Quaternary Sci. Rev.* 131, 285-301.

1896 Markowska, M., Baker, A., Treble, P.C., Andersen, M.S., Hankin, S., Jex, C.N., Tadros, C.V., Roach, R.,  
1897 2015. Unsaturated zone hydrology and cave drip discharge water response: Implications for  
1898 speleothem paleoclimate record variability. *J Hydrol* 529, 662-675.

1899 Markowska, M., Fohlmeister, J., Treble, P.C., Baker, A., Andersen, M.S., Hua, Q., 2019. Modelling the  
1900 <sup>14</sup>C bomb-pulse in young speleothems using a soil carbon continuum model. *Geochim. Cosmochim.*  
1901 *Acta* 261, 342-367.

- 1902 Martin-Chivelet, J., Munoz-Garcia, M.B., Edwards, R.L., Turrero, M.J., Ortega, A.I., 2011. Land surface  
1903 temperature changes in Northern Iberia since 4000 yr BP, based on delta C-13 of speleothems.  
1904 *Global and Planet. Change* 77, 1-12.
- 1905 Martin-Garcia, R., Alonso-Zarza, A.M., Martin-Perez, A., Schroder-Ritzrau, A., Ludwig, T., 2014.  
1906 Relationships between colour and diagenesis in the aragonite-calcite speleothems in Basajaun Etxea  
1907 cave, Spain. *Sediment Geol* 312, 63-75.
- 1908 Matthey, D., Collister, C., 2008. Controls on water drop volume at speleothem drip sites: An  
1909 experimental study. *J Hydrol* 358, 259-267.
- 1910 Matthey, D., Lowry, D., Duffet, J., Fisher, R., Hodge, E., Frisia, S., 2008. A 53 year seasonally resolved  
1911 oxygen and carbon isotope record from a modern Gibraltar speleothem: Reconstructed drip water  
1912 and relationship to local precipitation. *Earth Planet. Sci. Lett.* 269, 80-95.
- 1913 Matthey, D.P., Atkinson, T.C., Barker, J.A., Fisher, R., Latin, J.P., Durell, R., Ainsworth, M., 2016. Carbon  
1914 dioxide, ground air and carbon cycling in Gibraltar karst. *Geochim. Cosmochim. Acta* 184, 88-113.
- 1915 Matthey, D.P., Fairchild, I.J., Atkinson, T.C., 2009. Seasonal microclimate control on calcite fabrics,  
1916 stable isotopes and trace elements in modern speleothem from St. Michaels Cave, Gibraltar.  
1917 *Geochim. Cosmochim. Acta* 73, A849-A849.
- 1918 Matthey, D.P., Fairchild, I.J., Atkinson, T.C., Latin, J.-P., Ainsworth, M., Durell, R., 2010. Seasonal  
1919 microclimate control of calcite fabrics, stable isotopes and trace elements in modern speleothem  
1920 from St Michaels cave, Gibraltar in: Pedley, H.M., Rogerson, M. (Eds.), *Tufas and Speleothems:*  
1921 *Unravelling the Microbial and Physical Controls.* Geological Society of London Special Publication,  
1922 London, pp. 323-344.

- 1923 Maupin, C.R., Partin, J.W., Shen, C.C., Quinn, T.M., Lin, K., Taylor, F.W., Banner, J.L., Thirumalai, K.,  
1924 Sinclair, D.J., 2014. Persistent decadal-scale rainfall variability in the tropical South Pacific  
1925 Convergence Zone through the past six centuries. *Clim Past* 10, 1319-1332.
- 1926 McDermott, F., 2004. Palaeo-climate reconstruction from stable isotope variations in speleothems: a  
1927 review. *Quaternary Sci. Rev.* 23, 901-918.
- 1928 McDermott, F., Atkinson, T.C., Fairchild, I.J., Baldini, L.M., Matthey, D.P., 2011. A first evaluation of the  
1929 spatial gradients in delta O-18 recorded by European Holocene speleothems. *Global and Planet.*  
1930 *Change* 79, 275-287.
- 1931 McMillan, E.A., Fairchild, I.J., Frisia, S., Borsato, A., McDermott, F., 2005. Annual trace element cycles  
1932 in calcite-aragonite speleothems: evidence of drought in the western Mediterranean 1200-1100 yr  
1933 BP. *J. of Quaternary Sci.* 20, 423-433.
- 1934 Menne, M.J., Durre, I., Vose, R.S., Gleason, B.E., Houston, T.G., 2012. An Overview of the Global  
1935 Historical Climatology Network-Daily Database. *J Atmos Ocean Tech* 29, 897-910.
- 1936 Mickler, P.J., Stern, L.A., Banner, J.L., 2006. Large kinetic isotope effects in modern speleothems.  
1937 *Geol. Soc. Am. Bull.* 118, 65-81.
- 1938 Millo, C., Strikis, N.M., Vonhof, H.B., Deininger, M., da Cruz, F.W., Wang, X.F., Cheng, H., Edwards,  
1939 R.L., 2017. Last glacial and Holocene stable isotope record of fossil dripwater from subtropical Brazil  
1940 based on analysis of fluid inclusions in stalagmites. *Chem. Geol.* 468, 84-96.
- 1941 Mischel, S.A., Scholz, D., Spötl, C., 2015.  $\delta^{18}\text{O}$  values of cave drip water: a promising proxy for the  
1942 reconstruction of the North Atlantic Oscillation? *Climate Dynamics* 45, 3035-3050.



- 1943 Moerman, J.W., Cobb, K.M., Partin, J.W., Meckler, A.N., Carolin, S.A., Adkins, J.F., Lejau, S., Malang,  
1944 J., Clark, B., Tuen, A.A., 2014. Transformation of ENSO-related rainwater to dripwater  $\delta^{18}\text{O}$   
1945 variability by vadose water mixing. *Geophys Res Lett* 41, 7907-7915.
- 1946 Moquet, J.S., Cruz, F.W., Novello, V.F., Strikis, N.M., Deininger, M., Karmann, I., Santos, R.V., Millo,  
1947 C., Apaestegui, J., Guyot, J.L., Siffedine, A., Vuille, M., Cheng, H., Edwards, R.L., Santini, W., 2016.  
1948 Calibration of speleothem delta O-18 records against hydroclimate instrumental records in Central  
1949 Brazil. *Global and Planet. Change* 139, 151-164.
- 1950 Morellón, M., Valero-Garcés, B., Vegas-Villarrúbia, T., González-Sampériz, P., Romero, O., Delgado-  
1951 Huertas, A., Mata, P., Moreno, A., Rico, M., Corella, J.P., 2009. Lateglacial and Holocene  
1952 palaeohydrology in the western Mediterranean region: the Lake Estanya record (NE Spain).  
1953 *Quaternary Science Reviews* 28, 2582-2599.
- 1954 Moreno, A., Pérez-Mejías, C., Bartolomé, M., Sancho, C., Cacho, I., Stoll, H., Delgado-Huertas, A.,  
1955 Hellstrom, J., Edwards, R.L., Cheng, H., 2017. New speleothem data from Molinos and Ejulve caves  
1956 reveal Holocene hydrological variability in northeast Iberia. *Quaternary Research* 88, 223-233.
- 1957 Moreno, A., Sancho, C., Bartolomé, M., Oliva-Urcia, B., Delgado-Huertas, A., Estrela, M.J., Corell, D.,  
1958 López-Moreno, J.I., Cacho, I., 2014. Climate controls on rainfall isotopes and their effects on cave  
1959 drip water and speleothem growth: the case of Molinos cave (Teruel, NE Spain). *Climate Dynamics*  
1960 43, 221-241.
- 1961 Moseley, G.E., Spötl, C., Cheng, H., Boch, R., Min, A., Edwards, R.L., 2015. Termination-II  
1962 interstadial/stadial climate change recorded in two stalagmites from the north European Alps.  
1963 *Quaternary Science Reviews* 127, 229-239.
- 1964 Müller, W., Fietzke, J., 2016. The role of LA-ICP-MS in palaeoclimate research. *Elements* 12, 329-334.

1965 Müller, W., Shelley, M., Miller, P., Broude, S., 2009. Initial performance metrics of a new custom-  
1966 designed ArF excimer LA-ICPMS system coupled to a two-volume laser-ablation cell. *J. Anal. At.*  
1967 *Spectrom.* 24, 209-214.

1968 Müller, W., Valley, J.W., Warter, V., Kodzon, R., Evans, D., Orland, I.J., 2015. Natural high-  
1969 temperature metamorphic calcite as compositionally homogenous microanalytical standard?,  
1970 *Goldschmidt 2015, Prague.*

1971 Murata, F., Terao, T., Hayashi, T., Asada, H., Matsumoto, J., 2007. Relationship between atmospheric  
1972 conditions at Dhaka, Bangladesh, and rainfall at Cherrapunjee, India. *Natural Hazards* 44, 399-410.

1973 Myers, C.G., Oster, J.L., Sharp, W.D., Bennartz, R., Kelley, N.P., Covey, A.K., Breitenbach, S.F.M.,  
1974 2015. Northeast Indian stalagmite records Pacific decadal climate change: Implications for moisture  
1975 transport and drought in India. *Geophysical Research Letters* 42, 4124-4132.

1976 Nagra, G., Treble, P.C., Andersen, M.S., Bajo, P., Hellstrom, J., Baker, A., 2017. Dating stalagmites in  
1977 mediterranean climates using annual trace element cycles. *Sci. Rep.* 7, 621.

1978 Noronha, A.L., Johnson, K.R., Southon, J.R., Hu, C., Ruan, J., McCabe-Glynn, S., 2015. Radiocarbon  
1979 evidence for decomposition of aged organic matter in the vadose zone as the main source of  
1980 speleothem carbon. *Quaternary Sci. Rev.* 127, 37-47.

1981 O'Neil, J.R., Clayton, R.M., Mayeda, T., 1969. Oxygen isotope fractionation in divalent metal  
1982 carbonates. *J. Chem. Phys.* 30, 5547-5558.

1983 Oerter, E.J., Sharp, W.D., Oster, J.L., Ebeling, A., Valley, J.W., Kodzon, R., Orland, I.J., Hellstrom, J.,  
1984 Woodhead, J.D., Hergt, J.M., Chadwick, O.A., Amundson, R., 2016. Pedothem carbonates reveal  
1985 anomalous North American atmospheric circulation 70,000–55,000 years ago. *Proc Natl Acad Sci U S*  
1986 *A* 113, 919-924.

- 1987 Onac, B.P., Pace-Graczyk, K., Atudirei, V., 2008. Stable isotope study of precipitation and cave drip  
1988 water in Florida (USA): implications for speleothem-based paleoclimate studies. *Isot. Environ. Health*  
1989 *Stud.* 44, 149-161.
- 1990 Orland, I.J., Bar-Matthews, M., Ayalon, A., Matthews, A., Kozdon, R., Ushikubo, T., Valley, J.W., 2012.  
1991 Seasonal resolution of Eastern Mediterranean climate change since 34 ka from a Soreq Cave  
1992 speleothem. *Geochimica Et Cosmochimica Acta* 89, 240-255.
- 1993 Orland, I.J., Bar-Matthews, M., Kita, N.T., Ayalon, A., Matthews, A., Valley, J.W., 2008. Seasonal  
1994 climate change as revealed by ion microprobe analysis of delta O-18 in Soreq Cave (Israel)  
1995 speleothems. *Geochimica Et Cosmochimica Acta* 72, A709-A709.
- 1996 Orland, I.J., Bar-Matthews, M., Kita, N.T., Ayalon, A., Matthews, A., Valley, J.W., 2009. Climate  
1997 deterioration in the Eastern Mediterranean as revealed by ion microprobe analysis of a speleothem  
1998 that grew from 2.2 to 0.9 ka in Soreq Cave, Israel. *Quaternary Res.* 71, 27-35.
- 1999 Orland, I.J., Burstyn, Y., Bar-Matthews, M., Kozdon, R., Ayalon, A., Matthews, A., Valley, J.W., 2014.  
2000 Seasonal climate signals (1990-2008) in a modern Soreq Cave stalagmite as revealed by high-  
2001 resolution geochemical analysis. *Chem. Geol.* 363, 322-333.
- 2002 Orland, I.J., Edwards, R.L., Cheng, H., Kozdon, R., Cross, M., Valley, J.W., 2015. Direct measurements  
2003 of deglacial monsoon strength in a Chinese stalagmite. *Geology* 43, 555-558.
- 2004 Orland, I.J., He, F., Bar-Matthews, M., Chen, G., Ayalon, A., Kutzbach, J.E., 2019. Resolving seasonal  
2005 rainfall changes in the Middle East during the last interglacial period. *Proc Natl Acad Sci U S A* 116,  
2006 24985-24990.
- 2007 Orr, P.C., 1952. Excavations in Moaning Cave. *Santa Barbara Museum of Natural History Bulletin* 1, 1-  
2008 19.

- 2009 Ortega, R., Maire, R., Deves, G., Quinif, Y., 2005. High-resolution mapping of uranium and other trace  
2010 elements in recrystallized aragonite-calcite speleothems from caves in the Pyrenees (France):  
2011 Implications for U-series dating. *Earth Planet. Sci. Lett.* 237, 911-023.
- 2012 Oster, J.L., Montañez, I.P., Kelley, N.P., 2012. Response of a modern cave system to large seasonal  
2013 precipitation variability. *Geochim. Cosmochim. Acta* 91, 92-108.
- 2014 Pacton, M., Breitenbach, S.F.M., Lechleitner, F.A., Vaks, A., Rollion-Bard, C., Gutareva, O.S., Osintcev,  
2015 A.V., Vasconcelos, C., 2013. The role of microorganisms in the formation of a stalactite in Botovskaya  
2016 Cave, Siberia – paleoenvironmental implications. *Biogeosciences* 10, 6115-6130.
- 2017 Parton, A., Farrant, A.R., Leng, M.J., Telfer, M.W., Groucutt, H.S., Petraglia, M.D., Parker, A.G., 2015.  
2018 Alluvial fan records from southeast Arabia reveal multiple windows for human dispersal. *Geol.* 43,  
2019 295-298.
- 2020 Peel, M.C., Finlayson, B.L., McMahon, T.A., 2007. Updated world map of the Köppen-Geiger climate  
2021 classification. *Hydrology and Earth System Sciences* 11, 1633-1644.
- 2022 Perrin, J., Jeannin, P.-Y., Zwahlen, F., 2003. Epikarst storage in a karst aquifer: a conceptual model  
2023 based on isotopic data, Milandre test site, Switzerland. *Journal of Hydrology* 279, 106-124.
- 2024 Prokop, P., Walanus, A., 2003. Trends and periodicity in the longest instrumental rainfall series for  
2025 the area of most extreme rainfall in the world, northeast India. *Geographia Polonica* 76, 25-35.
- 2026 Pu, J., Wang, A., Shen, L., Yin, J., Yuan, D., Zhao, H., 2016. Factors controlling the growth rate, carbon  
2027 and oxygen isotope variation in modern calcite precipitation in a subtropical cave, Southwest China.  
2028 *Journal of Asian Earth Sciences* 119, 167-178.

2029 Railsback, L.B., Brook, G.A., Chen, J., Kalin, R., Fleisher, C., 1994. Environmental controls on the  
2030 petrology of a late Holocene speleothem from Botswana with annual layers of aragonite and calcite.  
2031 *J Sediment Res A64*, 147-155.

2032 Railsback, L.B., Liang, F.Y., Romani, J.R.V., Grandal-d'Anglade, A., Rodriguez, M.V., Fidalgo, L.S.,  
2033 Mosquera, D.F., Cheng, H., Edwards, R.L., 2011. Petrographic and isotopic evidence for Holocene  
2034 long-term climate change and shorter-term environmental shifts from a stalagmite from the Serra  
2035 do Courel of northwestern Spain, and implications for climatic history across Europe and the  
2036 Mediterranean. *Palaeogeography Palaeoc. 305*, 172-184.

2037 Railsback, L.B., Liang, F.Y., Vidal-Romani, J.R., Garrett, K.B., Sellers, R.C., Vaquero-Rodriguez, M.,  
2038 Grandal-d'Anglade, A., Cheng, H., Edwards, R.L., 2017. Radiometric, isotopic, and petrographic  
2039 evidence of changing interglacials over the past 550,000 years from six stalagmites from the Serra do  
2040 Courel in the Cordillera Cantabrica of northwestern Spain. *Palaeogeography Palaeoc. 466*, 137-152.

2041 Ramakrishnan, P.S., Subhash, C.R., 1988. Vegetation, biomass and productivity of seral grasslands of  
2042 Cherrapunji in north-east India. *Vegetatio 74*, 47-53.

2043 Ridley, H., Baldini, J., Prufer, K., Walczak, I., Breitenbach, S., 2015a. High-resolution monitoring of Yok  
2044 Balum Cave, Belize: An investigation of seasonal ventilation regimes and the atmospheric and drip-  
2045 flow response to a local earthquake. *Journal of Cave and Karst Studies 77*, 183-199.

2046 Ridley, H.E., Asmerom, Y., Baldini, J.U.L., Breitenbach, S.F.M., Aquino, V.V., Prufer, K.M., Culleton,  
2047 B.J., Polyak, V., Lechleitner, F.A., Kennett, D.J., Zhang, M., Marwan, N., Macpherson, C.G., Baldini,  
2048 L.M., Xiao, T., Peterkin, J.L., Awe, J., Haug, G.H., 2015b. Aerosol forcing of the position of the  
2049 intertropical convergence zone since AD1550. *Nat. Geosci. 8*, 195–200.

2050 Riechelmann, D.F.C., Deininger, M., Scholz, D., Riechelmann, S., Schroder-Ritzrau, A., Spotl, C.,  
2051 Richter, D.K., Mangini, A., Immenhauser, A., 2013. Disequilibrium carbon and oxygen isotope

2052 fractionation in recent cave calcite: Comparison of cave precipitates and model data. *Geochim.*  
2053 *Cosmochim. Acta* 103, 232-244.

2054 Riechelmann, D.F.C., Schroder-Ritzrau, A., Scholz, D., Fohlmeister, J., Spotl, C., Richter, D.K., Mangini,  
2055 A., 2011. Monitoring Bunker Cave (NW Germany): A prerequisite to interpret geochemical proxy  
2056 data of speleothems from this site. *J Hydrol* 409, 682-695.

2057 Riechelmann, S., Breitenbach, S.F.M., Schroder-Ritzrau, A., Mangini, A., Immenhauser, A., 2019.  
2058 Ventilation and Cave Air PCO<sub>2</sub> in the Bunker-Emst Cave System (NW Germany): Implications for  
2059 Speleothem Proxy Data. *J Cave Karst Stud* 81, 98-112.

2060 Riechelmann, S., Schröder-Ritzrau, A., Spötl, C., Riechelmann, D.F.C., Richter, D.K., Mangini, A.,  
2061 Frank, N., Breitenbach, S.F.M., Immenhauser, A., 2017. Sensitivity of Bunker Cave to climatic forcings  
2062 highlighted through multi-annual monitoring of rain-, soil-, and dripwaters. *Chemical Geology* 449,  
2063 194-205.

2064 Rittner, M., Müller, W., 2012. 2D mapping of LA-ICPMS trace element distributions using R.  
2065 *Computers & Geosciences* 42, 152-161.

2066 Roberts, M.S., Smart, P.L., Baker, A., 1998. Annual trace element variations in a Holocene  
2067 speleothem. *Earth Planet. Sci. Lett.* 154, 237-246.

2068 Ronay, E.R., Breitenbach, S.F.M., Oster, J.L., 2019. Sensitivity of speleothem records in the Indian  
2069 Summer Monsoon region to dry season infiltration. *Sci Rep* 9, 5091.

2070 Sade, Z., Halevy, I., 2017. New constraints on kinetic isotope effects during CO<sub>2</sub>(aq) hydration and  
2071 hydroxylation: Revisiting theoretical and experimental data. *Geochim. Cosmochim. Acta* 214, 246-  
2072 265.

2073 Santer, B.D., Po-Chedley, S., Zelinka, M.D., Cvijanovic, I., Bonfils, C., Durack, P.J., Fu, Q., Kiehl, J.,  
2074 Mears, C., Painter, J., Pallotta, G., Solomon, S., Wentz, F.J., Zou, C.-Z., 2018. Human influence on the  
2075 seasonal cycle of tropospheric temperature. *Science* 361, eaas8806.

2076 Schubert, B.A., Jahren, A.H., 2015. Seasonal temperature and precipitation recorded in the intra-  
2077 annual oxygen isotope pattern of meteoric water and tree-ring cellulose. *Quaternary Science*  
2078 *Reviews* 125, 1-14.

2079 Schwarz, K., Barth, J.A.C., Postigo-Rebollo, C., Grathwohl, P., 2009. Mixing and transport of water in a  
2080 karst catchment: a case study from precipitation via seepage to the spring. *Hydrology and Earth*  
2081 *System Sciences* 13, 285-292.

2082 Scroxton, N., Burns, S.J., Dawson, P., Rhodes, J.M., Brent, K., McGee, D., Heijnis, H., Gadd, P.,  
2083 Hantoro, W., Gagan, M., 2018. Rapid measurement of strontium in speleothems using core-scanning  
2084 micro X-ray fluorescence. *Chemical Geology* 487, 12-22.

2085 Shen, C.C., Lin, K., Duan, W., Jiang, X., Partin, J.W., Edwards, R.L., Cheng, H., Tan, M., 2013. Testing  
2086 the annual nature of speleothem banding. *Sci Rep* 3, 2633.

2087 Sherwin, C.M., Baldini, J.U.L., 2011. Cave air and hydrological controls on prior calcite precipitation  
2088 and stalagmite growth rates: Implications for palaeoclimate reconstructions using speleothems.  
2089 *Geochim. Cosmochim. Acta* 75, 3915-3929.

2090 Shopov, Y.Y., Ford, D.C., Schwarcz, H.P., 1994. Luminescent microbanding in speleothems - high-  
2091 resolution chronology and paleoclimate. *Geol.* 22, 407-410.

2092 Sliwinski, M.G., Kitajima, K., Kodzon, R., Spicuzza, M., Denny, A., Valley, J.W., 2017. In situ  $\delta^{13}\text{C}$  and  
2093  $\delta^{18}\text{O}$  microanalysis by SIMS: A method for characterizing the carbonate components of natural and  
2094 engineered CO<sub>2</sub>-reservoirs. *International Journal of Greenhouse Gas Control* 57, 116-133.

2095 Sliwinski, M.G., Kodzon, R., Kitajima, K., Denny, A., Spicuzza, M., Valley, J.W., 2015. In-Situ, Micron-  
2096 Scale  $\delta^{13}\text{C}$  &  $\delta^{18}\text{O}$  Analyses (by SIMS) of Chemo-Isotopically Zoned Carbonate Cements of  
2097 Diagenetic Origin—A Case Study on the Implications for the Thermal and Burial History of the Eau  
2098 Claire Fm., Illinois Basin (USA). AAPG Annual Convention and Exhibition.

2099 Smart, P.L., Friedrich, H., 1987. Water movement and storage in the unsaturated zone of a maturely  
2100 karstified aquifer, Mendip Hills, England, The conference on environmental problems in karst  
2101 terrains and their solution. National Water Well Association, Bowling Green, Kentucky, pp. 57-87.

2102 Smith, C.L., Fairchild, I.J., Spötl, C., Frisia, S., Borsato, A., Moreton, S.G., Wynn, P.M., 2009.  
2103 Chronology building using objective identification of annual signals in trace element profiles of  
2104 stalagmites. *Quat Geochronol* 4, 11-21.

2105 Spengler, R.N., 2019. *Fruit from the Sands: The Silk Road Origins of the Foods We Eat*, 1 ed.  
2106 University of California Press, Oakland, California.

2107 Spötl, C., Fairchild, I.J., Tooth, A.F., 2005. Cave air control on dripwater geochemistry, Obir Caves  
2108 (Austria): implications for speleothem deposition in dynamically ventilated caves. *Geochim.*  
2109 *Cosmochim. Acta* 69, 2451-2468.

2110 Spötl, C., Matthey, D., 2006. Stable isotope microsampling of speleothems for palaeoenvironmental  
2111 studies: A comparison of microdrill, micromill and laser ablation techniques. *Chem. Geol.* 235, 48-58.

2112 Stoll, H., Mendez-Vicente, A., Gonzalez-Lemos, S., Moreno, A., Cacho, I., Cheng, H., Edwards, R.L.,  
2113 2015. Interpretation of orbital scale variability in mid-latitude speleothem  $\delta^{18}\text{O}$ : Significance of  
2114 growth rate controlled kinetic fractionation effects. *Quaternary Science Reviews* 127, 215-228.

2115 Stoll, H.M., Müller, W., Prieto, M., 2012. I-STAL, a model for interpretation of Mg/Ca, Sr/Ca and  
2116 Ba/Ca variations in speleothems and its forward and inverse application on seasonal to millennial  
2117 scales. *Geochemistry Geophysics Geosystems* 13, 09004.



- 2118 Surić, M., Lončarić, R., Lončar, N., Buzjak, N., Bajo, P., Drysdale, R.N., 2017. Isotopic characterization  
2119 of cave environments at varying altitudes on the eastern Adriatic coast (Croatia) – Implications for  
2120 future speleothem-based studies. *Journal of Hydrology* 545, 367-380.
- 2121 Tabersky, D., Nishiguchi, K., Utani, K., Ohata, M., Dietiker, R., Fricker, M.B., de Maddalena, I.M.,  
2122 Koch, J., Gunther, D., 2013. Aerosol entrainment and a large-capacity gas exchange device (Q-GED)  
2123 for laser ablation inductively coupled plasma mass spectrometry in atmospheric pressure air. *J. Anal.*  
2124 *At. Spectrom.* 28, 831-842.
- 2125 Tadros, C.V., Treble, P.C., Baker, A., Fairchild, I., Hankin, S., Roach, R., Markowska, M., McDonald, J.,  
2126 2016. ENSO-cave drip water hydrochemical relationship: a 7-year dataset from south-eastern  
2127 Australia. *Hydrology and Earth System Sciences* 20, 4625-4640.
- 2128 Tan, M., Baker, A., Genty, D., Smith, C., Esper, J., Cai, B.G., 2006. Applications of stalagmite laminae  
2129 to paleoclimate reconstructions: Comparison with dendrochronology/climatology. *Quaternary Sci.*  
2130 *Rev.* 25, 2103-2117.
- 2131 Taylor, W., Shnaider, S., Abdykanova, A., Fages, A., Welker, F., Irmer, F., Seguin-Orlando, A., Khan, N.,  
2132 Douka, K., Kolobova, K., Orlando, L., Krivoshapkin, A., Boivin, N., 2018. Early pastoral economies  
2133 along the Ancient Silk Road: Biomolecular evidence from the Alay Valley, Kyrgyzstan. *Plos One* 13,  
2134 e0205646.
- 2135 Thompson, G.M., Lumsden, D.N., Walker, R.L., Carter, J.A., 1975. Uranium series dating of  
2136 stalagmites from Blanchard Springs Caverns, U.S.A. *Geochim. Cosmochim. Acta* 39, 1211-1218.
- 2137 Treble, P., Shelley, J.M.G., Chappell, J., 2003. Comparison of high resolution sub-annual records of  
2138 trace elements in a modern (1911-1992) speleothem with instrumental climate data from southwest  
2139 Australia. *Earth Planet. Sci. Lett.* 216, 141-153.

2140 Treble, P.C., Bradley, C., Wood, A., Baker, A., Jex, C.N., Fairchild, I.J., Gagan, M.K., Cowley, J., Azcurra,  
2141 C., 2013. An isotopic and modelling study of flow paths and storage in Quaternary calcarenite, SW  
2142 Australia; implications for speleothem paleoclimate records. *Quaternary Sci. Rev.* 64, 90-103.

2143 Treble, P.C., Chappell, J., Gagan, M.K., McKeegan, K.D., Harrison, T.M., 2005a. In situ measurement  
2144 of seasonal  $\delta^{18}\text{O}$  variations and analysis of isotopic trends in a modern speleothem from southwest  
2145 Australia. *Earth Planet. Sci. Lett.* 233, 17-32.

2146 Treble, P.C., Chappell, J., Shelley, J.M.G., 2005b. Complex speleothem growth processes revealed by  
2147 trace element mapping and scanning electron microscopy of annual layers. *Geochim. Cosmochim.*  
2148 *Acta* 69, 4855-4863.

2149 Treble, P.C., Schmitt, A.K., Edwards, R.L., McKeegan, K.D., Harrison, T.M., Grove, M., Cheng, H.,  
2150 Wang, Y.J., 2007. High resolution Secondary Ionisation Mass Spectrometry (SIMS)  $\delta^{18}\text{O}$   
2151 analyses of Hulu Cave speleothem at the time of Heinrich Event 1. *Chem. Geol.* 238, 197-212.

2152 Tremaine, D.M., Froelich, P.N., Wang, Y., 2011. Speleothem calcite formed in situ: Modern  
2153 calibration of  $\delta^{18}\text{O}$  and  $\delta^{13}\text{C}$  paleoclimate proxies in a continuously-monitored natural cave system.  
2154 *Geochim. Cosmochim. Acta* 75, 4929-4950.

2155 Valley, J.W., Kita, N.T., 2009. In situ oxygen isotope geochemistry by ion microprobe, MAC short  
2156 course: secondary ion mass spectrometry in the earth sciences, pp. 19-63.

2157 Vanghi, V., Borsato, A., Frisia, S., Howard, D., Gloy, G., Hellstrom, J., Bajo, P., 2019. High-resolution  
2158 synchrotron X-ray fluorescence investigation of calcite coralloid speleothems: Elemental  
2159 incorporation and their potential as environmental archives. *Sedimentology* 66, 2661–2685.

2160 Verheyden, S., Genty, D., Deflandre, G., Quinif, Y., Keppens, E., 2008. Monitoring climatological,  
2161 hydrological and geochemical parameters in the Pere Noel cave (Belgium): implication for the  
2162 interpretation of speleothem isotopic and geochemical time-series. *Int J Speleol* 37, 221-234.

2163 Vonhof, H.B., van Breukelen, M.R., Postma, O., Rowe, P.J., Atkinson, T.C., Kroon, D., 2006. A  
2164 continuous-flow crushing device for on-line delta H-2 analysis of fluid inclusion water in  
2165 speleothems. *Rapid Commun. Mass Spectrom.* 20, 2553-2558.

2166 Waite, A.J., Swart, P.K., 2015. The inversion of aragonite to calcite during the sampling of skeletal  
2167 archives: Implications for proxy interpretation. *Rapid Commun Mass Spectrom* 29, 955-964.

2168 Walczak, I.W., 2016. Holocene climate variability revealed using geochemistry and Computed  
2169 Tomography scanning of stalagmites from the North Atlantic Basin, *Earth Sciences*. Durham  
2170 University, Durham, p. 199.

2171 Walczak, I.W., Baldini, J.U.L., Baldini, L.M., McDermott, F., Marsden, S., Standish, C.D., Richards, D.A.,  
2172 Andreo, B., Slater, J., 2015. Reconstructing high-resolution climate using CT scanning of unsectioned  
2173 stalagmites: A case study identifying the mid-Holocene onset of the Mediterranean climate in  
2174 southern Iberia. *Quaternary Sci. Rev.* 127, 117-128.

2175 Wang, C., Bendle, J.A., Greene, S.E., Griffiths, M.L., Huang, J., Moossen, H., Zhang, H., Ashley, K., Xie,  
2176 S., 2019a. Speleothem biomarker evidence for a negative terrestrial feedback on climate during  
2177 Holocene warm periods. *Earth Planet. Sci. Lett.* 525, 115754.

2178 Wang, J.K., Johnson, K.R., Borsato, A., Amaya, D.J., Griffiths, M.L., Henderson, G.M., Frisia, S., Mason,  
2179 A., 2019b. Hydroclimatic variability in Southeast Asia over the past two millennia. *Earth Planet. Sci.*  
2180 *Lett.* 525, 115737.

2181 Wang, X.F., Edwards, R.L., Auler, A.S., Cheng, H., Kong, X.G., Wang, Y.J., Cruz, F.W., Dorale, J.A.,  
2182 Chiang, H.W., 2017. Hydroclimate changes across the Amazon lowlands over the past 45,000 years.  
2183 *Nature* 541, 204–207.

2184 Wang, Y.J., Cheng, H., Edwards, R.L., An, Z.S., Wu, J.Y., Shen, C.-C., Dorale, J.A., 2001. A high-  
2185 resolution absolute-dated late Pleistocene monsoon record from Hulu Cave, China. *Science* 294,  
2186 2345-2348.

2187 Webb, M., Dredge, J., Barker, P.A., Müller, W., Jex, C., Desmarchelier, J., Hellstrom, J., Wynn, P.M.,  
2188 2014. Quaternary climatic instability in south-east Australia from a multi-proxy speleothem record. *J.*  
2189 *of Quaternary Sci.* 29, 589-596.

2190 Welte, C., Wacker, L., Hattendorf, B., Christl, M., Fohlmeister, J., Breitenbach, S.F.M., Robinson, L.F.,  
2191 Andrews, A.H., Freiwald, A., Farmer, J.R., Yeman, C., Synal, H.A., Gunther, D., 2016. Laser Ablation -  
2192 Accelerator Mass Spectrometry: An Approach for Rapid Radiocarbon Analyses of Carbonate Archives  
2193 at High Spatial Resolution. *Anal. Chem.* 88, 8570-8576.

2194 Wiedenbeck, M., Bugoi, R., Duke, M.J.M., Dunai, T., Enzweiler, J., Horan, M., Jochum, K.P., Linge, K.,  
2195 Kosler, J., Merchel, S., Morales, L.F.G., Nasdala, L., Stalder, R., Sylvester, P., Weis, U., Zoubir, A., 2012.  
2196 GGR Biennial Critical Review: Analytical Developments Since 2010. *Geostandards and Geoanalytical*  
2197 *Research* 36, 337-398.

2198 Wong, C.I., Banner, J.L., Musgrove, M., 2011. Seasonal dripwater Mg/Ca and Sr/Ca variations driven  
2199 by cave ventilation: Implications for and modeling of speleothem paleoclimate records. *Geochimica*  
2200 *et Cosmochimica Acta* 75, 3514-3529.

2201 Wong, C.I., Breecker, D.O., 2015. Advancements in the use of speleothems as climate archives.  
2202 *Quaternary Science Reviews* 127, 1-18.

2203 Woodhead, J.D., Hellstrom, J., Hergt, J.M., Greig, A., Maas, R., 2007. Isotopic and elemental imaging  
2204 of geological materials by laser ablation inductively coupled plasma-mass spectrometry.  
2205 *Geostandards and Geoanalytical Research* 31, 331-343.

- 2206 Woodhead, J.D., Horstwood, M.S.A., Cottle, J.M., 2016. Advances in isotope ratio determination by  
2207 LA-ICP-MS. *Elements* 12, 317-322.
- 2208 Wortham, B.E., Montanez, I.P., Rowland, D.J., Lerche, M., Browning, A., 2019. Mapping Fluid-Filled  
2209 Inclusions in Stalagmites Using Coupled X-Ray and Neutron Computed Tomography: Potential as a  
2210 Water Excess Proxy. *Geochemistry Geophysics Geosystems* 20, 2647-2656.
- 2211 Wu, X., Zhu, X., Pan, M., Zhang, M., 2014. Seasonal variability of oxygen and hydrogen stable  
2212 isotopes in precipitation and cave drip water at Guilin, southwest China. *Environmental Earth  
2213 Sciences* 72, 3183-3191.
- 2214 Wycech, J.B., Kelly, D.C., Kozdon, R., Orland, I.J., Spero, H.J., Valley, J.W., 2018. Comparison of  $\delta^{18}O$   
2215 analyses on individual planktic foraminifer (*Orbulina universa*) shells by SIMS and gas-source mass  
2216 spectrometry. *Chemical Geology* 483, 119-130.
- 2217 Wynn, P.M., Fairchild, I.J., Borsato, A., Spotl, C., Hartland, A., Baker, A., Frisia, S., Baldini, J.U.L., 2018.  
2218 Sulphate partitioning into calcite: Experimental verification of pH control and application to  
2219 seasonality in speleothems. *Geochim. Cosmochim. Acta* 226, 69-83.
- 2220 Wynn, P.M., Fairchild, I.J., Frisia, S., Spotl, C., Baker, A., Borsato, A., EIMF, 2010. High-resolution  
2221 sulphur isotope analysis of speleothem carbonate by secondary ionisation mass spectrometry.  
2222 *Chem. Geol.* 271, 101-107.
- 2223 Wynn, P.M., Fairchild, I.J., Spotl, C., Hartland, A., Matthey, D., Fayard, B., Cotte, M., 2014. Synchrotron  
2224 X-ray distinction of seasonal hydrological and temperature patterns in speleothem carbonate.  
2225 *Environ Chem* 11, 28-36.
- 2226 Yonge, C.J., Ford, D.C., Gray, J., Schwarcz, H.P., 1985. Stable isotope studies of cave seepage water.  
2227 *Chemical Geology* 58, 97-105.

2228 Zeng, G., Luo, W., Wang, S., Du, X., 2015. Hydrogeochemical and climatic interpretations of isotopic  
2229 signals from precipitation to drip waters in Liangfeng Cave, Guizhou Province, China. *Environmental*  
2230 *Earth Sciences* 74, 1509-1519.

2231

2232 **Figure Captions:**

2233 Figure 1: Top Panel: Resolution of speleothem isotope records over time, compiled from the  
2234 SISALv1b database. Individual record resolution (small black circles) and mean resolution of  
2235 all available (black bars) and Holocene (blue bars) records published in a given year. Bottom  
2236 panel: Total number of stalagmite records identified (grey bars), total number of stalagmite  
2237 records in SISALv1b (black bars), and total number of Holocene records in SISALv1b (blue  
2238 bars).

2239 Figure 2: Illustration of different drip responses from Yok Balum Cave, Belize, over  
2240 approximately two months as captured by a series of automated drip loggers. Two clear rain  
2241 events and the subsequent drip responses are indicated by the vertical dashed red lines.  
2242 Rainfall amount is recorded directly over the cave site using a tipping bucket rain gauge.  
2243 Techniques are discussed in more detail in (Ridley et al., 2015a).

2244 Figure 3: A new drip categorisation scheme designed to emphasise cave drip seasonality.  
2245 The scheme does not use classification boundaries as such, but instead uses the data  
2246 distribution to understand the hydrology. The scheme uses descriptors that map onto  
2247 established drip terminology (see Panels B-D and main text for examples). A) Minimum and  
2248 maximum hourly drip rates extracted for every month of record for numerous cave drips  
2249 globally. The dashed line represents the 1:1 line, and all data points must necessarily plot

2250 over this (i.e., the minimum drip rate cannot exceed the maximum drip rate for any given  
2251 month). The closer a point plots to the dashed line, the lower the difference between  
2252 monthly maximum and minimum values for that point; if a point sits on the line the  
2253 minimum and maximum values for that month are identical. Panels B-D illustrate some  
2254 common drip types (using synthetic data) and their pattern when plotted on this diagram.  
2255 Panels B-D are schematic and are not based on actual collected datasets; the symbols used  
2256 are arbitrary and are not linked to the symbols used in Panel A.

2257 Figure 4: The simulated effects of sampling resolution on the climate signal extracted from a  
2258 stalagmite. The stalagmite data are from stalagmite YOK-G (Yok Balum Cave, Belize), which  
2259 was originally sampled with a micromill at a 100 micron (0.1 mm) step size (Ridley et al.,  
2260 2015b). The chronology for the stalagmite is precise at the seasonal scale. The rainfall data  
2261 (bottom panel) are from the Punta Gorda meteorological station (~30 km to the southeast  
2262 of the cave site).

2263 Figure 5: Schematic of a sampling scheme for achieving ~50 micron spatial resolution. Plan  
2264 view of a stalagmite surface with 1 mm conventional holes on the right and trenches cut for  
2265 low and high resolution. The red trench was milled with a 0.8 mm diameter drill and the (blue-  
2266 shaded) higher resolution trench was cut laterally, with each sample integrating 50  $\mu\text{m}$ . The  
2267 red corners highlight the area that is incorporated into subsequent steps, which in this case  
2268 includes material from the current and the previous sample. In this example each high-  
2269 resolution sample (e.g., yellow shaded area) integrates a minimal amount of powder of an  
2270 older sample (because the milling direction is upward).

2271 Figure 6: Several examples of output generated by different geochemical-based techniques  
2272 for extracting seasonal climate. A) Variability in sulphate in speleothem calcite (Obi84, Obir

2273 cave, Austria) as determined by SR- $\mu$ XRF (Wynn et al., 2014). The clear annual sulphur maxima  
2274 are evident as brighter green colours. B) Ion microprobe-resolved strontium and phosphorous  
2275 cycles apparent in stalagmite CC3 from Crag Cave, southwestern Ireland (Baldini et al., 2002).  
2276 The well-developed cycles illustrate stronger seasonality at the time of deposition ( $\sim$ 8.336 ka  
2277 BP) than currently present. C) Annual UV-luminescent banding in a stalagmite from Shihua  
2278 Cave, Beijing, China (adapted from Tan et al. (2006)). D) well-develop carbon isotope ratio  
2279 cycles in stalagmite YOK-G from Yok Balum Cave, Belize, constructed using data obtained via  
2280 micromilling at a 100-micron spatial resolution and analyses of powders on an IRMS (Ridley  
2281 et al., 2015b) (see also Figure 4). E) Mg cycles apparent in stalagmite BER-SWI-13 from  
2282 Leamington Cave, Bermuda, resolved using LA-ICPMS-derived Mg data (Walczak, 2016). All  
2283 panels show three to four cycles, interpreted as annual.

2284 Figure 7: A synthetic rainfall input signal (orange circles) with an annual temperature range of  
2285 15 °C compared with two mean model outputs, one derived using an annual temperature  
2286 range of  $10 \pm 6$  °C (grey line), and another derived using an annual temperature range of  $15 \pm$   
2287 6 °C (blue line). At the beginning of the simulated rainfall input signal record (year = 0), April  
2288 is the wettest month and November the driest month, but this shifts in polarity slowly through  
2289 the record, moving through a brief phase with no seasonality in rainfall (year = 7), and then  
2290 transitioning into a phase where April is the driest month (from year = 8). The vertical gridlines  
2291 highlight the month of April during every model year. The simulated rainfall input signal  
2292 amplitude and polarity is reproduced by the model very satisfactorily, provided that the  
2293 model temperature range is realistic, as it is in Model 2. Note that the polarity of the simulated  
2294 rainfall input signal is still reproduced by Model 1, but modelled rainfall seasonal amplitude  
2295 is too large in order to compensate for the low amplitude of the modelled temperature range.



2296 Figure 8: Temperature (top panel) and rainfall (bottom panel) modelling results (black  
2297 dashed lines) against 'noisy' synthetic input datasets (solid coloured lines) for seven model  
2298 years. The grey rectangle highlights one model year (Year 4) where the input rainfall signal  
2299 polarity was reversed; the model detects this shift. The modelling results presented are the  
2300 mean values of all successful model runs for each timeslice.

2301 Figure 9: Mean modelled monthly temperature and rainfall data against Global Historical  
2302 Climate Network (GHCN) and tree ring data. A) Stalagmite Keklik1 oxygen isotope ratio data  
2303 from Bir-Uja Cave, Kyrgyzstan (input data) (Fohlmeister et al., 2017). B) Centennial-scale  
2304 borehole temperature data from the Tian Shan region (Huang et al., 2000) from 1500 to  
2305 2000 C.E. (input data, shifted upwards for clarity) (blue diamonds), modelled July  
2306 temperature (black curve) (output), and NTREND summer temperature reconstruction for  
2307 Asia Grid 2 (AG2) (red curve) (Cook et al., 2013). C) Modelled January rainfall (black curve)  
2308 (output) and GHCN January rainfall for Tashkent (orange curve), both in % of total annual  
2309 rainfall. The grey rectangles highlight the years 1797 and 1815 C.E. discussed in the text.

2310 Figure 10: Global seasonality in annual temperature ( $^{\circ}\text{C}$ ) and annual precipitation (mm). A)  
2311 The annual temperature range was calculated as the maximum temperature of the warmest  
2312 month minus the minimum temperature of the coldest month averaged over the period  
2313 1970-2000. B) Precipitation seasonality was calculated as the precipitation amount of the  
2314 wettest month minus the precipitation amount of the driest month averaged over the  
2315 period 1970-2000. WorldClim Version 2 data (<https://www.worldclim.org/>) were obtained  
2316 at a 2.5 minute ( $\sim 4.5$  km at the equator) spatial resolution (Fick and Hijmans, 2017). The  
2317 data span the period 1970-2000 and thus may reflect anthropogenically-influenced  
2318 temperature seasonality as discussed in Santer et al. (2018). Therefore, although the general

2319 spatial pattern of temperature (and potentially precipitation) seasonality may persist into  
2320 the past, the magnitude of seasonality shifts may deviate from that presented here,  
2321 particularly when extending records into the preindustrial era.

2322 Figure 11: Global seasonality in amount-weighted precipitation  $\delta^{18}\text{O}$  (‰ VWMOW). The  
2323 amount-weighted mean (WM) monthly precipitation  $\delta^{18}\text{O}$  data (IAEA/WMO, 2001) were  
2324 used to determine the annual range in precipitation isotopes globally (calculated as the  
2325 maximum monthly WM  $\delta^{18}\text{O}$  minus minimum monthly WM  $\delta^{18}\text{O}$  at 267 stations (yellow  
2326 symbols) with a complete 12-month dataset over the period 1961-1999. GNIP station data  
2327 were interpolated onto a  $2.5^\circ \times 2.5^\circ$  global grid ( $\sim 278 \text{ km} \times 278 \text{ km}$ ) (IAEA, 2001).

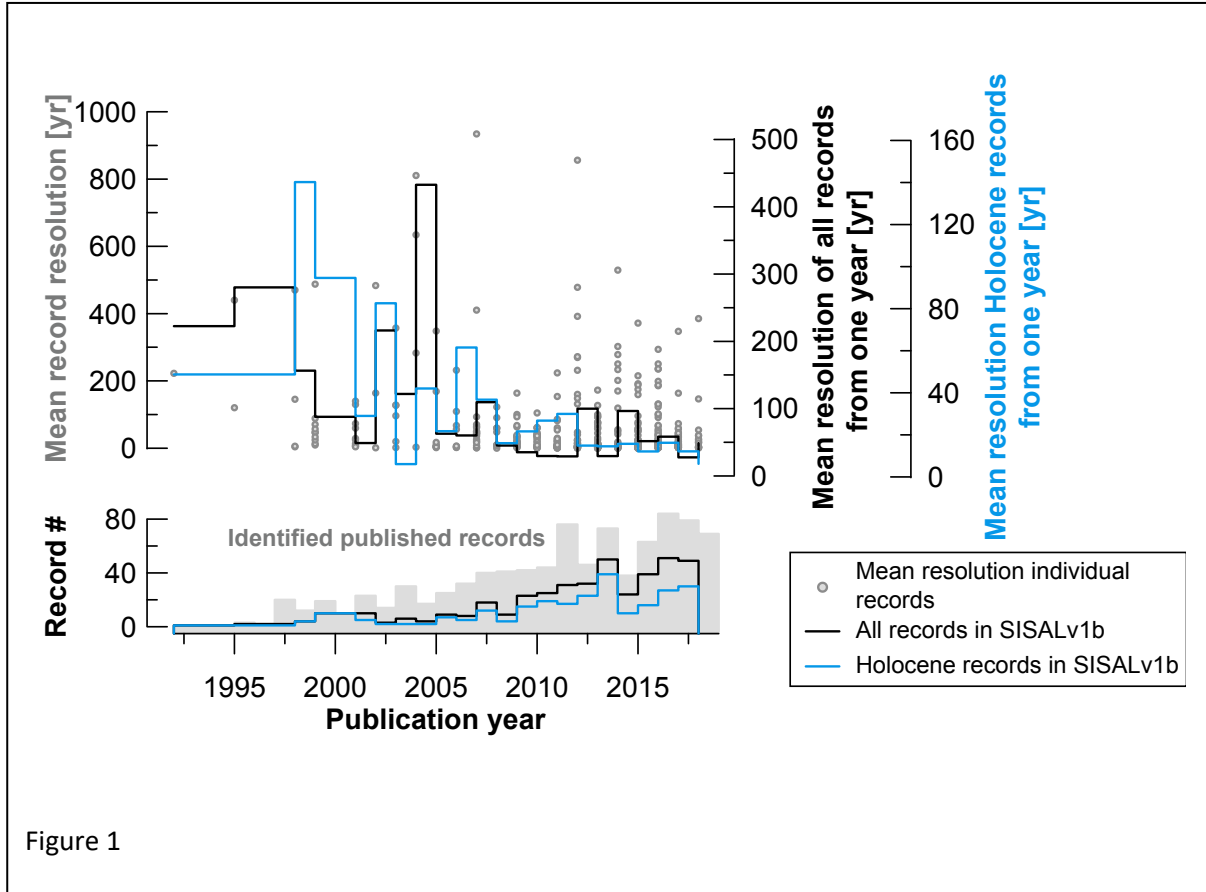
2328 Figure 12: A Hovmöller plot of the annual cycle of total-column precipitable water vapour  
2329 for Central America, based on daily ERA5 re-analysis data across the region from  $-110^\circ$  to  $-$   
2330  $80^\circ\text{W}$  and  $0^\circ$  to  $35^\circ\text{N}$  for the period 1979-2018. Also indicated are the latitudes of three key  
2331 cave sites that have yielded stalagmites which have produced oxygen isotope records of  
2332 rainfall.

2333

2334 Figures:

2335

2336



2337

2338

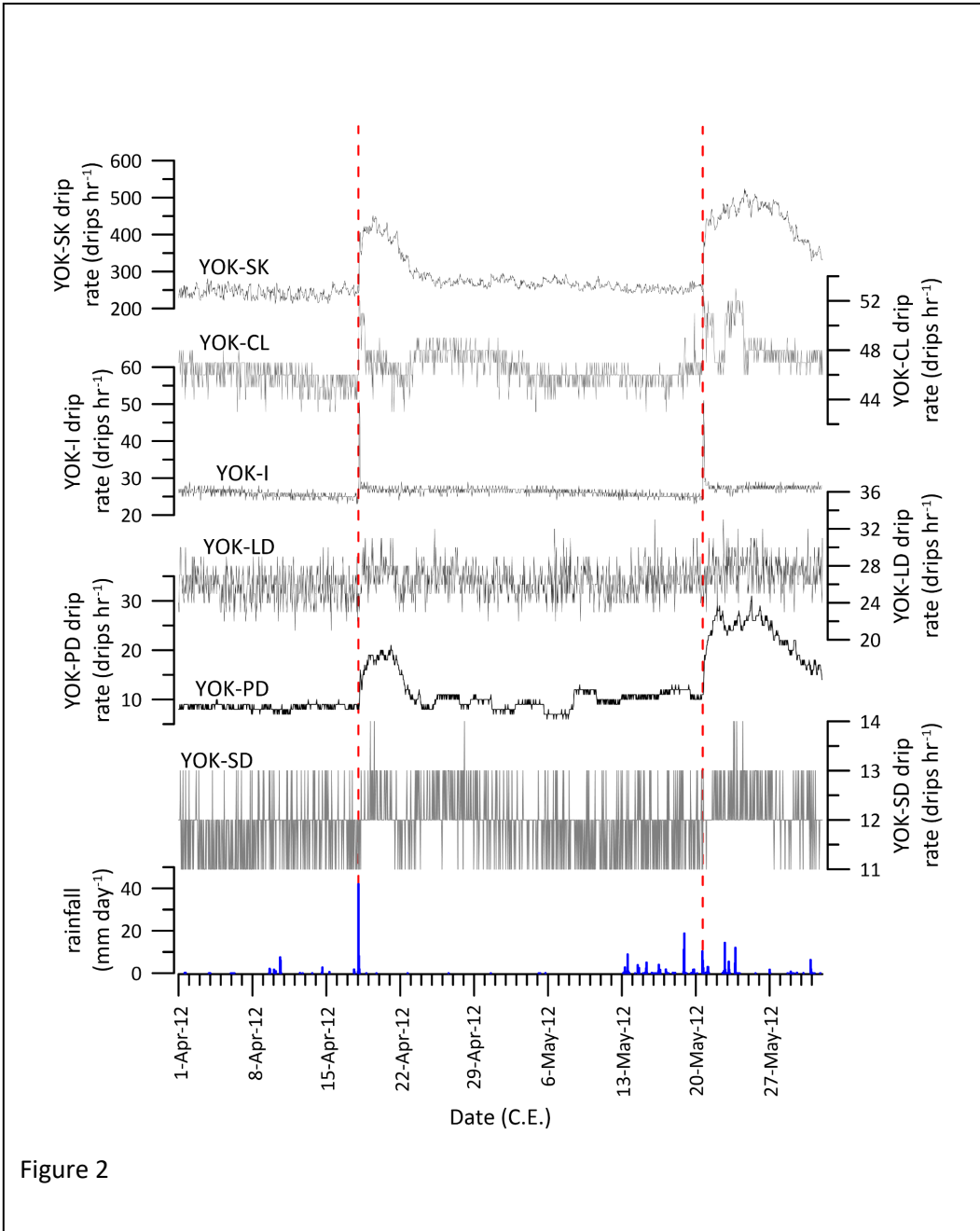


Figure 2

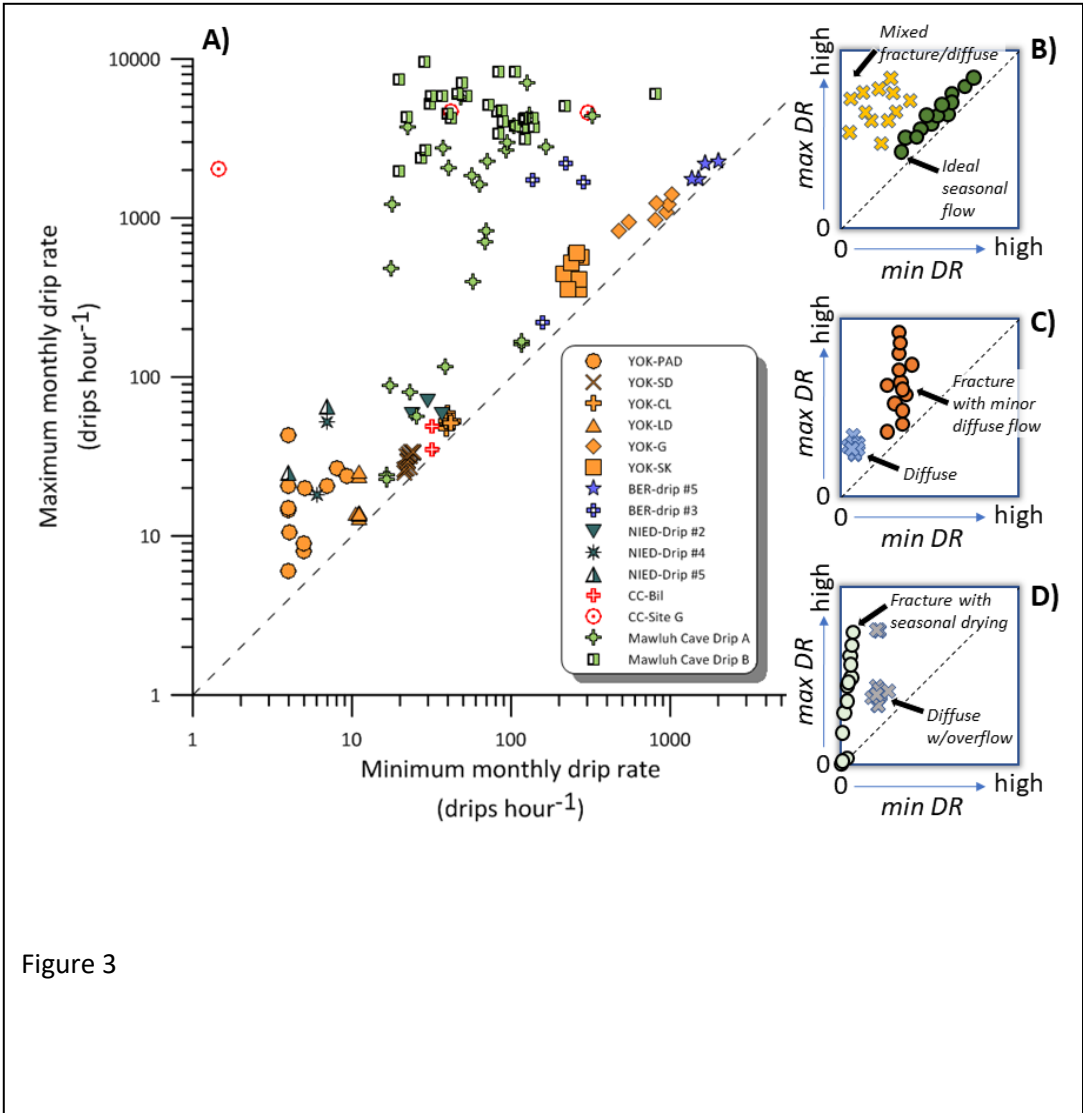


Figure 3

2342

2343

2344

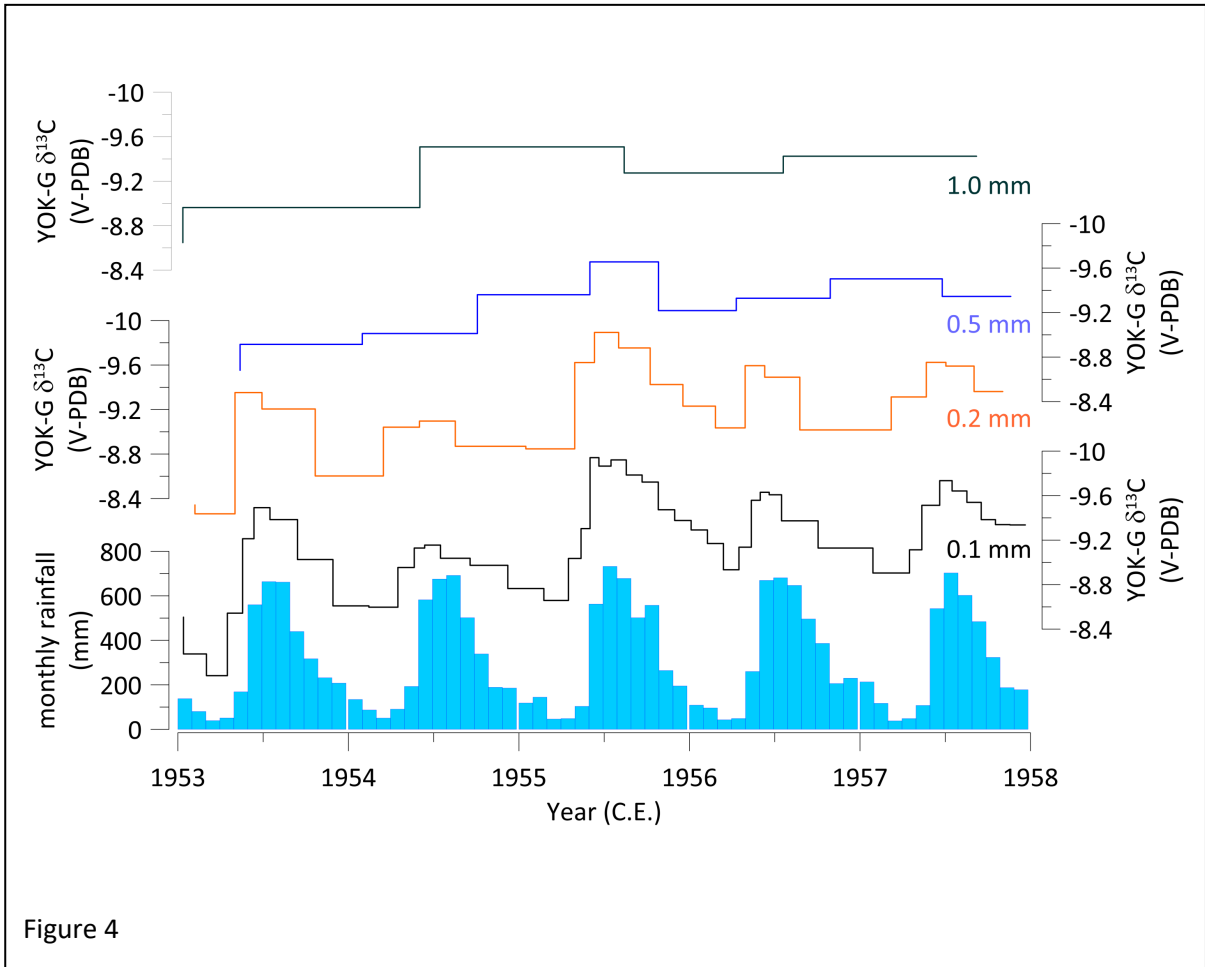


Figure 4

2345

2346

2347

2348

2349

2350

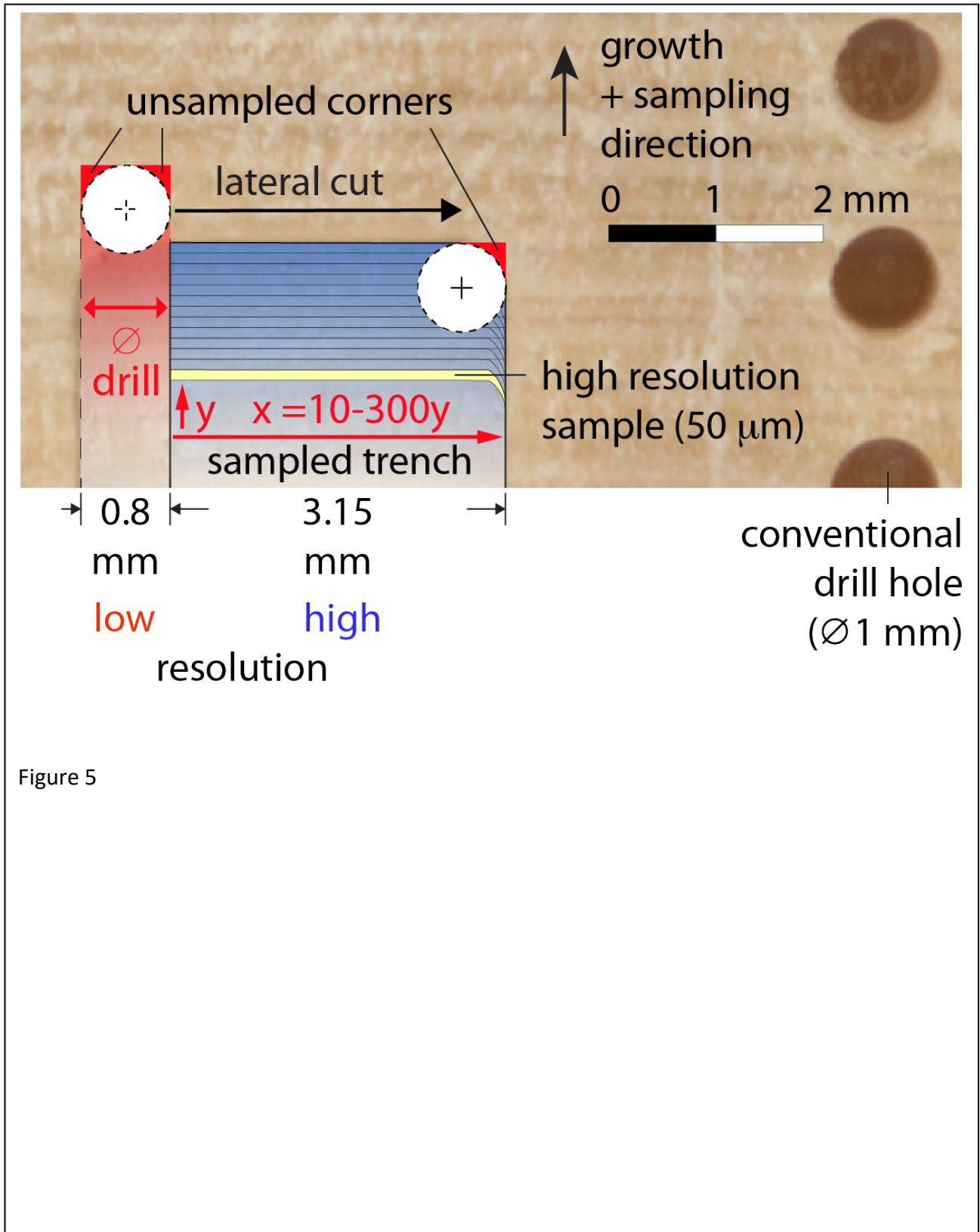


Figure 5

2353

2354

2355

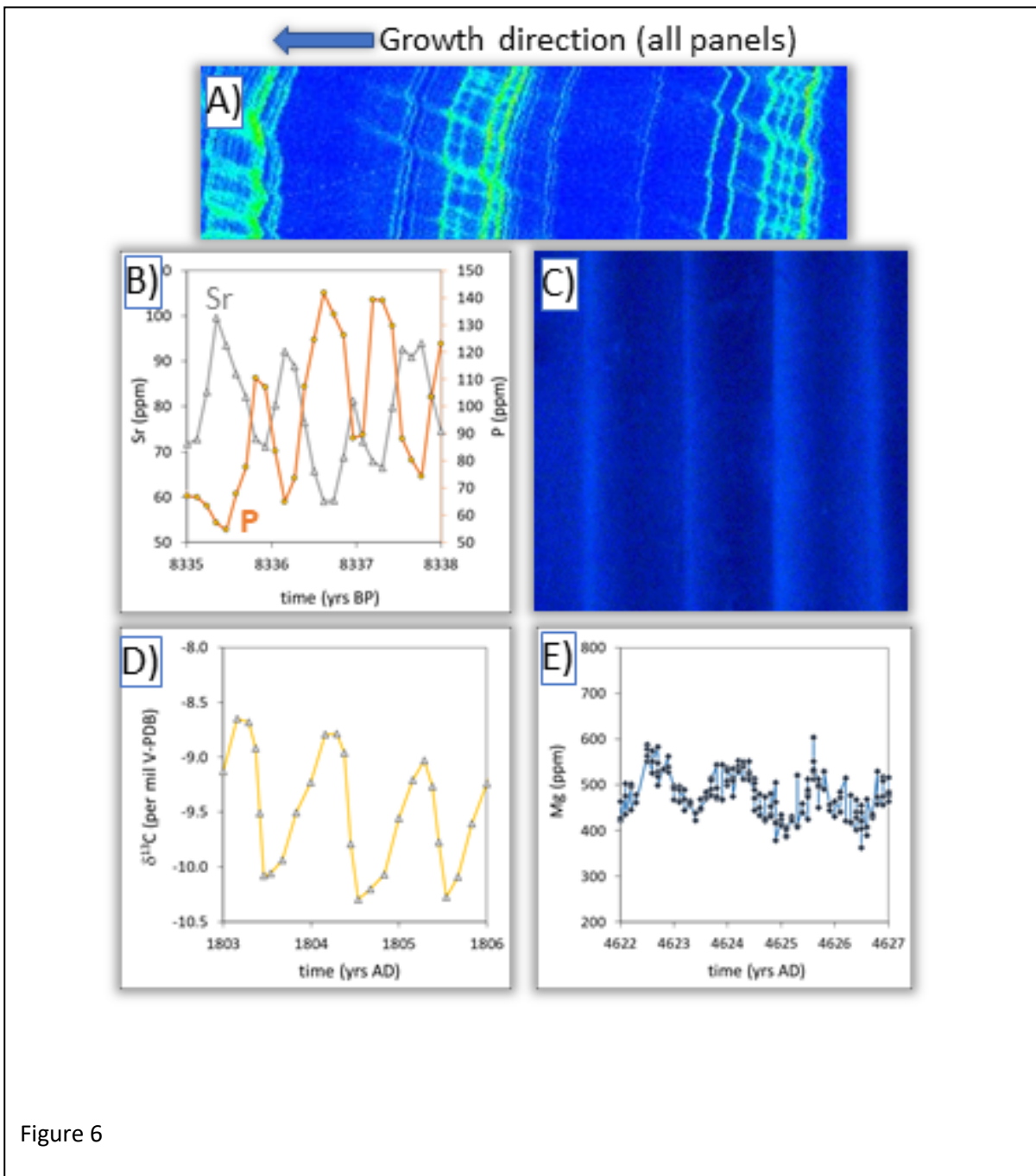


Figure 6

2356



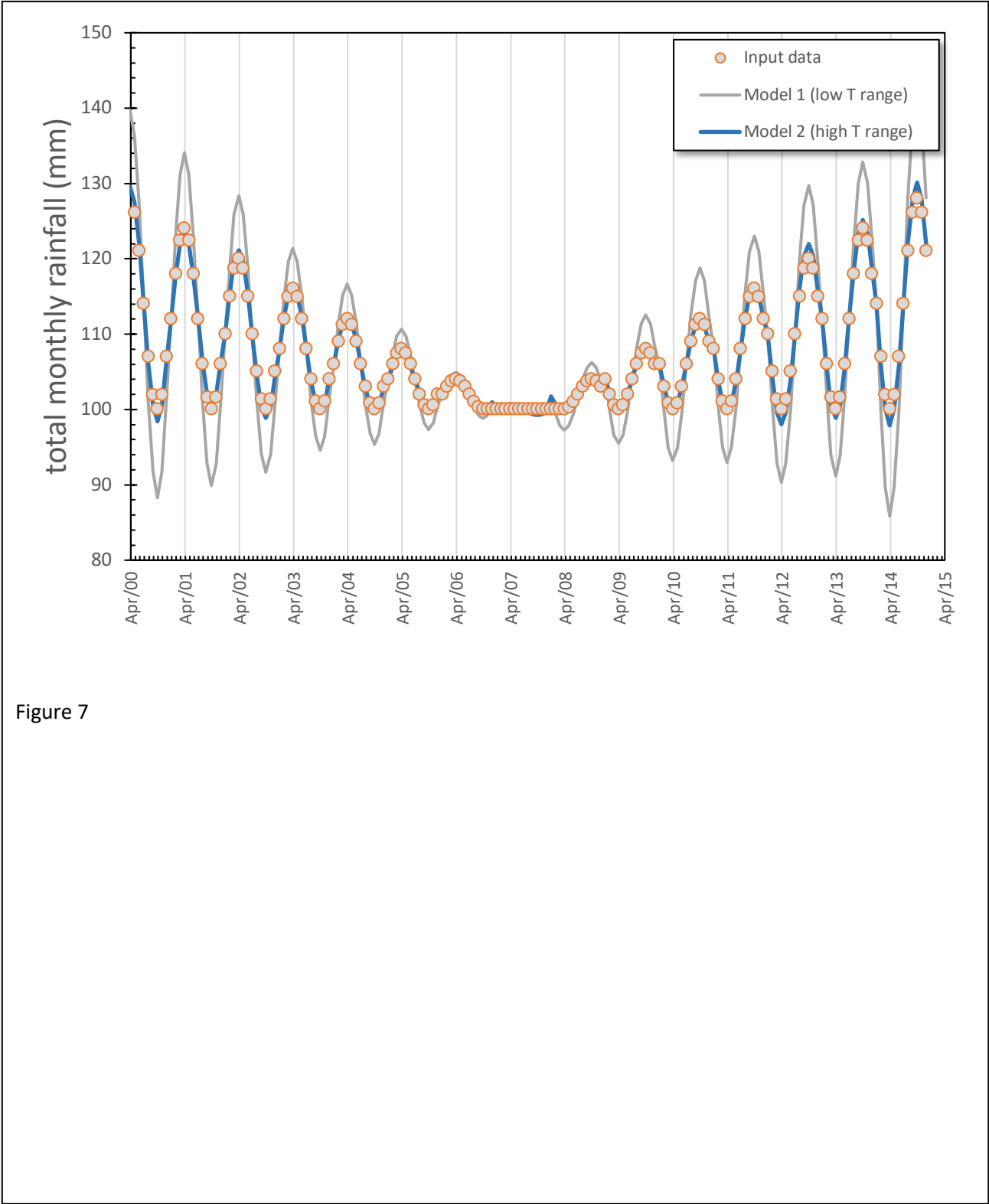
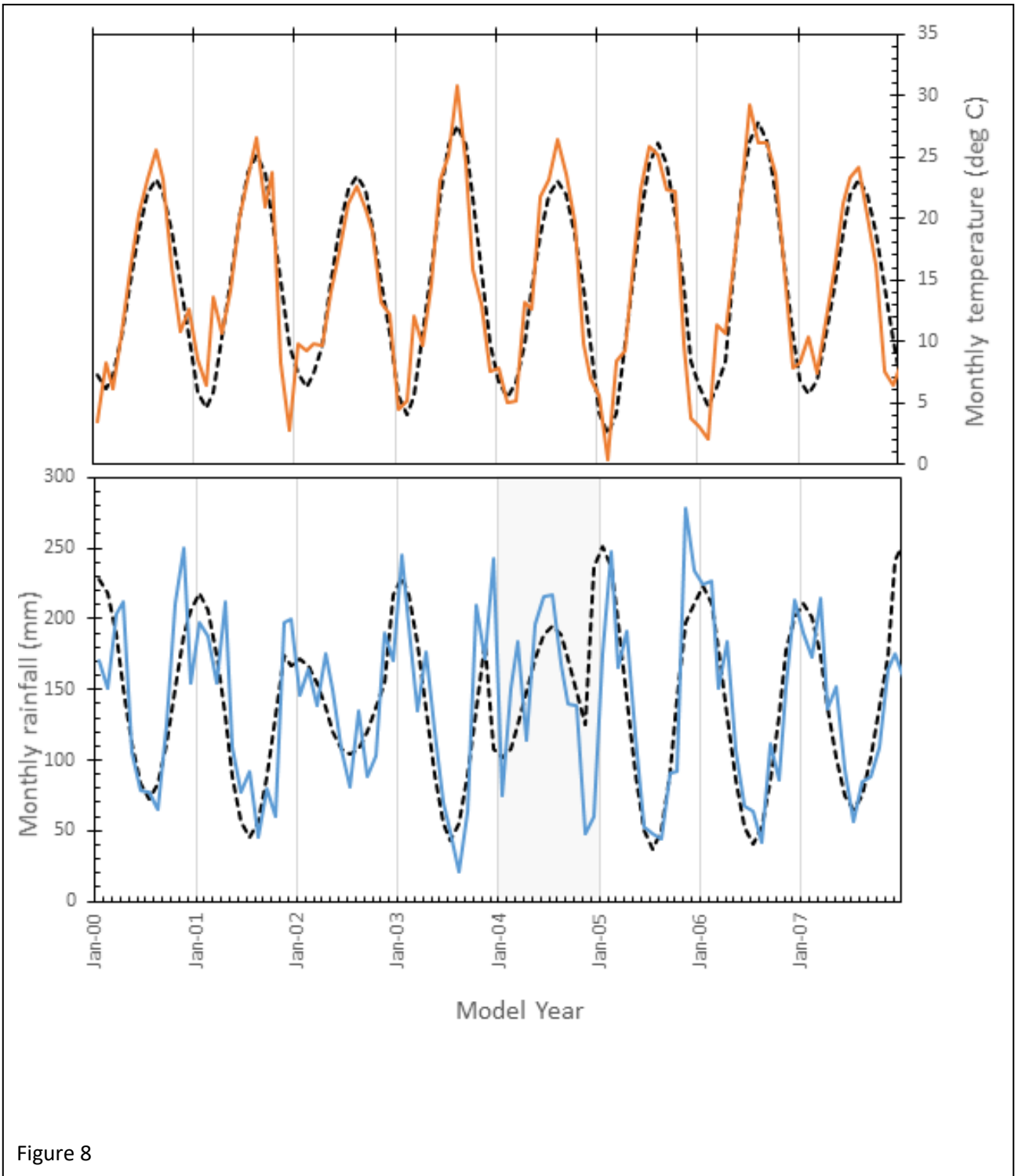


Figure 7



2359

2360

2361

2362

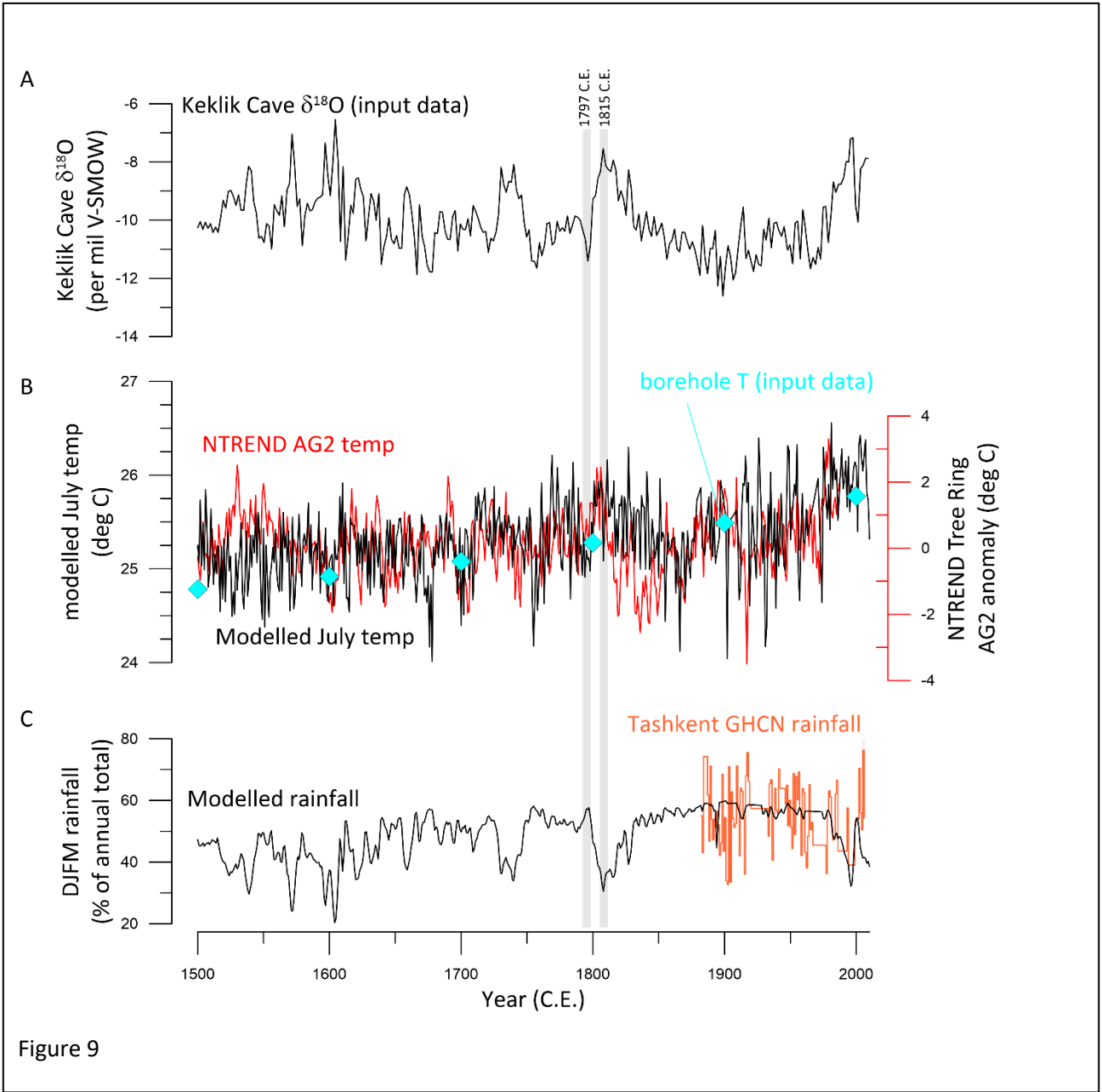


Figure 9

2363

2364

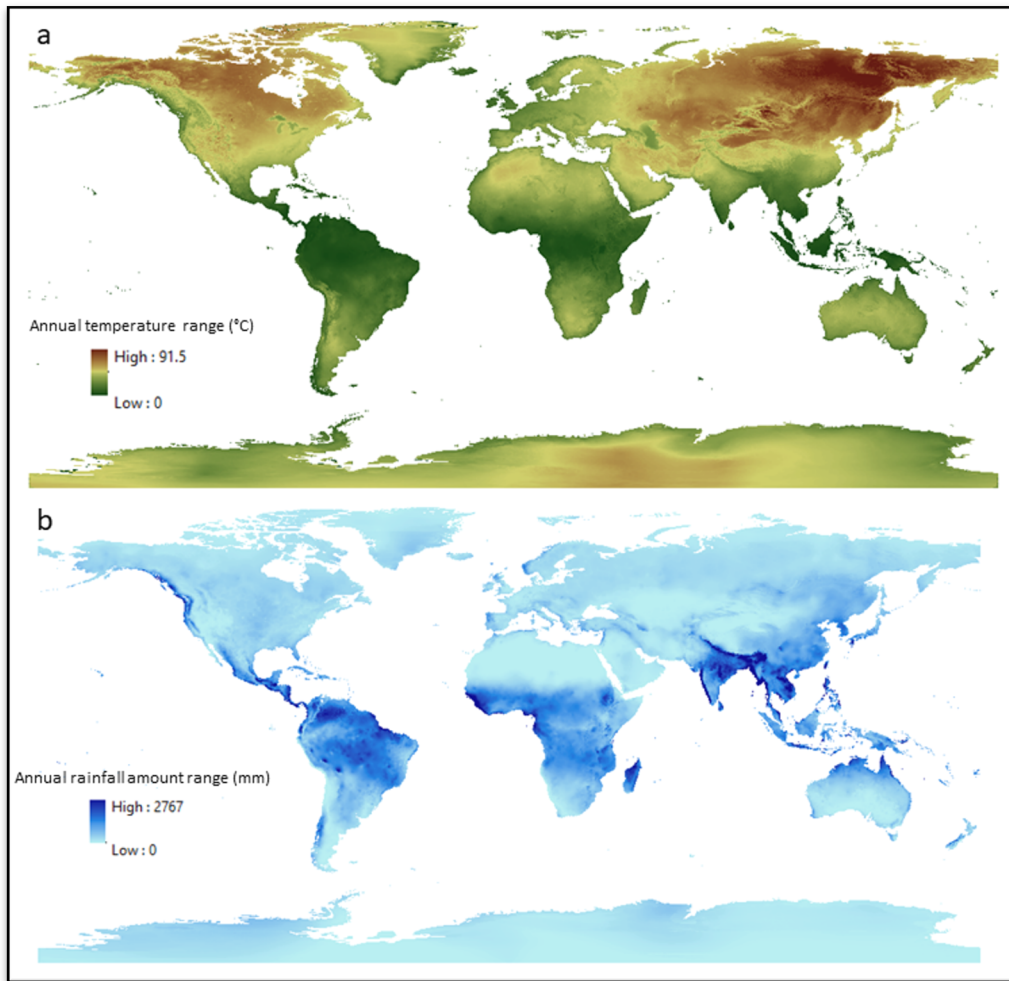


Figure 10

2367

2368

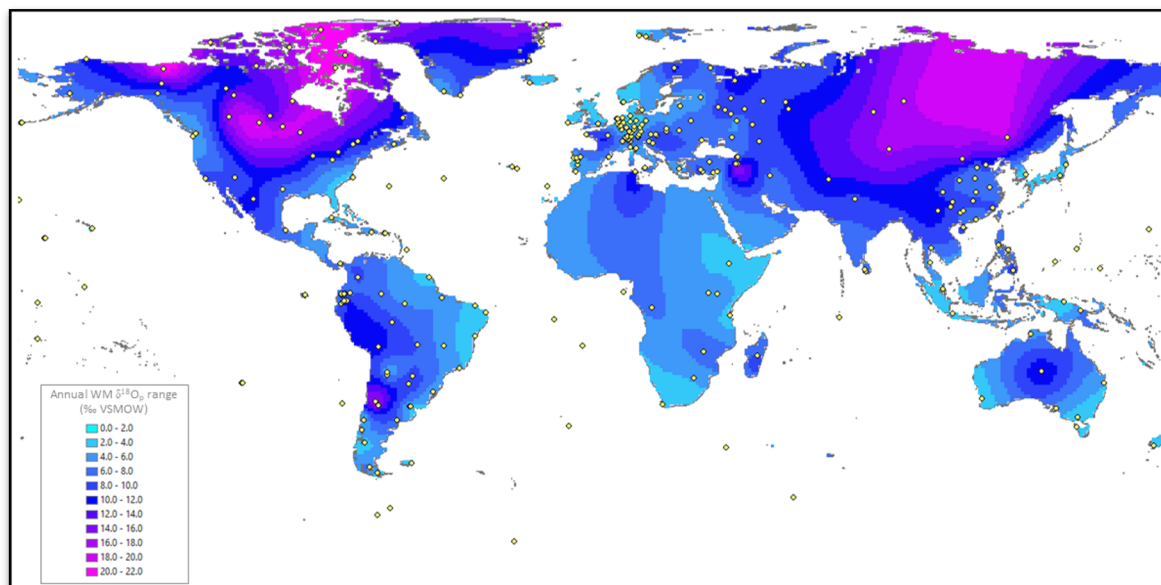
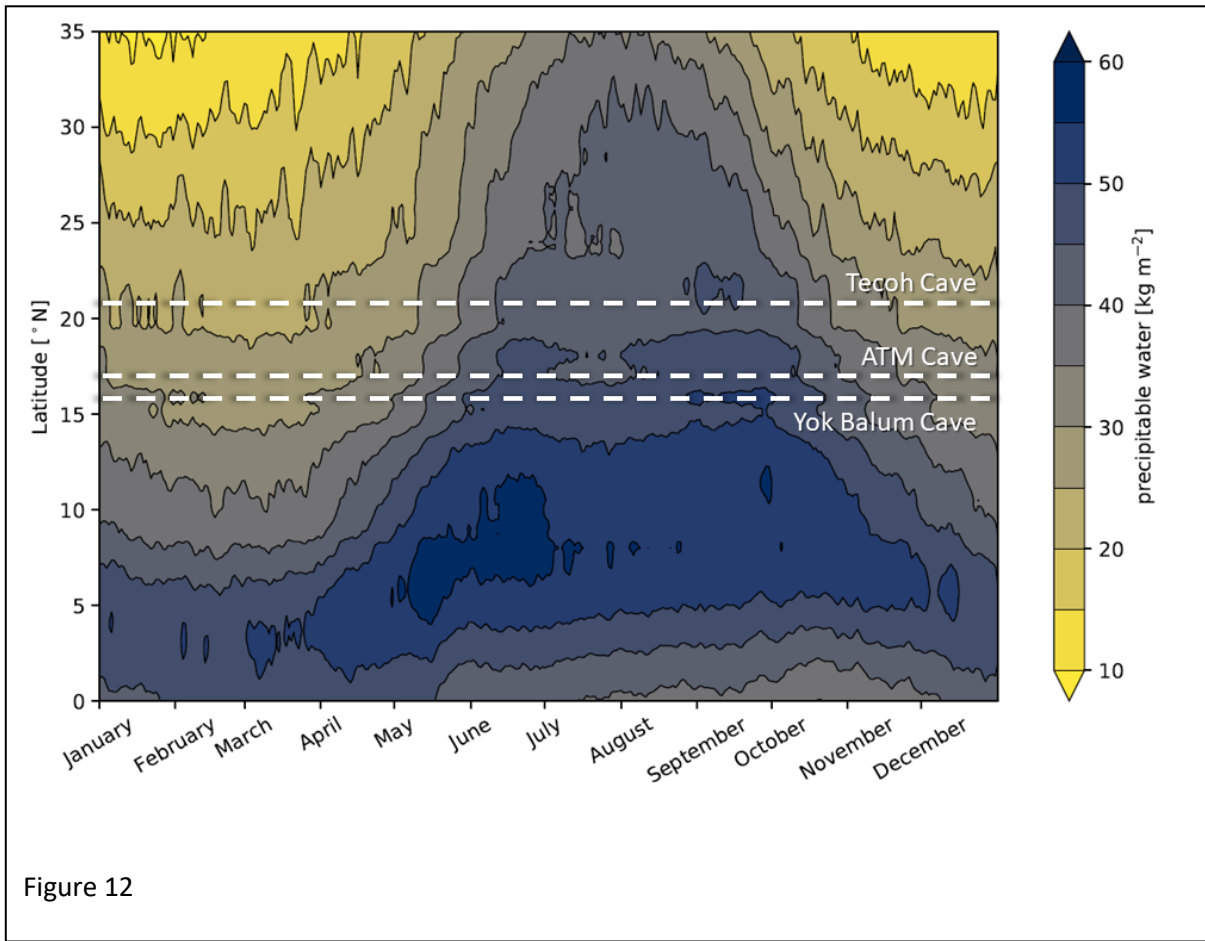


Figure 11

2369



2370

2371

2372